UNIVERSITÉ DU QUÉBEC À CHICOUTIMI

THESIS SUBMITTED TO THE

UNIVERSITY OF QUEBEC AT CHICOUTIMI

IN PARTIAL FULFILLMENT OF

THE REQUIREMENTS FOR THE DEGREE OF

DOCTOR OF PHILOSOPHY IN ENGINEERING

BY

EHAB A. ELSHARKAWI

EFFECTS OF METALLURGICAL PARAMETERS ON THE DECOMPOSITION OF π-AlFeMgSi PHASE IN AL-SI-MG ALLOYS AND ITS INFLUENCE ON THE MECHANICAL PROPERTIES

JUNE 2011

UNIVERSITÉ DU QUÉBEC À CHICOUTIMI

THÈSE PRÉSENTÉ À

L'UNIVERSITÉ DU QUÉBEC À CHICOUTIMI

COMME EXIGENCE PARTIELLE

DU DOCTORAT EN INGÉNIERIE

PAR

EHAB A. ELSHARKAWI

EFFETS DES PARAMETRES MÉTALLURGIQUES SUR LA DECOMPOSITION
DE LA PHASE π-AlFeMgSi DANS LES ALLIAGES AL-SI-MG ET SON
INFLUENCE SUR LES PROPRIÉTÉS MÉCANIQUES

JUIN 2011

This thesis is dedicated to the memory of my parents.

RÉSUMÉ

La formation de la phase intermétallique de fer π-AlFeMgSi dans les alliages Al-Si-Mg est connue pour son effet néfaste sur la ductilité et la résistance, elle est contrôlée par la teneur en Mg et en Fe de l'alliage, ainsi que par la vitesse de solidification. La présente étude a été réalisée en vue d'enquêter sur tous les paramètres métallurgiques affectent la formation des phases intermétalliques π de fer, et à son tour, le rôle de la phase π en ce qui concerne les propriétés de traction et d'impact des alliages Al-Si-Mg. Les paramètres étudiés incluent la teneur en Mg et en Fe, l'addition de Be, la vitesse de refroidissement, la modification au Sr ainsi que les durées des mises en solution. Une parfaite compréhension de ces paramètres et de leurs effets sur la composition de la phase π des intermétalliques de fer permettra d'élargir la base de données disponibles concernant la formation de cette phase et des méthodes requises pour réduire ses effets négatifs en vue d'améliorer les propriétés mécaniques des alliages Al-Si-Mg.

l'évaluation microstructurale a été réalisée au moyen de la métallographie quantitative en utilisant la microsonde électronique (EPMA) et la microscopie électronique à balayage (MEB). Les résultats indiquent que l'augmentation du Mg ainsi que du Fe augmente la quantité de phase π-AlMgFeSi formée. Tous les alliages contenant de faibles niveaux de fer, peu importe la teneur en Mg montrent de faible quantité de phase π d'intermétalliques de fer. L'ajout de traces de Be a un effet observable dans la réduction du nombre de phase π formé dans tous les alliages étudiés. Les particules de la phase π d'intermétalliques de Fe semblent s'être ségrégées loin du Si modifié dans les alliages modifiés au Sr, en particulier ceux qui se solidifie à une vitesse de refroidissement faible.

L'effets des différents temps de mise en solution sur la décomposition de la phase π ont été étudiées afin d'examiner comment ce type de décomposition affecte la chimie de la matrice elle-même. Après 8 heures de traitement thermique à une teneur de %Mg, la phase π a montré une décomposition complète sous forme d'aiguilles fines de phase β. La phase π, cependant, a montré une décomposition partielle en aiguilles de phase β à des niveaux

supérieur à 0,4%Mg. Ce type de décomposition a été examiné aux fins de cette étude sur de longues périodes de traitement de mise en solution dans des échantillons d'alliage Al-7%Si-0.55%Mg-0.1%Fe obtenus à différents taux de refroidissement afin d'évaluer le mécanisme de décomposition des phases π-β. Les résultats obtenus montrent que la fraction volumique de la phase π-AlFeMgSi diminue de manière significative en prolongeant la durée de mise en solution. Le montant le plus élevé de la phase β nouvellement formée a été observée dans l'intervalle des temps de mise en solution de 60 à 80 heures. Une analyse de la composition chimique de la matrice à l'aide de la spectroscopie dispersive en longueur d'onde (WDS) à différents stades de mise en solution a révélé que la décomposition de la phase π-β au cours du traitement thermique résultats d'une nette augmentation de la teneur en Mg dans la matrice. Par ailleurs, aucun changement n'a été observé dans les stœchiométries calculées des phases intermétalliques π et β au cours du traitement thermique pour tous les échantillons des alliages étudiés.

L'étude a également étudié la décomposition de π-AlFeMgSi en aiguilles de phase β au cours de longues périodes de traitement thermique et ses effets sur les propriétés mécaniques des alliages Al-7%Si-0.55%Mg-0.1%Fe. Les résultats obtenus à partir des valeurs calculées de l'indice de qualité montre que le temps de mise en solution optimale pour les alliages modifiés au Sr est de l'ordre de 12 heures. Une utilisation prolongée de la durée de mise en solution conduit à la décomposition d'une grande quantité de la phase π en aiguilles de phase β, environ 85%, ce qui permet une légère amélioration des propriétés de traction à 80 heures par rapport au traitement standard. Cette amélioration peut être attribuée à l'augmentation du taux de Mg dans la matrice résultant de la décomposition de la phase π, et qui est alors disponible pour la précipitation du Mg_2Si lors du vieillissement ultérieur.

Une analyse des résultats obtenus à partir des essais de Charpy en utilisant des échantillons non entaillés montre que la plus grande amélioration dans les énergies d'initiation et de propagation est obtenue pour les alliages tels que coulés et traités thermiquement lorsque ces alliages sont solidifiées à une vitesse de refroidissement faible

et modifié avec du strontium. Une augmentation du temps de mise en solution améliore les propriétés d'impact des alliages par rapport à l'état tel que coulé. Conformément à cette constatation, le temps recommandé de mise en solution pour obtenir une énergie d'initiation et de propagation maximale est de 20 heures pour tous les alliages étudiés. Les résultats montrent également que les propriétés d'impact sont plus sensibles aux changements qui surviennent dans la microstructure qui résultent de la mise en solution et de la modification au Sr, à savoir, la morphologie du Si eutectique et de la phase π, plutôt que ceux liés aux propriétés de traction, à savoir, à la teneur en Mg dans la matrice.

L'analyse de la fracture a été réalisée en utilisant un microscope à balayage électronique équipé d'un système d'analyse d'élément EDX. Les résultats obtenus montrent que le comportement à la rupture lors des essais de traction et d'impact des alliages Al-7%Si-0.55%Mg-0.1%Fe sont contrôlés principalement par la morphologie du silicium eutectique. Les intermétalliques de fer de phase π agissent en tant que sites d'initiation de fissures et fournissent un chemin facile pour la propagation des fissures dans les deux alliages, non-modifiés et modifiés au strontium. L'analyse de la fracture de l'échantillon traité pendant 80 heures montre la présence d'aiguilles de phase β nouvellement formées qui fournissent une source supplémentaire pour l'initiation de la fissure, et donc tous les alliages traités pendant 80 heures présentent les valeurs d'énergie les plus bases.

ABSTRACT

The formation of the π-AlFeMgSi iron intermetallic phase in Al-Si-Mg alloys is known for its detrimental effect on ductility and strength, in that it is controlled by the Fe and Mg content of the alloy, as well as by the cooling rate. The current study was carried out with a view to investigating all the metallurgical parameters affecting the formation of the π-phase iron intermetallic and, in turn, the role of the π-phase as it relates to the tensile and impact properties of Al-Si-Mg alloys. The parameters investigated include Mg content, Fe content, Be addition, cooling rate, Sr modification, and solution heat treatment time. A full understanding of these parameters and their effect on π-phase iron intermetallics will widen the background data available concerning the formation of this phase and the methods required to reduce its detrimental effect with a view to improving the mechanical properties of Al-Si-Mg alloys.

Microstructural assessment was carried out by means of quantitative metallography using electron probe microanalysis (EPMA) and scanning electron microscopy (SEM). The results indicate that increasing the Mg and Fe content increases the amount of the π-AlMgFeSi phase formed. All the alloys containing low levels of iron regardless of the amount of Mg-content show low amounts of π-phase iron intermetallic. The addition of trace amounts of Be has an observable effect in reducing the amount of the π-phase formed in all the alloys studied. The π-phase iron intermetallic particles appear to be segregated away from the modified Si in the Sr-modified alloys, particularly those solidified at a low cooling rate.

The effects of different solution treatment times on the decomposition of the π-phase were investigated in order to examine how this type of decomposition affected the chemistry of the matrix itself. After 8 hours of solution heat treatment and at Mg content of 0.4wt%, the π-phase showed complete decomposition into fine β-phase needles. The π-phase, however, showed only partial decomposition into β-AlFeSi phase needles at Mg levels of over 0.4%wt. This type of decomposition was examined for the purposes of this study over

extended periods of solution heat treatment time in Al-7Si-0.55Mg-0.1Fe alloy samples obtained at different cooling rates in order to evaluate the mechanism of π- to β-phase decomposition. The results obtained show that the volume fraction of π-AlFeMgSi phase decreases significantly at prolonged solution treatment times. The highest amount of the newly-formed β-phase was observed in the solution treatment time range of 60 to 80 hours. An analysis of the chemical composition of the matrix using wavelength-dispersive spectroscopy (WDS) at different stages of solution heat treatment revealed that the π- to β- phase decomposition during solution heat treatment results in a distinct increase in the Mg content of the matrix. Furthermore, no changes were observed in the calculated stoichiometries of the π-phase or the β-phase intermetallics during solution treatment in all the alloy samples studied.

The study also investigated the decomposition of π-AlFeMgSi into β-phase needles during extended periods of solution heat treatment and its effects on the mechanical properties of Al-7Si-0.55Mg-0.1Fe alloys. The results obtained from the calculated quality index values show that the optimum solution treatment time for Sr-modified alloys is of the order of 12 hours. Using prolonged solution treatment time leads to the decomposition of a large amount of π-phase into β-phase needles, approximately 85%, thereby providing a slight improvement in the tensile properties at 80 hrs compared to standard heat treatment times; this improvement may be attributed to the increased amount of Mg in the matrix resulting from the decomposition of the π-phase, and which is then available for precipitation as Mg_2Si upon subsequent aging.

An analysis of the results obtained from the Charpy impact test using unnotched samples shows that the greatest improvement in the initiation and propagation energies is obtained for the as-cast and heat-treated alloys when these alloys are solidified at a low cooling rate and modified with strontium. An increase in the solution treatment time improves the impact properties of the alloys compared to the as-cast condition. In accordance with this finding, the recommended solution treatment time at which the maximum initiation and propagation energy values can be obtained is 20 hours for all alloys studied. The results

ix

also show that the impact properties are more sensitive to the changes occurring in the microstructure which result from solution heat treatment and Sr modification, namely, the eutectic Si and π-phase morphologies, rather than those related to the tensile properties i.e., to the Mg content in the matrix.

Fracture analysis was carried out using a scanning electron microscope equipped with an EDX system for element analysis. The results obtained show that the tensile and impact fracture behavior of the Al-7Si-0.55Mg-0.1Fe alloys are controlled mainly by the morphology of eutectic silicon. The π-phase iron intermetallics act as crack initiation sites and provide an easy path for crack propagation in both non-modified and Sr-modified alloys. The fracture analysis of the 80-hr solution-treated sample shows the presence of newly formed β-phase needles which provide an additional source for crack initiation, and thus all the 80-hr solution-treated alloys show the lowest energy values.

ACKNOWLEDGMENTS

TABLE OF CONTENTS

LIST OF FIGURES

CHAPTER 3

CHAPTER 4

CHAPTER 5

LIST OF TABLES

CHAPTER 1

INTRODUCTION

CHAPTER 1

INTRODUCTION

1.1   Defining the Problem

The automotive and aerospace fields are rapidly growing areas of interest for the application of Al-7Si-Mg casting alloys. Much research has been conducted with a view to increasing the strength of these commercially popular alloys. The mechanical properties of such alloys are strongly affected by the nature of the iron intermetallics existing in the structure. When iron is added to Al-7%Si-Mg alloys, it forms a platelet-like β-Al$_5$FeSi iron-intermetallic phase, or β-phase, having sharp edges. The high stress concentrations at these sharp edges enhance crack initiation and thus decrease the ductility of the castings.[1] In the case where Mg is present, the π-AlFeMgSi iron-intermetallic phase, or π-phase, forms.

Magnesium is added to Al-7Si-Mg alloys to promote the formation of the Mg$_2$Si phase which precipitates during aging, hardens the alloy and, consequently, improves the tensile strength.[2,3] Increasing the magnesium content beyond 0.45wt% in the Al-7Si-Mg alloys results in an increase in the matrix strength after the application of heat treatment. Moreover, the volume fraction of the iron-rich intermetallics in such alloys is larger than it is in 356 alloys containing 0.45wt% Mg as a result of the formation of larger amounts of the π-AlFeMgSi iron-intermetallic phase.[4,5] The stability of the π-phase in 357 alloys after

applying the standard heat treatment causes a reduction in the amount of free Mg, found in solid solution, which is available for forming Mg_2Si precipitates during the aging step. The strength of this kind of alloy is thus lower than expected, leading to the saturation of the UTS and YS values.[6, 7] The presence of the π-phase iron intermetallic and Si particles has a significant effect by reducing the ductility of 357 alloys.[8,3] Heat treatment of Al-7Si-Mg alloys is carried out to obtain an optimum combination of strength and ductility. Solution heat treatment results in the dissolution of Mg_2Si particles, the homogenization of the casting, and a transformation of the eutectic silicon morphology by fragmentation and spheroidization; also the dissolution or decomposition of the π-phase iron rich intermetallic may be observed.[4, 9, 10] Alloy composition, solidification rate, and solution heat treatment are the main parameters which closely affect the formation and dissolution of the π-phase and consequently the mechanical properties of Al-7Si-Mg alloys.

It becomes clear that reducing the π-phase iron intermetallic is highly recommended since it has the aim of improving the strength and ductility of 357 alloys. In this regard, it should be mentioned that, to date, the formation of the π-phase has usually been suppressed by the addition of beryllium. In view of the fact that beryllium poses health hazards, however, its use is not to be recommended. Other means must, therefore, be required to reduce the amount of the π-phase by dissolution or by decomposition into another less detrimental phase in the Al-7Si-Mg alloys with the intention of improving strength and ductility. There are very limited and mixed studies concerning the stability of π-phase during heat treatment and its effect on the mechanical properties, as well as the factors controlling the formation of this phase in Al-7Si-Mg alloys. It is believed that the data

collected in this comprehensive study will help to block the existing gap in the literature in this area.

1.2   Objectives

This study was carried out for the purpose of developing a fundamental understanding of the effects that metallurgical parameters will have on the microstructural constituents of Al-7Si-Mg alloys. Far more emphasis than hitherto will be placed on the formation of the π-phase iron intermetallic compound and on the changes observed in its morphology in Be-free and Be-containing Al-7Si-Mg alloys, and how this phase could affect on the mechanical properties of such alloys . This aim will be accomplished by fulfilling the following objectives.

1- Understanding the role of iron, magnesium, and beryllium, as well as the interaction between them, on the microstructural constituents and in the formation of the iron-intermetallic π-phase in Al-7Si-Mg alloys.

2- Studying the effects of solution heat treatment time and of solidification rates on the amount and the morphological changes of the π-phase iron intermetallic observed in non-modified and Sr-modified 357 alloys.

3- Correlating the results obtained from the impact and tensile tests with the earlier microstructural characterization so as to determine the effects of the changes in the

morphology of the π-phase after application of heat treatments on the mechanical properties of non-modified and Sr-modified 357 alloys.

4- Examining the role of the π-phase iron intermetallic and Si-particles on the fracture behaviour of as-cast and T6-aged non-modified and Sr-modified 357 alloys.

CHAPTER 2

REVIEW OF THE LITERATURE

CHAPTER 2

REVIEW OF THE LITERATURE

2.1   Introduction

The main reason for which aluminum-silicon alloys have become vital in various industrial applications is that they present a combination of positive factors including their light weight in conjunction with a number of favourable physical and mechanical properties. The presence of silicon with aluminum imparts high fluidity to the alloy, with good feedability characteristics, low shrinkage, and satisfactory crack resistance.[11,12] The silicon content of standardized commercial aluminum-silicon casting alloys is in the range 5 to 23 wt%; the alloys are classified as hypoeutectic (5-10 wt%), eutectic (11.7%Si), or hypereutectic (above 13%Si). The properties of a specific alloy may be attributed to the individual physical properties of its main phase components, namely α-aluminum solid solution, iron intermetallic volume fraction, and the morphology of the silicon particles.

The addition of magnesium to aluminum-silicon alloys creates an extremely important and useful family of compositions which combines outstanding casting characteristics with excellent properties after heat treatment. Corrosion resistance also is high, while a low level of thermal expansion is maintained.[9] The most commonly known of the Al-Si-Mg group are the 356 and A357 alloys, both of which contain 7 wt% Si but have

different Mg levels of approximately 0.45 wt% and 0.7 wt% Mg, respectively. Alloys 356 and 357 have been widely used for automotive and aerospace applications requiring the highest strength with reasonable ductility. A357 alloys also contain a small amount of beryllium which is added in order to improve strength and ductility through its effect on the morphology and chemistry of the β-phase iron-containing intermetallic.[13]

The solid solubility of iron in molten aluminum is about 0.03-0.05 wt% at the eutectic temperature of 655°C. Thus, most of the iron present above this level appears in the form of iron intermetallic phases. When iron combines with Al and Si, it forms a β-Al$_5$FeSi intermetallic phase displaying a platelet-like shape. In the case where Mg is present, another intermetallic tends to form and is called the π-phase whereby Al$_9$FeMg$_3$Si$_5$ may be produced. Experimental studies have demonstrated that the formation of iron intermetallic compounds is influenced by alloy composition as well as by the cooling rate. Iron intermetallic phases have a crystal structure which differs from that of aluminum; normally they have high hardness and strength values, with low plasticity compared to the Al-matrix. Thus, iron intermetallic phases appear to have a significant effect on Al-Si-Mg alloys by reducing strength values and ductility.[8,10,14] It is thus essential to acquire an understanding of the factors which affect the formation and dissolution of this type of iron intermetallic compound in order to understand the concepts involved in improving the mechanical properties of Al-7Si-Mg alloys. This aim forms the basis of the current chapter.

2.2   Iron Intermetallic Phases in Al-7Si-Mg Alloys

2.2.1   Formation of Iron Intermetallics in Al-Si-Mg Alloys

Bäckerud et al.[15] reported that the main reactions to be observed in the Al-7Si-0.56Mg alloy containing 0.14wt%Fe are (i) the formation of primary α-Al dendrites, (ii) the formation of the Al-Si eutectic along with β-phase iron-intermetallic, and (iii) the formation of secondary eutectic phases, as may be seen in Table 2.1. The cooling curve and its first derivative are shown in Figure 2.1. It will be observed that there are two possible reactions required for the formation of the π-phase: the first is a result of the transformation of the β-Al$_5$FeSi phase into the π-phase through a peritectic reaction, as will be found listed under Reaction 3b in Table 2.1; the second, on the other hand, forms as a result of the quaternary eutectic reaction occurring at the end of the solidification sequence, as listed under Reaction 5. The general microstructure of Al-7%Si-Mg alloys consists of (i) primary α-Al; (ii) Mg$_2$Si displaying Chinese script morphology; (iii) β-phase (Al$_5$FeSi) with its plate-like morphology; and (iv) the script-like π-phase (Al$_8$FeMg$_3$Si$_6$), as shown in Figure 2.2.

Table 2.1 Reactions expected to occur in A357.2 alloys.[15]

Reaction No.	Reaction	Temperature (^{o}C)
1	Dendritic network	611
2a	L $\rightarrow$ Al + Si	577
3a	L $\rightarrow$ Al + Si +Al$_5$FeSi	575
3b	L + Al$_5$FeSi $\rightarrow$ Al + Si + Al$_8$Mg$_3$FeSi$_6$	567
4	L $\rightarrow$ Al + Mg$_2$Si + Si	555
5	L $\rightarrow$ Al + Si +Mg$_2$Si + Al$_8$Mg$_3$FeSi$_6$	550
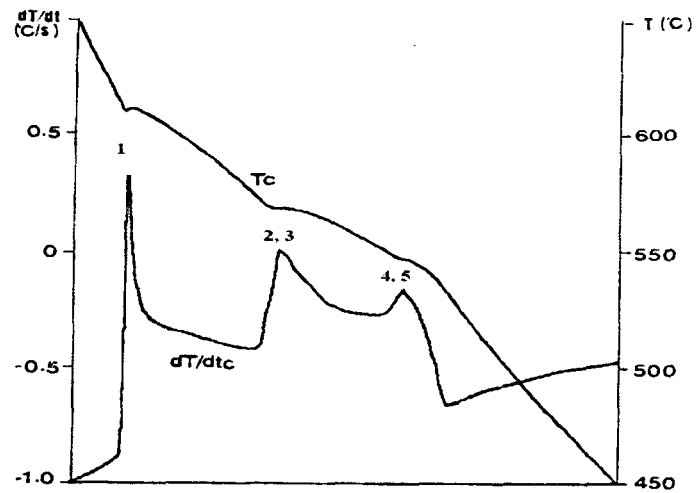
Figure 2.1 Cooling curve and its derivative for alloy A357.2.[15]
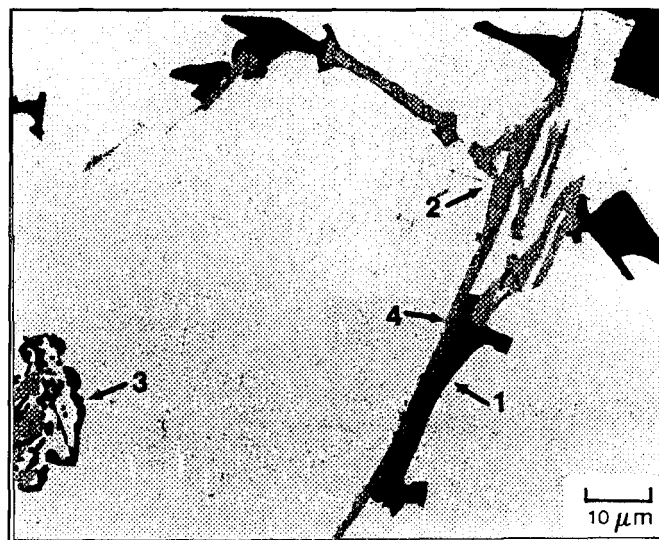
Figure 2.2 Optical micrograph of non-modified 357 alloy: (1) eutectic silicon, (2) $Al_8Mg_3FeSi_6$ Chinese script, (3) Mg_2Si Chinese script, and (4) Al_5FeSi needles.[15]

2.2.2   Composition and Morphology of β and π Iron Intermetallic Phases

Phragmén[16] reported that the composition of the β-Al$_5$FeSi phase is 27% Fe and 13.5% Si; this β-phase has a monoclinic structure with the parameters a = b = 6.12 A°, c = 41.5 A°, and a density of 3.30-3.35 g/cm^3, appearing in the form of thin platelets or needles in the microstructure. The β-Al$_5$FeSi phase grows in a lateral or faceted mode and contains multiple (001) growth twins parallel to the growth direction.[17] The possible morphology of β-Al$_5$FeSi is shown in Figure 2.2. The first suggestion of the stoichiometry of the π-phase by Foss et al.[18] was Al$_9$FeMg$_3$Si$_5$; this stoichiometry deviates from the Al$_8$FeMg$_3$Si$_6$ suggested by others. The π-phase is a quaternary phase having a script-like morphology often linked with β-Al$_5$FeSi.[20] The chemical composition of this phase is 10.9% Fe, 32.9% Si, and 14.1% Mg, with lattice parameters of a = 0.663 nm, c = 0.794 nm, and a density of 2.82 g/cm^3. Figure 2.3 shows the only two possible morphologies for the π-phase.[19, 20, 21, 22]
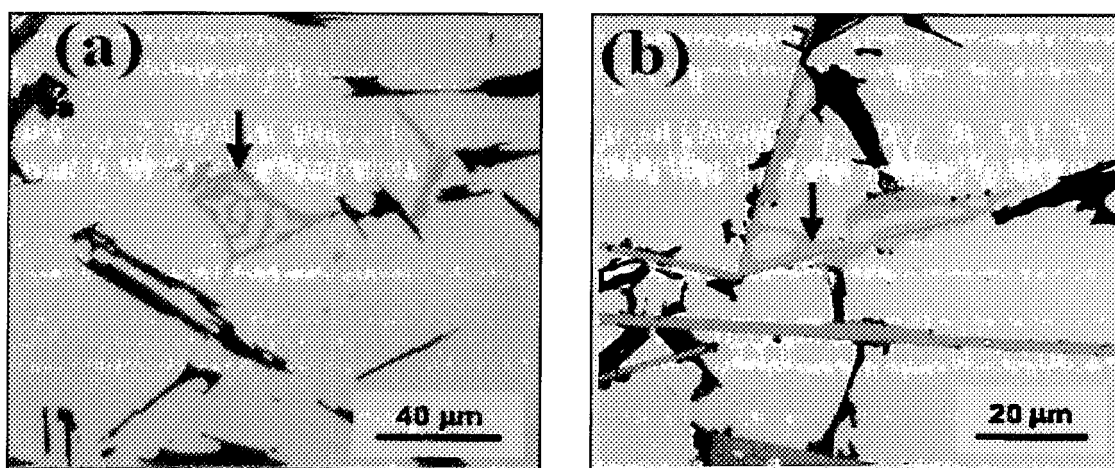
Figure 2.3 Microstructure of alloy Al-5Si-1Cu-0.5Mg showing the two possible types of π-Al$_8$Mg$_3$FeSi$_6$ morphologies; (a) Chinese script-like morphology, and (b) π-phase connected with β-Al$_5$FeSi.[22]

2.3   Factors Affecting the Formation of Iron Intermetallic Phases

2.3.1   Effects of Iron Content

It has been observed that increasing the level of iron in Al-7Si-Mg alloys increases the number and size of β and π intermetallic phases.[23, 24] Lu *et al.*[25] reported that increasing the iron level from 0.3 to 0.7 wt% causes a major change in the precipitation sequence of the β-phase. At low iron levels, the β-phase forms at lower temperatures through the ternary eutectic reaction displaying a small needle-like morphology. At high iron levels, most of the β-phase will precipitate at a high temperature prior to the eutectic and has a large-size platelet-like morphology. These large β-phase Al_5FeSi platelet sizes tend to prevent the flow of liquid metal during solidification, thereby reducing casting soundness.[26, 27]

Tang *et al.*[17] studied the effects of increasing the iron from 0.3 to 0.6 wt% at different cooling rates in Al-7Si alloys; they found that the average length of the β-platelets increases with an increase in iron content. This study was in full agreement with the findings of Vorren *et al.*[28] who measured the maximum length of the β-phase as a function of secondary dendrite arm spacing and iron content for 356 alloys. Results obtained by these authors indicate that there is a variation in the formation mechanism or growth rate of β-plates as a result of changing the iron content and solidification rate, as can be seen in Figure 2.4. A further study was carried out by Musmar[29] on the effects of iron content on the formation temperature of the β-phase using two different techniques of thermal
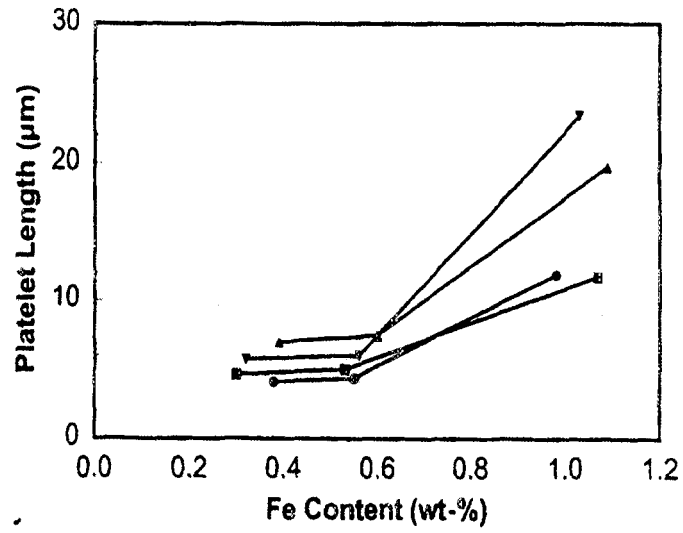
Figure 2.4 Effects of increasing iron content on length of β-Al$_5$FeSi phase.[28]
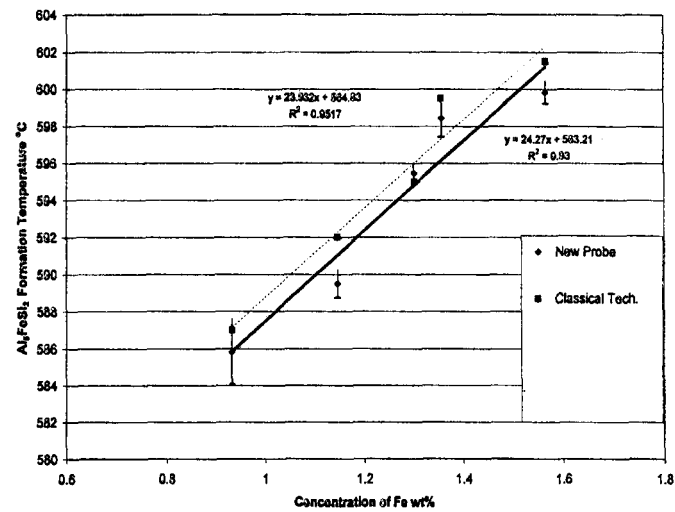
Figure 2.5 Temperature at which β-Al$_5$FeSi phase forms with regard to different levels of iron content.[29]

analysis; his findings showed that as the iron levels increase from 0.93 to 1.6 wt%, the temperature at which the β-phase forms also increases, as shown in Figure 2.5. Taylor *et al.*[30] studied the effects of Fe content on the volume fraction of the three intermetallic phases, Mg_2Si, β, and π for the as-cast Al-7Si-0.4Mg alloy; they found that all the intermetallic phases appear to increase with the Fe content, as shown in Figure 2.6 which illustrates that the dominant phase in all of the as-cast alloys studied is the π-phase.
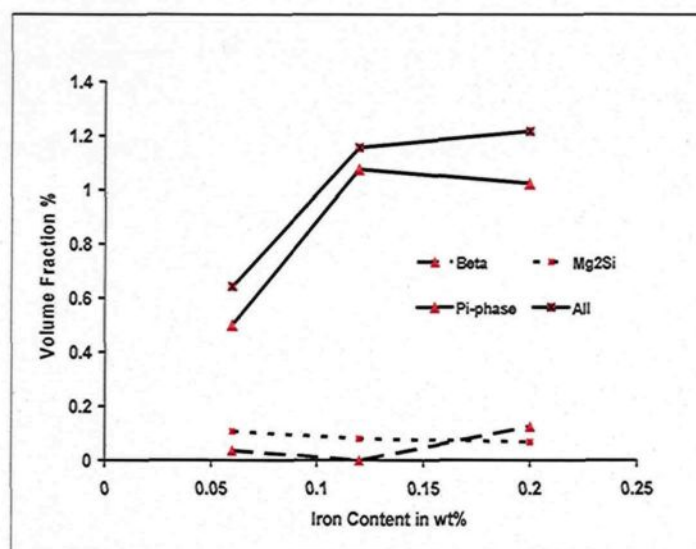
Figure 2.6 Volume fraction of the Mg_2Si, β and π phases present in the as-cast Al-7Si-xMg-0.12%Fe alloy.[30]

2.3.2 Effects of Magnesium Content

Cáceres *et al.*[31] studied the microstructure behavior of two Al-7Si-Mg casting alloys, having a magnesium content of either 0.4 or 0.7 wt% each. They observed that the iron intermetallic phases in high magnesium content alloys are larger than they are in alloys containing low levels of magnesium, and that the iron rich intermetallic phases in low Mg

alloys were exclusively small β-phase plates, while large π-phase ($Al_9FeMg_3Si_5$) particles were dominant in high-Mg alloys with a small proportion of the β-phase, as shown in Table 2.2.

Bäckerud et al.[15] studied the solidification characteristics of three types of Al-7Si-Mg casting alloys at three different cooling rates; they observed that the addition of Mg changes the solidification sequence and the type of iron intermetallic phase formed in this particular type of alloy. Taylor et al.[30] investigated the effects of Mg content on the amounts of intermetallic phases formed in Al-7Si-0.21Fe-xMg cast alloys. The results reveal that the π-phase and β-phase volume fractions remain constant regardless of the Mg content, whereas the amount of Mg_2Si appears to increase generally, as shown in Figure 2.7. In their study on the mechanism of eutectic nucleation in hypoeutectic Al-Si alloys, Makhlouf and Shankar[32] reported that increasing the Mg content in the Al-14.5Si-0.22Fe alloy produces a significant change in the rheological characteristics of the melt, preventing the formation of the β-phase, which acts as a nucleating site for eutectic Si, by changing this phase into π-phase which is less effective in nucleating the Al-Si eutectic. Consequently, the eutectic Si particles become very fine.

Table 2.2 Volume fraction of iron rich intermetallics as a function of types of alloys.[31]

Alloy	**356**	**356+Sr**	**357**	**357+Sr**
Volume Fraction of Intermetallics (%)	0.52 ±0.03	0.53±0.01	1.46±0.06	1.34±0.04
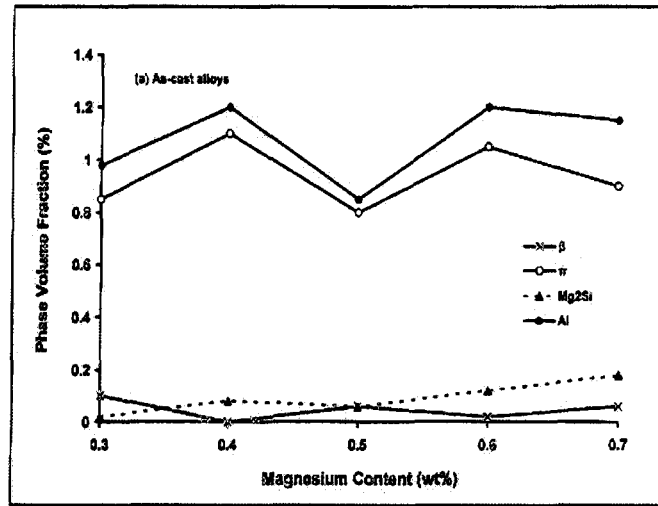
Figure 2.7 Volume fraction of Mg_2Si, β, and π phases in as-cast A-7Si-0.12Fe-xMg alloys as a function of Mg content.[30]

Samuel *et al.*[33] reported that the addition of Mg to molten 319-type alloys, in amounts of up to 0.5wt% leads to the precipitation of Mg_2Si and the $Al_8Mg_3FeSi_6$ phase. At magnesium contents of more than 1%, the volume fraction of the β-phase is reduced as a result of all the β-phase which had undergone transformation into the π-phase. This observation is in full agreement with another study carried out by Wang *et al.*[34] who reported that increasing the Mg content from 0.4 to 0.7 wt% in 357 alloys significantly increases the potential for the formation of the Mg-containing iron intermetallic $Al_8Mg_3FeSi_6$ phase.

2.3.3 Cooling Rate

Secondary Dendrite Arm Spacing (SDAS), defined as the distance between the protruding adjacent secondary arms of a dendrite, has been used in recent years to describe the metallurgical structure of cast materials. The smaller the SDAS value, the smaller the

size of defects such as segregation, microshrinkage, and gas porosity, which are detrimental to mechanical properties.[35] High cooling rate has a direct effect on reducing the quantities of β, π, and Mg_2Si intermetallic phases observed within the microstructure of Al-7Si-Mg alloys. A rapid solidification process can also be used to suppress the formation of some precipitates or otherwise modify their morphology.[36,37] Bäckerud et al.[15] stated that the type and morphology of the Fe-intermetallic phases in 356 and 357 alloys depend not only on alloy composition, but also on the cooling rate. Cáceres et al.[31] reported that the average size of Fe-intermetallics in 357 alloys is affected by the cooling rate in both unmodified and Sr-modified alloys, as shown in Figure 2.8. This observation was also confirmed by the findings of J. Barresi et al.[38]
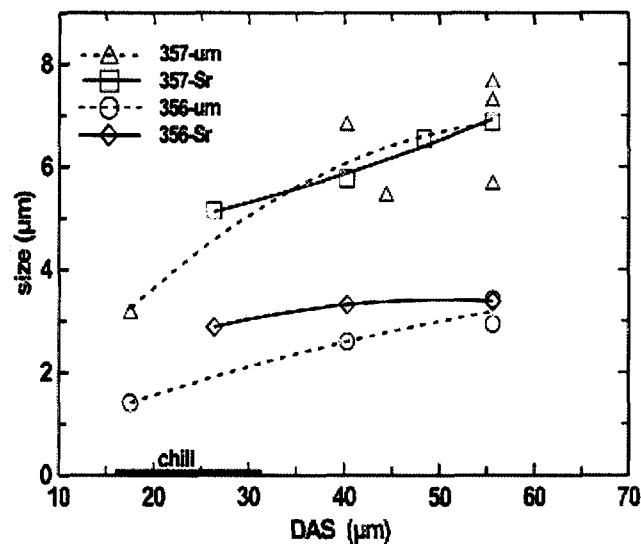
Figure 2.8 The average size of iron intermetallic particles as a function of DAS.[31]

Shabestari and Gruzleski[39] studied the effects of cooling rate on the formation and

morphology of intermetallic compounds in Al-12.7Si alloys containing 0.1%Cr with three

levels of iron (0.4%, 0.8%, 1.2%), and five different levels of manganese ranging from 0.0

to 0.5 %. According to these researchers, the morphology and volume fraction of all types

of intermetallics depend on the cooling rate, while the volume percentage of intermetallics

decreases significantly with an increasing cooling rate. The effects of cooling rate on the

morphology and the volume percent of intermetallic compounds in alloys containing 0.8%

Fe are shown in Figure 2.9.
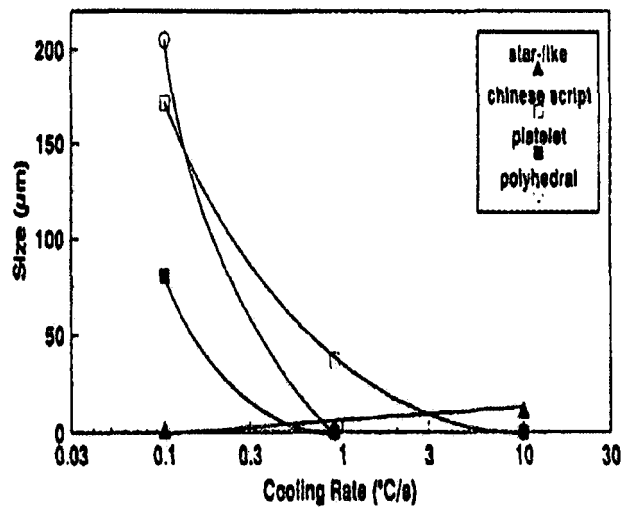
Figure 2.9 Effects of cooling rate on the volume percent of intermetallic at 0.8%Fe.[39]

A study was also carried out by Vorren et al.[28] with regard to the effects of

cooling rate on the length of the β-phase in Al-7Si-0.3Mg alloys; these researchers found

that, at specific levels of Fe content, there is a critical DAS value or cooling rate, at which

there is a variation in the formation mechanism or growth rate of the β-phase, and also

observed that the π-phase iron intermetallic was observed over the whole range of iron content and solidification rates. The size of the π-phase, however, was observed to be weakly dependent on the solidification rate. Gustafsson et al.[20] studied the effects of Fe, Cr, and solidification rate on the microstructure of Al-7%Si-xMg-yFe containing different levels of Mg and Fe. They observed that coarse π-phase and fine α-phase formed in all of the alloys investigated, whereas increasing the DAS from 20µm to 60µm results in an increase in the length of β- platelets at two different iron levels, namely 0.2 and 0.5wt %, as shown in Figure 2.10.
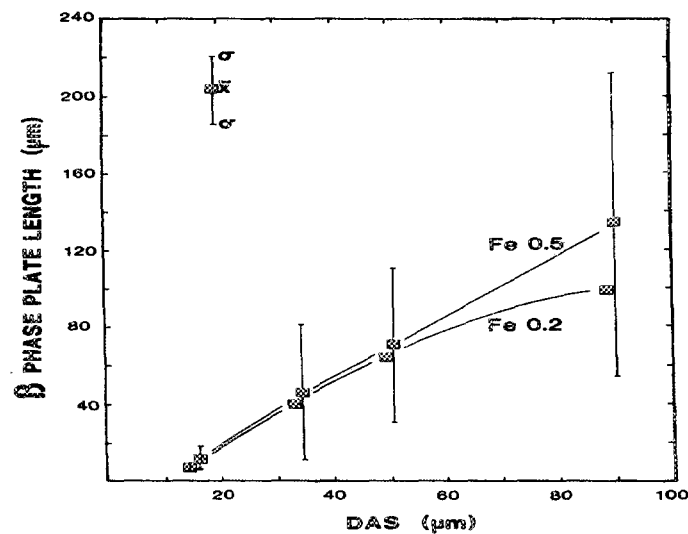
Figure 2.10 Length measurement of β-platelet in A356 alloys containing different iron levels.[20]

According to the literature in the field, it would appear that increasing the cooling rate has a considerable effect on the refining of all iron-intermetallic phases in Al-7Si-Mg alloys and can be considered one of the better techniques available for reducing the detrimental effects of iron intermetallics on the mechanical properties.

2.4   Mechanical Properties of Al-7Si-Mg Alloys

2.4.1   Effects of Size of Iron Intermetallic Phases

The size, shape, and volume fraction of the iron-intermetallic phases have a significant effect on the mechanical properties. Thus, the larger elongated particles are more detrimental to the mechanical properties than are the rounded particles.[40,41,42] Figures 2.11 (a) and (b) show the three-dimensional morphology of the β-platelets and the α-$Al_{12}(Fe,Mn)_3Si_2$ particles.[43]
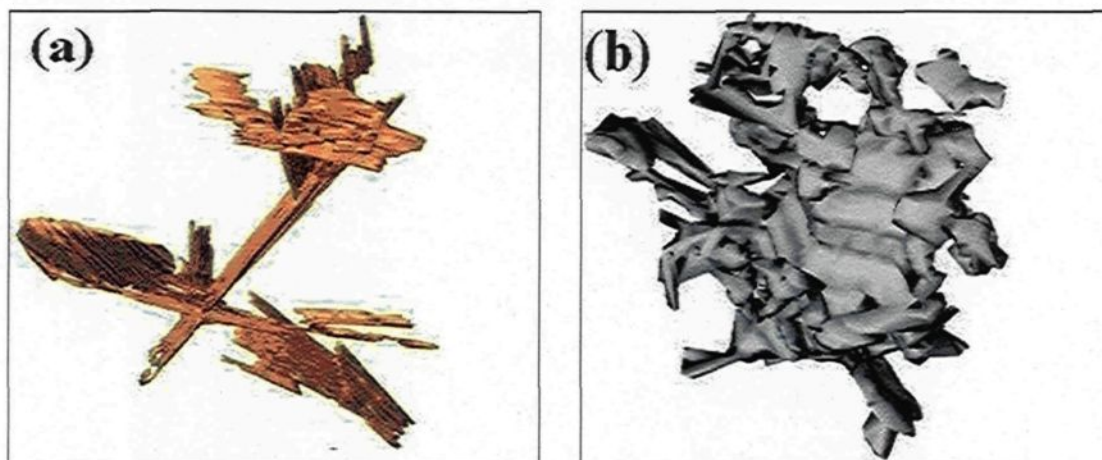
Figure 2.11 Three-dimensional reconstruction of (a) β-Al_5FeSi platelets; and (b) α-$Al_{15}(Fe,Mn)_3Si_2$ particle.[43]

The sharp edges and branching of the β-platelets make them more detrimental to the mechanical properties than the polyhedral structure of the α-phase. There have been numerous studies carried out to determine the reason for which β-phase intermetallic particles are detrimental to such a degree. Murali et al.[44] reported that the β-phase intermetallic is large in size, brittle, and having a high aspect ratio; such features will tend to promote the initiation and propagation of cracks throughout the matrix, thereby reducing

ductility. Wang *et al.*[34] reported that the detrimental effects to be observed with regard to the β-phase may be ascribed to the stress concentration at the sharp edges of the needles in the Al-matrix. Vorren *et al.*[28] explained that these detrimental effects may be attributable to the weak bonding between the β-phase and the matrix.

Wang *et al.*[34] also found that π-phase particle-cracking plays an important role in the reduction of the ductility of Sr-modified A357 alloys, while Ma *et al.*[45] observed that the π-phase iron intermetallic phases provide additional sources for crack initiation sites in the microstructure of 319 alloys, and hence for lower impact properties. The same authors studied the effects of β-phase size on the tensile properties and impact energy of non-modified and Sr-modified 356 alloys. They observed that there is a decrease in the tensile strength and impact energy with respect to an increase in the length of β-phase iron intermetallics, as there is also a rapid decrease in the tensile strength and impact energy occurring at smaller β-phase sizes, which would indicate that even the iron present in small amounts can cause deterioration of the tensile and impact properties, as can be shown in Figures2.12 (a) and (b). Based on earlier studies, it becomes clear that it is essential either to lower the levels of the iron content or to change the morphology of the β and π intermetallic phases in order to bring about an improvement in the mechanical properties.
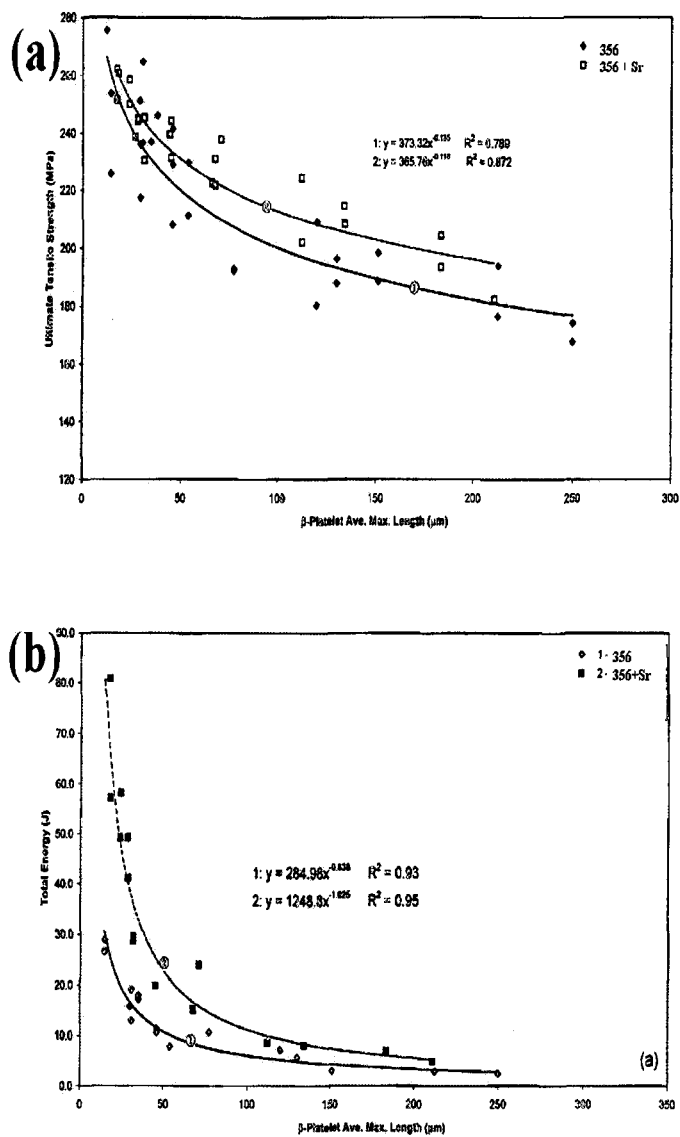
Figure 2.12 Effects of average length of β-platelet on (a) ultimate tensile stress; and (b) total impact energy.

2.4.2 Effects of Alloying Elements and Impurities

2.4.2.1 Fe Content

As described earlier in the previous section, the mechanical properties of cast aluminum alloys are commonly affected by iron content even in the case of very low amounts. Extensive literature on the subject has been published investigating the effects of Fe content on the mechanical properties of Al-Si alloys as a result of an increase in the iron intermetallic phases. These phases then increase the number of crack initiation sites, thus facilitate crack initiation and propagation through the matrix after the material has yielded. Consequently, ductility is observed to be more noticeably affected by an increase in the iron content than is the yield stress.[38, 46, 47]

Closset and Gruzleski[21] determined the effects of Fe on the Quality Index in A356 alloys, as shown in Figure 2.13. The results provided in this figure reveal the decreases in the Quality Index upon increasing the Fe content from 0.16 to 0.4%wt. The Quality Index was used extensively to relate the mechanical properties of Al-7Si-Mg alloys to different microstructural conditions; it can also be used as a tool for the design engineer to select the most favorable conditions which best fulfill the requirements of the components used for certain applications.[48,49,50] The concept of Quality Index (Q) was developed by Drouzy *et al.*[51], and is defined by the equation: $Q = UTS + d \, \text{Log} \, (\%El_f)$, where UTS , d, and $\%El_f$ stand for ultimate strength, empirical coefficient, and elongation to fracture, respectively. For Al-7Si-Mg alloys, the value of the empirical coefficient is 150 MPa. In this equation, the Quality (Q) is more sensitive to the ductility than to tensile strength, thus the effects of

the Fe content in reducing the quality values mainly results from reducing the ductility in

A356 alloys
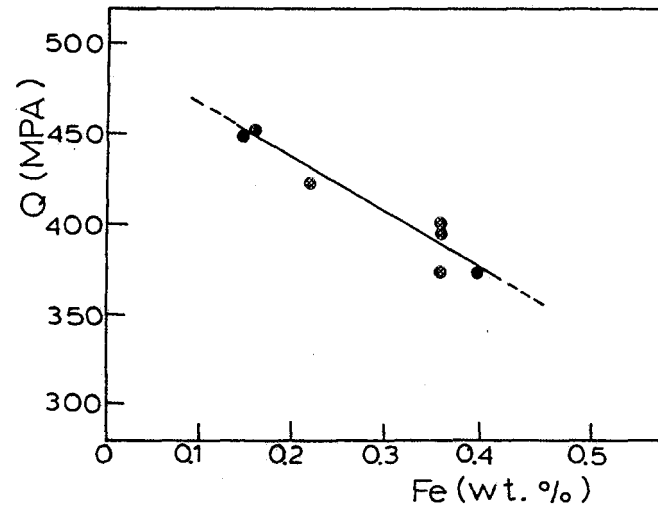
Figure 2.13 Variation of the quality index with Fe content.[21]

A significant decrease in the yield strength at Fe contents higher than 0.06%Fe, as

shown in Figure 2.14 have been observed by the Granger *et al.*[52] Similar results were

observed in a study carried out by Murali *et al.*[1, 44] regarding the effects of Fe content and

solidification rate on the tensile properties and impact toughness in 356 and 357 alloys. The

authors reported that as the iron content increases in 356 alloys from 0.2 to 0.8wt%, the

UTS and YS decrease significantly, by 20 and 18%, respectively, as shown in Figure 2.15;

also that there is a decrease of 66% observed in the total impact energy in 357 alloys, as

will be seen in Figure 2.16.
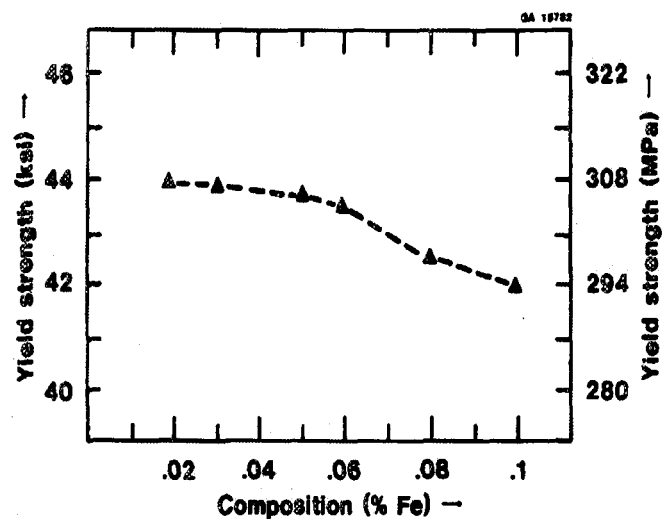
Figure 2.14 Effect of Fe on the yield strength in an A357 alloy.[52]
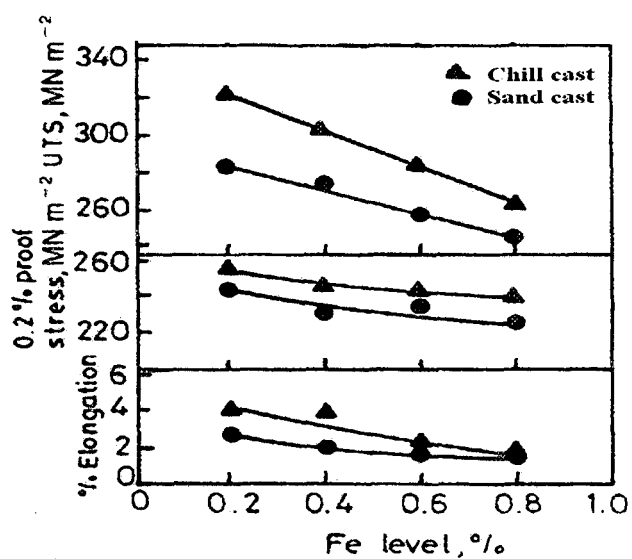
Figure 2.15 Effects of Fe impurity on the mechanical properties of 356 alloys.[44]
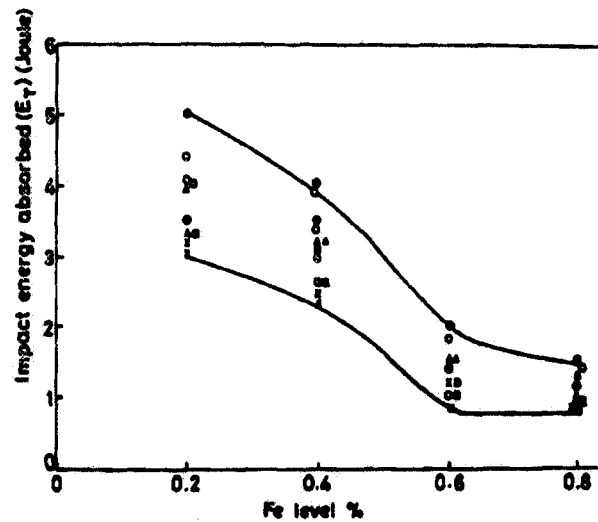
Figure 2.16   Effects of Fe content and solidification rate on the total impact energy for 357 alloys.[44]

Similar results were reported in research carried out by Tsukuda et al.[53,54] who found that an increase in the iron-content from 0.02 to 2 wt % decreases the impact strength of the as-cast and T6 heat-treated permanent mold Al-7Si-0.23Mg-0.13Ti-0.005%Na alloy castings, as shown in Figure 2.17. Kaneko et al.[55] studied the influence of iron on the impact energy of squeeze-cast Al-7Si-0.3Mg alloys; the results reveal that an increase in the iron-content from 0.15 to 0.3 wt % results in a decrease in impact energy from 1.5 to 1.2 J/mm2.The authors proposed that the maximum iron-content for obtaining optimum mechanical properties should be 0.3 wt %. Results from another study carried out by Nagel et al.[56] on the effects of Fe, Mg, and heat treatment in permanent mold A357 castings, reveal that all of the mechanical properties clearly improve at a low iron content, namely 0.05 wt %. Thus, using low iron content is highly recommended with a view to improving the mechanical properties.
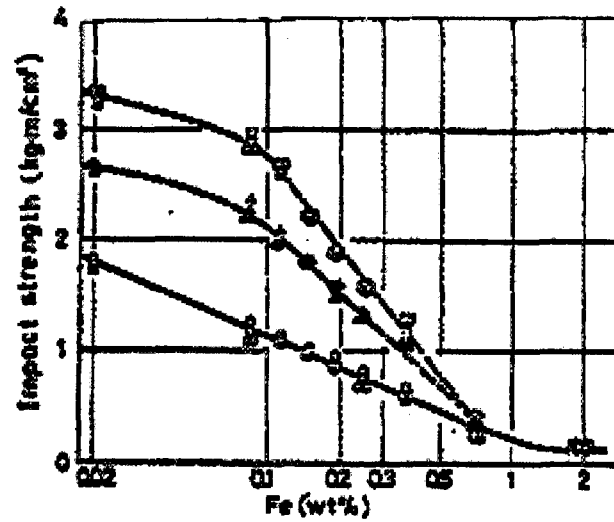
Figure 2.17 Effects of Fe on mechanical properties of T6 - Al-7%Si-0.23%Mg-0.13%Ti-0.005%Na alloy.[53]
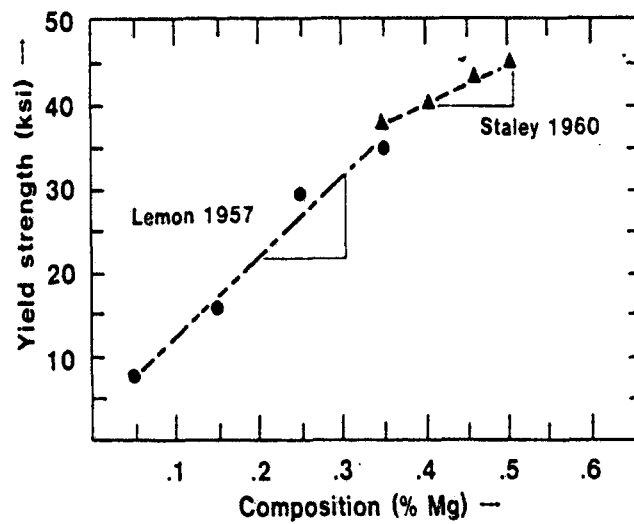
Figure 2.18 Effect of Mg on T6 yield strength in hypoeutectic Al-Si alloys[52]

2.4.2.2 Magnesium Content

The addition of magnesium allows the casting to be heat-treated, whereby magnesium silicate precipitates, which harden the alloy and impart a specific combination of strength and ductility. High magnesium levels increase the number of Mg_2Si precipitates which form during aging, thereby increasing the YS and the UTS of the material.[1,57,58] Granger and co-workers[52] pointed out that increasing the magnesium even in small amounts will result in an increase in the yield strength of Be-free Al-7Si-Mg alloys, as shown in Figure 2.18.

A study carried out by Cáceres et al.[31] on the effects of different Mg levels in the mechanical properties of Al-7Si-Mg alloys, plotted their data against data reported from other resources, as shown in Figure 2.19. The authors found that the yield stress increases linearly with $(Mg)^{1/2}$ and they also observed that the yield strength of the high Mg content alloys, as occurs in 357 alloys, is somewhat lower than predicted. The low yield strength for the high Mg alloys is due to the presence of the π-phase iron intermetallic, which in itself consumes large amounts of magnesium from the solid solution, thereby reducing the amount of Mg available to form Mg_2Si precipitates after ageing.[5, 59]

In support of the negative effects of the π-phase upon lowering the strength values of high Mg content Be-free 357 alloys, another study carried out by Mäller et al.[7] concerning the influence of magnesium content on the T6 tensile properties of A356 and
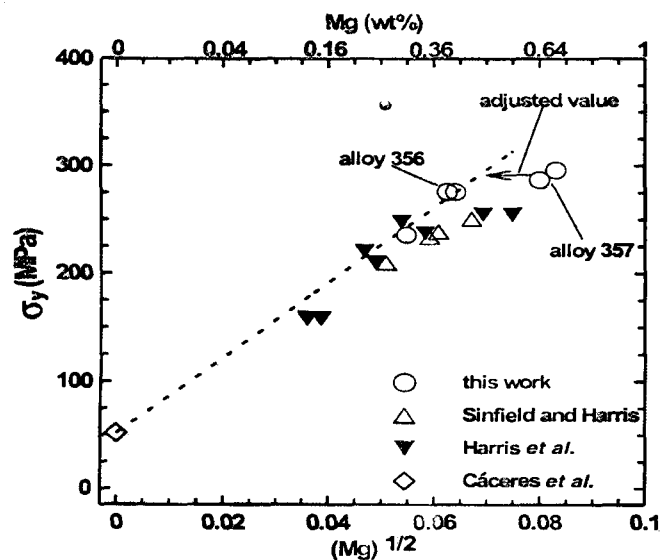
Figure 2.19 The yield stress as a function of Mg content.[31]
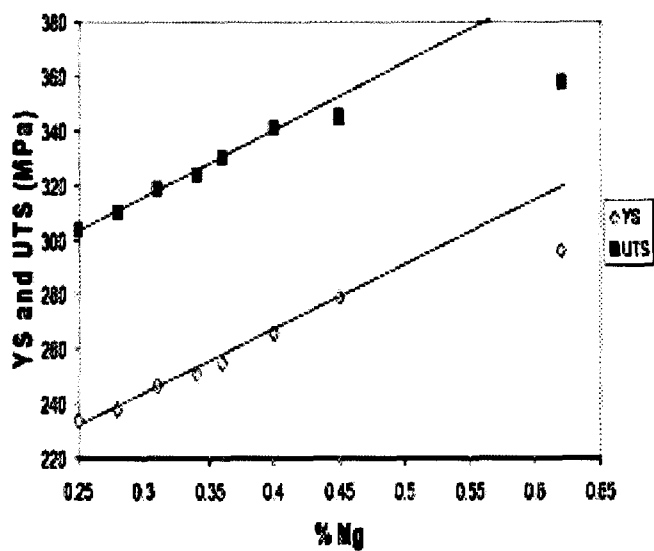
Figure 2.20 Yield strength and ultimate tensile strength of T6-A356 as a function of the bulk Mg concentration of the alloys.[7]

F357 alloys. The authors observed that increasing the Mg content from 0.25 to 0.45 wt% has a noticeable effect in increasing the UTS and YS, although increasing this content beyond 0.45wt% causes an increase in YS and UTS to less than expected values. The expected values were obtained, however, by a linear extrapolation of the strength of lower Mg content in A356 alloys to actual F357 Mg concentrations, as shown in Figure 2.20.It has been reported that increasing the yield strength and ultimate tensile strength usually accompanied by a decrease in the ductility especially in the presence of high levels of Mg as in 357 alloys;[3, 31, 34] this reduction has already been discussed and explained by a number of authors. Cáceres et al.[31] attributed such a reduction to the existence of the π-phase which is larger than the silicon particles in Sr-modified 357 alloys. In agreement with this study, Wang et al.[34] also reported that the fracture of π-phase particles plays an important role in the reduction of ductility, especially in Sr-modified 357 alloys.

Tsukuda et al.[53] investigated the effects of various levels of Mg content on the impact strength of as-cast and T6 Al-7Si alloys at various levels of Fe addition. These researchers observed that increasing the amount of Mg from 0.15 to 2.2 wt% led to a significant reduction in the impact strength values at all Fe levels, as can be seen in Figure 2.21. This reduction in the impact strength may be attributed to the formation of large amounts of β-and π-iron intermetallic phases especially at higher levels of Mg and Fe content.
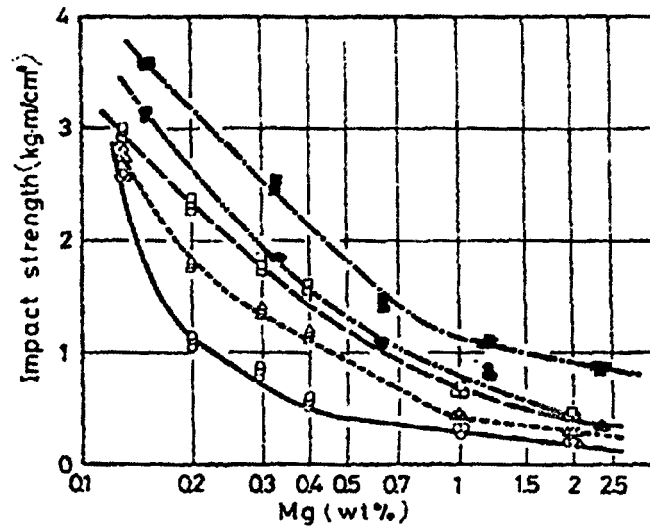
Figure 2.21 Effects of Mg on the mechanical properties of Al-7Si-0.006Fe-0.07Ti-0.005Na and Al-7Si-0.2Fe-0.13Ti-0.005Na T6-tempered permanent-mold casting.[53]

In their study of the effects of Mg, Fe, and solidification rate on the fracture toughness of Al-7Si-xMg-yFe, Murali *et al.*[44] observed that, at 0.2 wt% Fe for all the solidification rates studied, increasing the Mg content from 0.32 to 0.65 wt% causes a reduction in the total impact energy by about 50%. This reduction in the impact energy was attributed to the presence of the coarse β-phase in the microstructure which acts as a stress raiser and facilitates crack nucleation and propagation.[60]

2.4.2.3 Silicon Content

Several studies indicated that the morphology of the brittle Si particles, which precipitates out in the form of the excess silicon beyond the eutectic point during solidification have a significant effect on the mechanical properties of Al-Si alloys. Sharp-edged platelets of silicon, of an acicular structure, have a considerable effect in reducing the

tensile strength, ductility, and impact strength of as-cast Al-Si alloys.[61, 62, 63] Consequently, it becomes essential to change the morphology of Si particles in order to improve the mechanical properties of these alloys. Silicon particles become extremely fine if they are chemically treated by modifiers such as Na and Sr, or are otherwise thermally treated by solution heat treatment, as will be discussed in greater detail in subsequent sections.

Bayram and Uguz [64] studied the manner in which adding different Si levels to the non-modified and Na-modified Al-xSi-1.1Cu-0.9Mg-0.5Fe alloy might affect its mechanical properties. They observed that increasing the Si content from 5% to 11% causes an increase in the UTS in the case of the as-cast alloys while the Na-modified and heat-treated alloys display superior UTS values compared to the as-cast versions. This increase in the UTS may be attributed to the formation of Mg_2Si and Al_2Cu precipitates after application of the aging step. The same authors also observed that there is no effect to be observed resulting from an increase in the amount of Si content from 5 to 11 wt% acting upon the fracture toughness of notched Al-xSi-1.1Cu-0.9Mg-0.5Fe specimens. The fracture toughness is greatly affected by Si morphology, however; thus, as the Si particles become circular and finer through Na-modification, whether individually or in combination with heat treatment, the fracture toughness increases.

The previous study was found to be in full agreement with a study carried out by Tsukuda et al.[53] on the effects of different addition levels of Si, from 1-13 wt%, on the tensile strength values of as-cast and T6 Al-Si-0.03Mg-0.02Fe-0.15%Sb alloys; they observed that these values increase with increases the Si content The amount of elongation

to fracture, however, seems to be more negatively sensitive to the Si content in both as-cast

and T6 alloys, as shown in Figure 2.22.
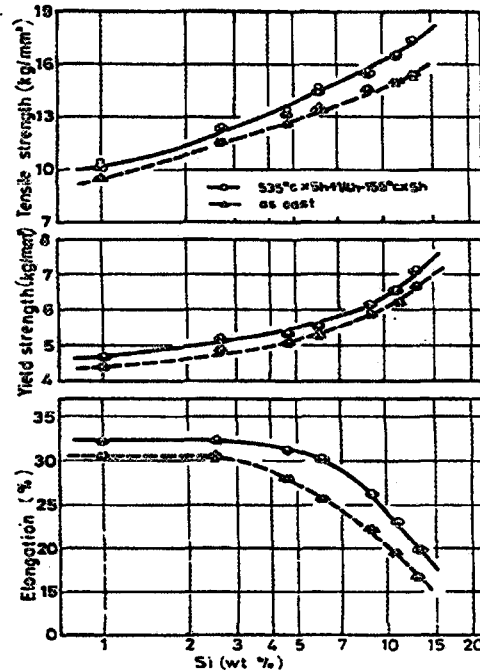
Figure 2.22 Effects of Si on mechanical properties of Al-Si-0.03Mg-0.02%Fe
-0.15%Sb.[53]

The same authors also studied the effects ensuing from an increase in the Si content

between 1 and 13 wt% with regard to the impact energy on the same alloys; they observed

a noticeable 84% reduction in the impact strength when the Si content increases from 2.5%

to 13 wt % for the as-cast and heat-treated alloys. The reason for the reduction in the impact

properties was attributed to the increase in the number of crack initiation sites resulted from

the increase in the silicon content.

Akira *et al.*[65], in their study on the tensile and impact properties of hypereutectic Al-Si alloy castings, obtained results indicated that increasing the Si-content of the alloy from 12 to 20%wt causes a noticeable decrease in the impact values, the tensile strength, the 0.2% proof stress, and the rupture elongation, as may be seen in Figure 2.23. The analysis of the fracture surface for broken samples reveals the cleavage fracture of coarse primary Si particles, as well as a number of fine dimples nucleated at the eutectic Si particles formed in the eutectic matrix. This observation implies that the presence of coarse primary Si particles in the hypereutectic has the effect of reducing the crack initiation resistance, thereby lessening the mechanical properties.
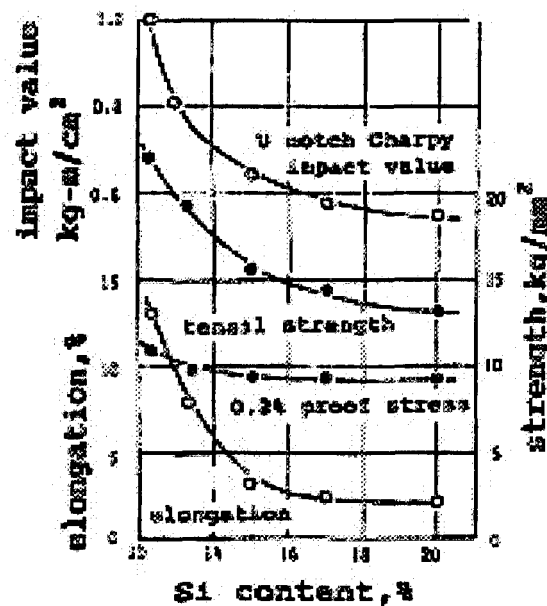
Figure 2.23 Relationship between Si content and the mechanical properties of hypereutectic Al-Si alloys.[65]

2.4.3 Modification

Modifiers are elements which are used mainly for transforming the morphology of the coarse acicular silicon in the eutectic structure of Al-Si alloys into a finer or more fibrous form in order to improve the mechanical properties. The most common modifying elements used are sodium and strontium, although recently the use of Sr has become more common than sodium.[66] The mechanism involved in the modification of the growth of the Si particles and the subsequent changes in its morphology has been described elsewhere.[19, 67] Modifiers can, however, also increase inclusion content in the melt through the formation of Sr oxides, as well as decrease the surface tension, and increase the freezing range of the alloys.[68, 69] Consequently, the addition of Sr is frequently associated with an increase in the amount of porosity.

In addition to the observable effects of Sr obtained when refining the coarse Si particles, it has also been reported that the iron intermetallic volume fraction is lower in the Sr-modified alloys compared to non-modified alloys. The lower volume fraction of the iron intermetallics in the Sr-modified alloys may be attributed to the effects of Sr modification on the fragmentation of iron intermetallics in the as-cast Al-Si alloys.[70] Peyman *et al.*[71] studied the influence of Sr addition on intermetallic compound morphologies in an Al-Si-Cu-Fe Cast alloy; they observed that the length and volume fraction of the β-phase decrease and that the number density of particles increases by means of adding 0.015 % Sr, as shown in Figures 2.24 (a) and (b). Thus, Sr proves to be an effective element in the modification and shortening of the needle-like β-intermetallic phase.
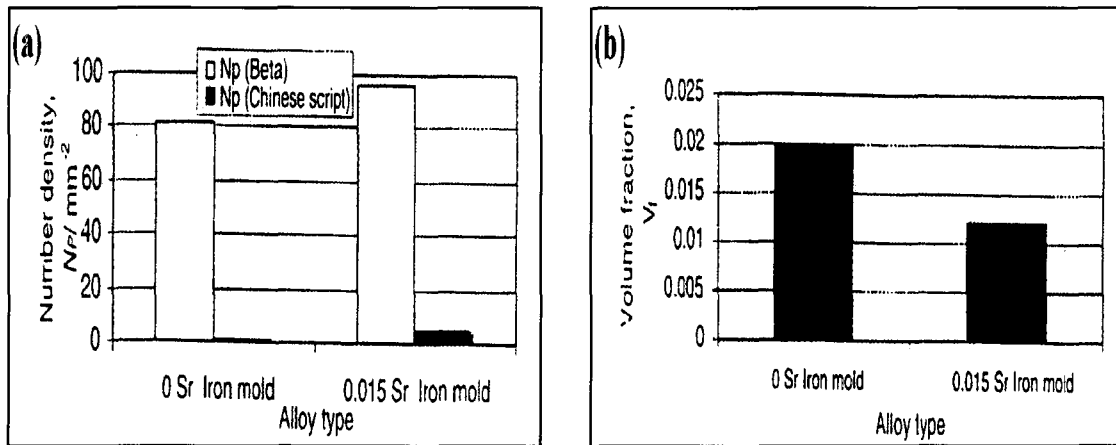
Figure 2.24 Effects of Sr addition on (a) number density and (b) volume fraction of β-phase of iron mold cast Al-6Si-3.5Cu-1.0Fe alloys.[71]

Samuel *et al.*[72] studied the effects of strontium on formation of the β-Al$_5$FeSi phase in 319 alloys. According to these researchers, the addition of strontium acts as a poison on the nucleation site of the β-needles, thereby reducing the number of sites ultimately available for nucleation. As a result, the β-iron phase precipitated at a smaller number of sites, leading to the precipitation of needles which were larger compared to those in the non-modified alloy. Pennors *et al.*[73] studied the effects of Sr modification on β-needles, together with the length, density, and area for alloy 319 at low cooling rates having different iron contents of 0.46% - 1.0% and 1.5%Fe; they found that, for the alloy containing 0.46%Fe and which solidified at a slow cooling rate, the optimum Sr levels lie closer to the limit of 400 ppm. As the iron level increases, the optimum Sr level will be observed to shift towards the higher limit.

The relationship between the Quality Index and the changes occurring in the microstructure of A356 alloys as a result of heat treatment and the addition of different

levels of pure Sr was investigated out by Closset and Gruzlezki.[21] They plotted the Q

values as a function of different cooling rates and Sr content, as shown in Figure 2.25. This

figure reveals an increase in the Q value with increases in Sr content, but at certain values

of the Sr content, the Q value starts to decrease for all the cooling rates studied. The

increase in the Q values observed with Sr additions of up to 0.03pct is a result of changes in

the acicular morphology of the Si particles to a fibrous form leading to decreases in the

crack initiation sites and thus also to an increase in the elongation to fracture. The apparent

reason for the drop in quality values, as the Sr content grew greater than 0.03 wt%, was the

over-modification of the Si particles and the formation of the Al_3SrSi intermetallic phase,

which is brittle and also not affected by heat treatment. The optimum mechanical properties

were also reported to be obtained in the Sr range from 0.005 to 0.015 pct.[74, 75]
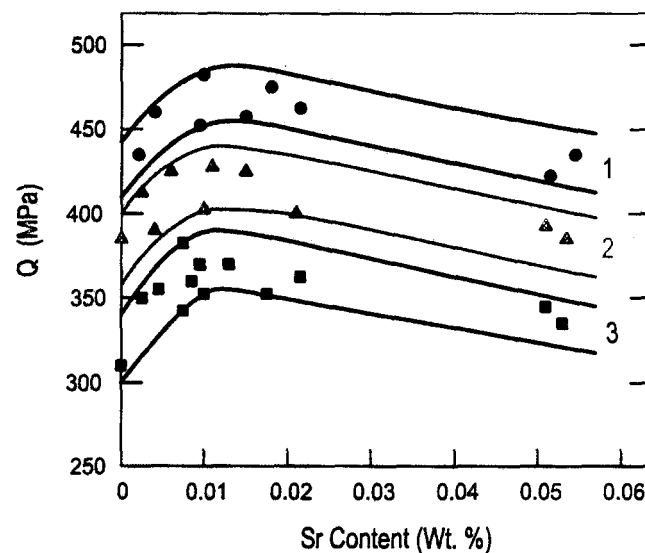
Figure 2.25 Variation of the Quality Index (Q) in relation to Sr content for different cooling rates.[21]

Paray[76] studied the effects of Sr modification on the total impact energy in terms of

the initiation and propagation energies of A356 alloys. Her results indicated that the crack

initiation energy may be improved by 53% through modification with Sr; this improvement

was attributed to the diminution of stress concentrations at the modified silicon-aluminum

interface. She also reported that the addition of Sr results in a reduction in the size of Si

particles, producing an improvement of 147% in the propagation energy through the

addition of Sr compared to non-modified alloys, as will be seen in Figure 2.26.
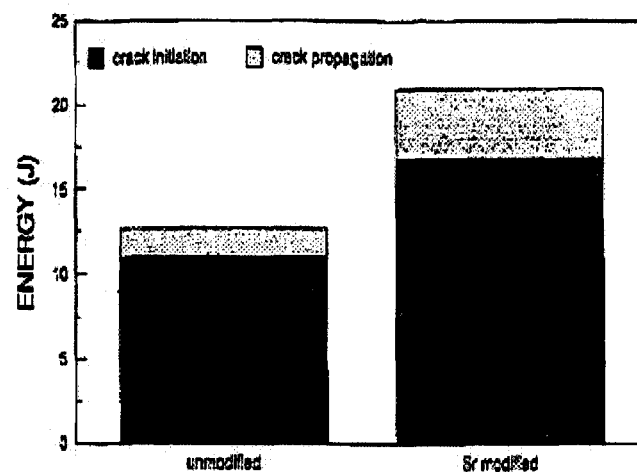
Figure 2.26 Different energies involved in the fracture of the as-cast impact samples.[76]

Hafiz and Kobayashi[77] investigated the influence of Sr level on eutectic Si

characteristics, namely aspect ratio (AR), equivalent diameter (DE), and shape factor (SF)

and their effects on impact toughness in terms of the crack initiation and crack propagation

energies of Al-12.6Si alloys. The authors revealed that the fracture initiation and

propagation energy is strongly influenced by the eutectic Si characteristics, as shown in

Figures 2.27 (a) and (b). As can be seen in these figures, the decrease in the aspect ratio of the Si particles and the improved circularity leads to a significant improvement in the impact initiation and propagation energies through decreases the void nucleation resistance especially in the early stages of the fracture process.
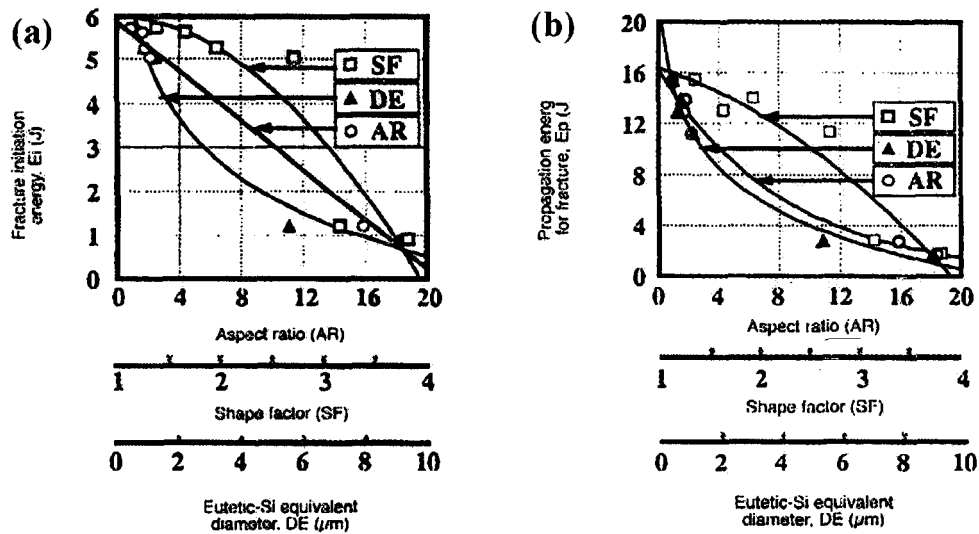
Figure 2.27 (a) Fracture initiation energy, and (b) fracture propagation energy as a function of eutectic Si characteristics.[77]

2.4.4 Cooling Rate

Since increasing the cooling rate is observed to have an effect on refining the eutectic Si particles, the SDAS, and the iron intermetallics, as well as reducing the amount of porosity, the mechanical properties are expected to improve. From the work of Verron et al.,[28] Figures 2.28 show the fracture toughness of Al-7Si-0.3Mg alloys versus secondary dendrite arm spacing at different levels of Fe content. It will be seen from these figure that increasing the SDAS has an effect by reducing the fracture toughness at all levels of Fe

content. The higher impact toughness can be also observed in the alloys contain 0.15%wt

Fe content. This increase in the toughness at 0.15%wt Fe content implies that it is

recommended to keep the level of iron very low in order to obtain superior mechanical

properties.
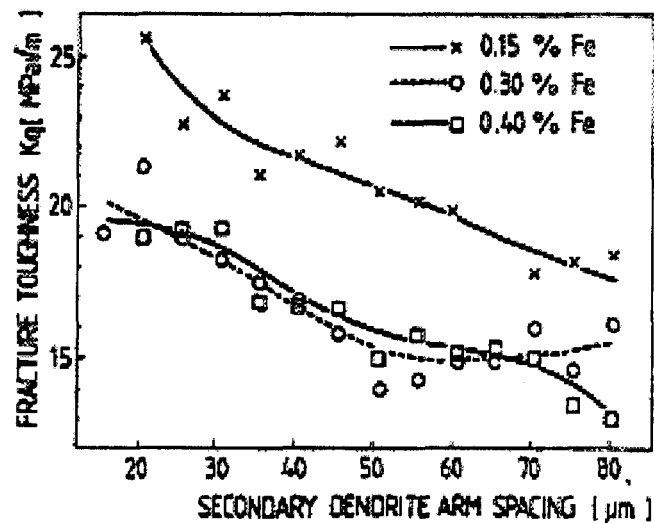
Figure 2.28 Fracture toughness versus secondary dendrite arm spacing at different levels of Fe content in Al-7Si-Mg alloys.[28]

Kamado et al.[78] studied the effects of the solidification condition on the mechanical

properties of a unidirectional solidified A356 alloy by means of stepwise regression

analysis. These researchers observed that the tensile properties and impact properties

become reduced significantly with increasing SDAS values, as shown in Figure 2.29(a) and

(b). The causes of this reduction may be ascribed to the increase in the Si particle size with

decreasing cooling rates, consequently, the crack initiation and propagation energies are

expected to diminish. The fracture analysis of the alloy samples solidified at a low cooling

rate reveal the cracks initiated at the matrix- silicon interface through the cleavage of the

silicon particles, and once the cracks had been triggered, they continued to interconnect and then propagated with ease.[79]
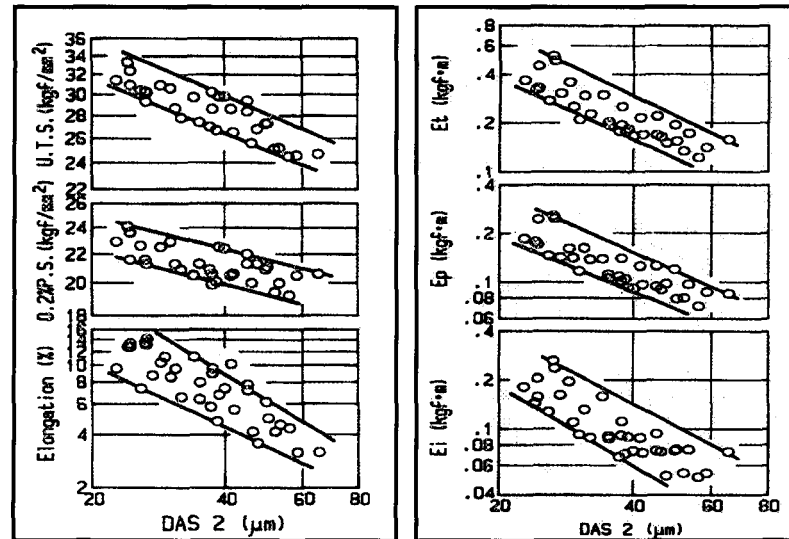
Figure 2.29 Effects of secondary dendrite arm spacing on tensile properties of 356 alloys in T6-condition.[78]

Shabestari and Shahari[80] studied the effects of cooling rate and modification using different modifiers on the Q values of T6-A356 alloys. A reduction in Q values was observed by the authors upon increasing the SDAS. This reduction is a result of the decrease in the % Elongation when increasing the SDAS, which has an effect on increasing the average diameter of Si particles. Strontium-modified alloys, however, have high Q values as a result of the higher % elongation when compared to the non-modified alloys, as shown in Figure 2.30. The ultimate tensile strength and yield stress of sand-cast T6-356 alloys were improved by means of the addition of Sr and by increasing the cooling rate, as has been reported by the same authors.
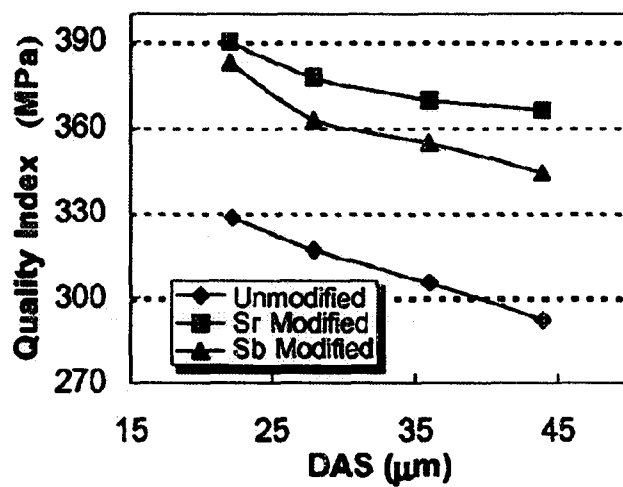
Figure 2.30 Quality index as a function of the dendrite arm spacing for sand cast heat treated alloys.[80]

2.4.5 Heat Treatment

The main objectives of heat treating cast Al-Si-Mg alloys include homogenization, stress relief, improved dimensional stability, and optimization of the strength and ductility parameters. Generally, Al-Si-Mg alloys are subjected to conventional T6 heat treatment conditions with the intention of obtaining an optimum combination of strength and ductility. The typical heat treatment specification of a T6 temper consists of solid solution treatment and quenching, followed by aging. The main effects of solution heat treatment are the dissolution of Mg_2Si particles, the homogenization of the casting, and a alteration the morphology of eutectic silicon by fragmentation and spheroidization at critical temperatures.[4, 57, 81] The recommended solution temperature for 356 and 357 alloys is 540 ± 5°C; this temperature was selected to obtain maximum concentrations of Mg and Si in solid solution, as shown in Figure 2.31.
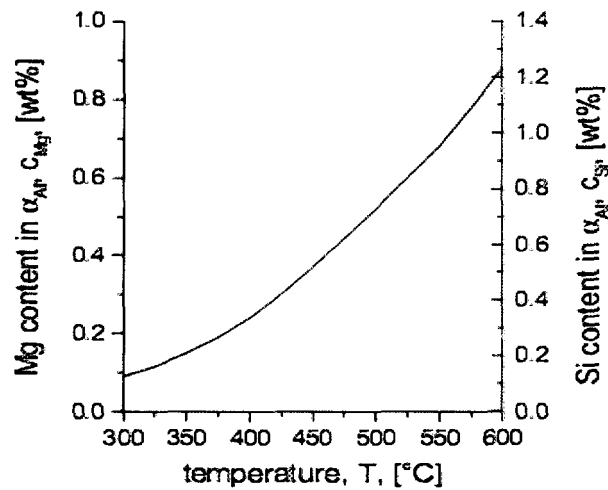
Figure 2.31 Solubility of Mg and Si in aluminum solid solution.[57]

The purpose of quenching is to preserve the solid solution formed at the solution heat-treating temperature by rapid cooling to room temperature. The quenching media and rate are parameters which control the mechanical properties; thus the highest strength can be ensured when the material is subjected to a rapid quenching rate. Aging is the final stage of heat treatment in cast Al alloys; this process can be natural or artificial and the mechanical properties depend on the aging temperature and time. The main objective of artificial aging is to heat-the as-quenched castings to an intermediate temperature between 150°C and 200°C for 4 to 8hrs in order to precipitate the excess solutes which were super saturated in α-Al during the solution heat treatment process. The improvement obtained in the mechanical properties during the artificial aging process is a result of the precipitation of metastable phases from the supersaturated solution. Al-Si-Mg alloys fulfill the following precipitation sequences:[4,82,83,84]

α_{ss} —— needle-shaped GP Zones —— rod-like β' precipitates —— platelets of Mg_2Si

Solution heat treatment may also be used as a useful technique for the dissolution or transformation of iron-rich intermetallic phases. A number of studies were carried out concerning the effects of solid solution heat treatment on the β- and π- iron intermetallic phases. Narayanan et al.[85] studied the effects of solution heat treatment on the dissolution behavior of β-phase iron intermetallics in a 319 alloy containing 1.0 pct iron; they found that, upon increasing the solution temperature, the β-phase platelets dissolve slowly through fragmentation along the width and dissolution at the plate tips. Additionally, the authors reported that the dissolution of iron intermetallics improves more obviously with increasing solution temperature than with solution treatment time. Villeneuve and Samuel[86] reported that solution heat treatment in Al-Si castings accelerates the dissolution of the β-phase by decomposition of Al_5FeSi into Al_6Fe and Si.

With regard to the π-phase iron intermetallic, Barresi et al. found that, in 357 alloys, there is a reduction in the amount of π-phase at different levels of Mg after heat treatment. Closset and Gruzleski[21] also studied the effects of solution heat treatment on Alloy 356. They observed that the dissolution of the π-phase depends on the levels of iron and magnesium present; thus, at low levels of 0.16 wt% Fe and 0.45 wt% Mg the π-phase dissolves, whereas it is only partially dissolved at higher Mg levels of 0.65%. Gustafsson et al.[20] studied the effects of T6 temper on the microstructure of the same alloy as was used

by Closset and Gruzleski;[21] they found that no changes were to be observed in the β-phases, although the π-phase was seen to dissolve after solution heat treatment.
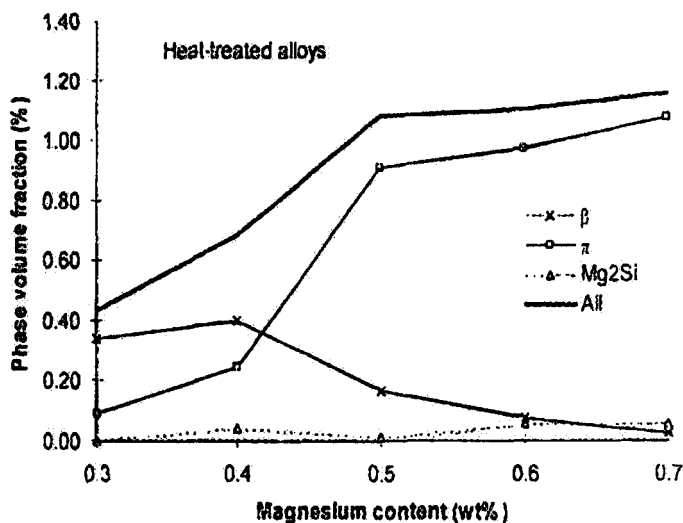
Figure 2.32 Volume fraction of the Mg₂Si, β- and π-phases present in the heat-treated Al-7Si-xMg-0.12%Fe alloy as a function of Mg content.[30]

A recent study was carried out by Taylor et al.[30] on the effects of a T6 temper on the π-phase in Al-7Si-xMg alloys containing 0.12 wt% Fe. They reported that, at low levels of 0.3-0.4 wt% Mg, the as-cast Chinese-script π-phase is reduced as a result of transformation into clusters of fine β-needles. At an intermediate Mg level of 0.5 wt%, there is a partial transformation of π-phase into β-phase needles, whereas no change was observed in the π-phase at high Mg levels of 0.6-0.7 wt%, as shown in Figure 2.32. This study was in agreement with the findings of Wang et al. who reported that, at Mg contents of lower than 0.5%, the π-phase in Al-7Si-Mg alloys decomposed into fine β-phase platelets as a result of the release of Mg into the matrix, although at high Mg contents of over 0.5wt % the π-

phase had a tendency to become slightly spheroidized, a fact which may be attributable to the solubility limit of Mg in the aluminum matrix.

An investigation was carried out by Shivkumar et al.[87] on the effects of T6 and T4 tempers in the tensile properties of non-modified and Sr-modified A356 alloys obtained from permanent mold and sand mold castings. Their results showed that the yield strength is not appreciably influenced by the change in Si-particle characteristics. The UTS and % elongation increases significantly with increases in the solution treatment time at 540°C, as shown in Figures 2.33 (a), (b), and (c). They also observed that upon modification with Sr the fracture mode changes from brittle to ductile especially in sand casting. Both non-modified and Sr-modified alloys obtained from permanent mold casting, however, showed ductile fracture mode. All the improvements in the tensile properties reported upon were related mainly to the changes which occurred in the Si particle aspect ratio and particle size during solution treatment.
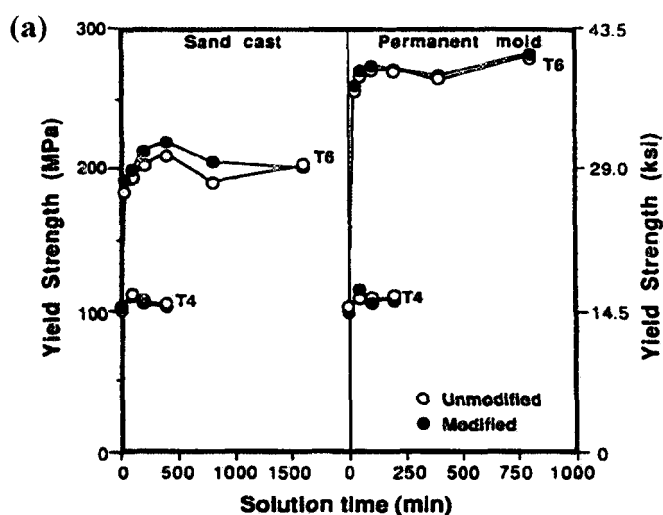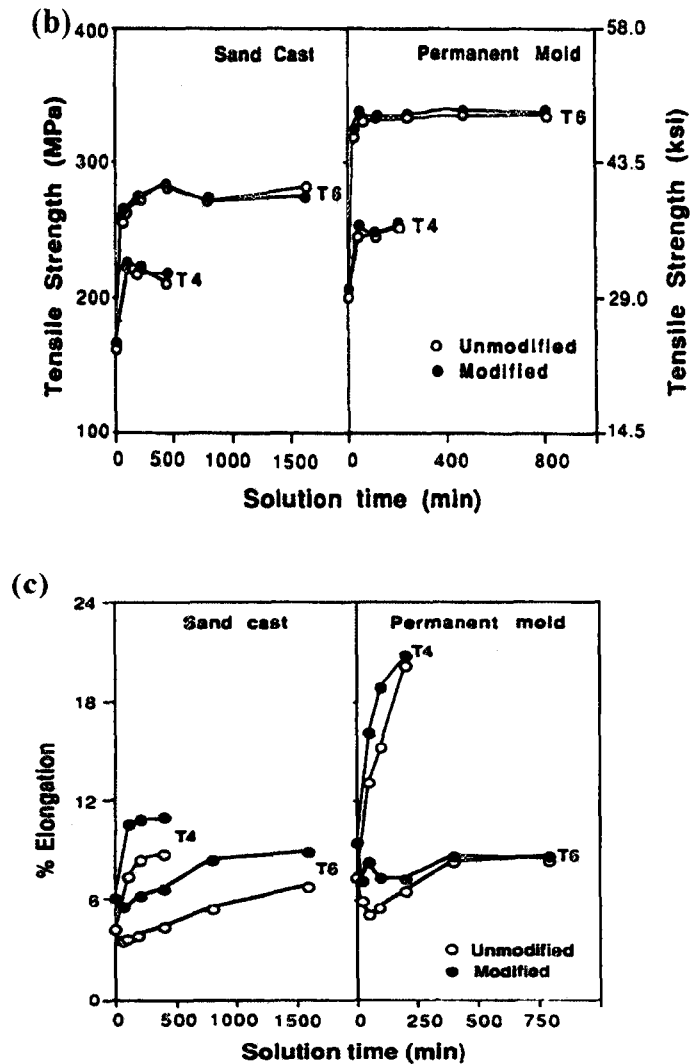
Figure 2.33 (a) Yield strength, (b) ultimate tensile strength and (c) % elongation as a function of solution time.[87]

Paray *et al.*[88] studied the effects of heat treatment on the impact properties of 356 alloys. They observed that after 1 hour of solution treatment, the improvement in both crack initiation and propagation energies was 129% and 153%, respectively, when compared to the as-cast alloys. For longer solution treatment times, the improvements in impact properties were observably large as a result of increasing the ductility of this alloy,

as indicated by increasing the crack propagation energy to 247% and 555% for 2 and 4 hours of solution treatment, respectively. The authors attributed the improvement occurring in the impact properties after 1 hour to the changes which occurred in the morphology of the Si particles. On the other hand, the improvement observed after prolonged solution treatment could be ascribed to the coarsening of the eutectic silicon particles. The results obtained from this research also showed that heat treatment is more effective than modification in improving the impact properties.

In conformity with this study, Tsukuda et al.[89] observed that by increasing solution heat treatment temperature and time, the impact strength also increases, as shown in Figure 2.34. Carolyn et al.,[90] in their study on the effects of solution treatment time on the impact properties of the 357 alloys, attributed the improvement in the impact energy resulting from
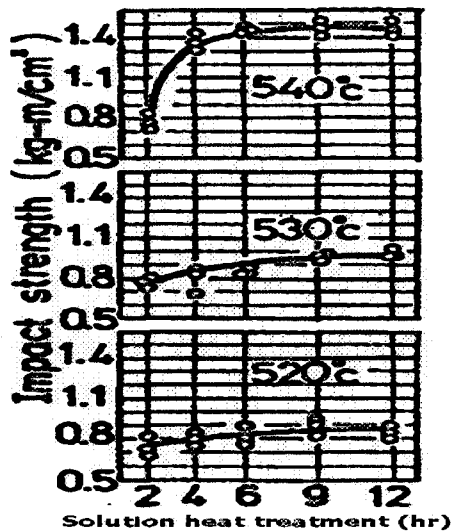
Figure 2.34   Effect of solution treatment time on the impact properties of Al6.85Si-0.3Mg0.2Fe-0.12Ti.[89]

an increase in the solution treatment time to the reduction in the aspect ratio and to the increase in the interparticle spacing of Si particles. They observed also that extended solution treatment time causes the sharp corners of Si particles to become blunt and to create a smoother particle-matrix interface, thereby contributing to the improvement observed in the fracture toughness.

2.4.6   Trace Elements

A number of methods have been put forward by various authors for reducing the detrimental effects of iron intermetallics. Generally, as described in previous sections, increasing the cooling rate, or using solution heat treatment, either individually or all in combination, will be observed to alleviate the problems involved in such detrimental effects of iron intermetallics on the mechanical properties. The addition of certain elements, mainly trace elements, to the melt has been reported to act as an effective neutralizer of the effects of iron in formation of iron intermetallic phases. There are several trace elements which are liable to neutralize the embrittlement effect of iron intermetallics; these include chromium, cobalt, manganese, molybdenum, and beryllium.[91,26]

Beryllium is used in Al-Si casting alloys to reduce the oxidation of the molten metal. The diffusion of the small beryllium ions into the oxide film causes a contraction of the oxide which establishes a denser, more protective film on the melt surface thereby impeding attack from the O_2 present in the atmosphere.[92] It has been reported that the presence of Be in premium quality aluminum alloys leads to the production of a clean melt

and to the formation of an oxidation layer which prevents Mg from oxidizing,[93] hence increasing the amount of Mg available to form Mg_2Si for the strengthening of the Al-Si-Mg alloys.

Beryllium is extensively reported in the literature as a neutralizing agent for the iron intermetallic phases which form in Al-7Si-Mg alloys. Yen *et al.*[94] observed that the amount of π-phase intermetallic in the Be-free 357 alloy is higher than it is in a Be-containing alloy, particularly in the presence of high Mg levels. They also noted that, in the Be-containing 357 alloy, the β-phase was replaced by the Chinese-script morphology of Al_8Fe_2Si in which it reduces the embrittlement effect of the β-Al_5FeSi phase. The same finding was reported by Wang and Xiong.[95]

Kumari *et al.*[96] found that the addition of 0.2% Be to Al-7Si-0.3Mg-0.8Fe results in the replacement of the β-phase in the α-Be-Fe phases; this phase tends to precipitate at temperatures which are higher than the formation temperature of the β-phase, consequently reducing the iron available to form this β-phase. Murali *et al.*[97] observed a certain amount of improvement in the mechanical properties of 356 alloys as a result of the addition of small amounts of Be; they attributed this improvement to the change in solidification behavior as well as to alterations in the morphology of the β-phase when changing into the Be-Fe Chinese-script phase. Murali *et al.*[98] investigated the effects that adding iron and trace elements, particularly beryllium, would have on the fracture toughness of Al-7Si-0.3Mg alloy specimens taken from two different squeeze-cast cranks; their results revealed significant decreases in the fracture toughness values for increasing iron levels of up to

0.7wt% for all the alloys studied except those containing trace amounts of Be, as can be seen in Figure 2.35. Slightly higher fracture toughness values were observed at all iron levels, a fact which may be attributed to grain refining and altering the morphology of β-phase to Be-Fe Phase (BeSiFe$_2$Al$_8$) by means of the Be additions.
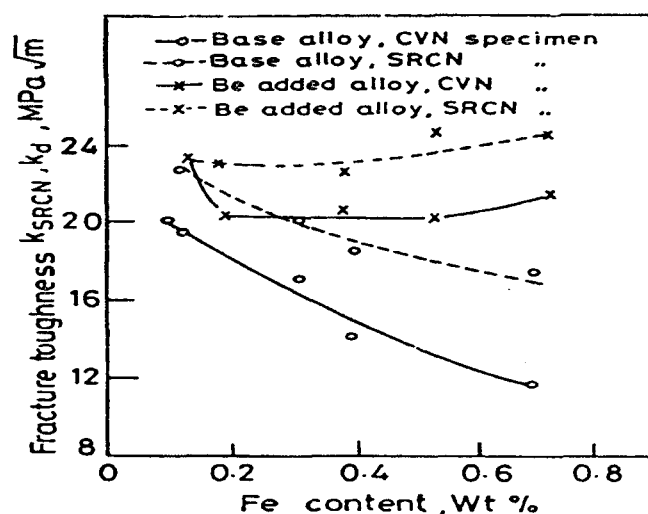
Figure 2.35 Effects of Be addition on the fracture toughness for Al-7Si-0.3Mg alloy with varying iron contents squeeze-cast at 66MPa.[98]

In the agreement of the positive effect of Be addition on enhancing the mechanical properties of Al-Si-Mg alloys, another study was carried out by Murali and co-workers[44] on the effect of different addition of trace elements on the tensile properties of Al-7Si-xFe alloys. The authors observed that the Be-containing alloys exhibit higher values for tensile strength at all levels of iron content, as indicated in Figure 2.36; they also observed that the ductility of the Be-containing alloys initially decreases, although it still remains higher than the values for the other alloys. The same authors attributed the improvement observed in the tensile properties for Be-containing alloys to the same previously reported reason as

given above. It should be noted here, that even though numerous benefits result from the addition of Be to Al-Si-Mg alloys, the presence of Be in Al-Si-Mg alloys is a potential health hazard,[93,52] and its elimination is, therefore, to be recommended strongly.
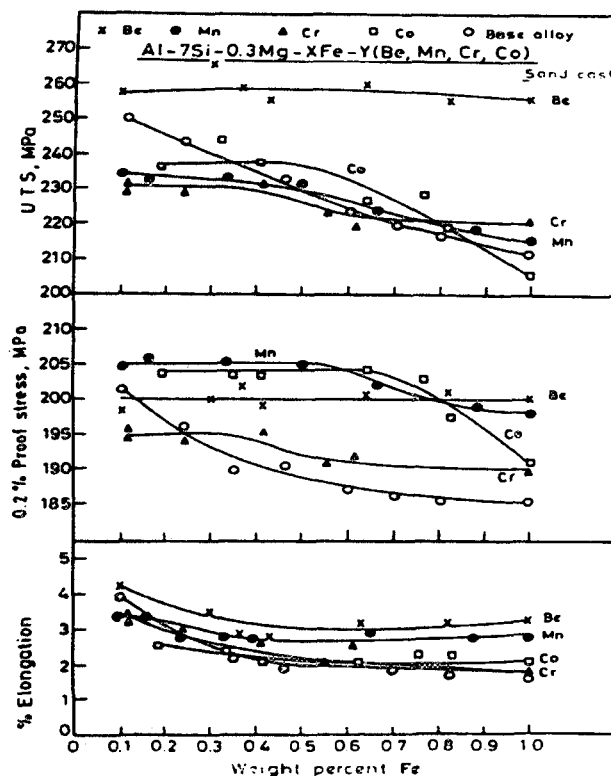
Figure 2.36 Effects of trace additions on the tensile properties with varying levels of Fe content.[44]

Based on the data reviewed in the literature, it has become apparent that the π-phase leads to a softening of the matrix and a lessening of the mechanical properties of the Al-7%Si-Mg alloys. Consequently, the ideal conditions in which to minimize the detrimental effects of the iron-intermetallic phases would be to start with the difficult step of removing the iron from the melt. Reducing the size of the π-phase by dissolution or

transformation to another less detrimental phase is highly to be desired in Al-Si-Mg alloys with a view to the ultimate improving of the ductility values.[52]

CHAPTER 3

EXPERIMENTAL PROCEDURES

CHAPTER 3

EXPERIMENTAL PROCEDURES

3.1   Introduction

The experimental procedures were designed with the aim of fulfilling the requirement objectives of the current study. In order to investigate the effects that Mg, Fe, and Be additions have on the formation of π-phase iron intermetallics, different levels of these elements were added to a 356 base alloy so as to produce a large variety of 356 and 357 alloys. Castings of these alloys were produced using a graphite mold preheated to 600°C following by air cooling for the purposes of phase identification and quantitative analysis of the iron intermetallics in the as-cast and heat treated conditions. Castings of a number of selected 357 alloys were produced using L-shaped metallic molds to study the effects of different solidification rates and solution heat treatment times on Si-particle characteristics and the π-phase iron intermetallic. With the intention of investigating the effects of the Si-particle characteristics and π-phase iron intermetallics on the tensile and impact properties of 357 alloys, two different metallic mold types were used, namely a copper end-chill metallic mold and an ASTM B-108 permanent mold, respectively, for preparing the test bars. Extensive microstructural examination was carried out on samples obtained from the L-shaped metallic molds, from the graphite mold and on some selected

samples obtained from impact and tensile-tested bars. The detailed experimental procedures applied to accomplishing the task involved in the current work will all be discussed in the following subsections.

3.2 Melt Preparation

The 356 alloy used in this study was supplied in the form of 12.5-Kg ingots. The chemical composition of the as-received 356 alloy is listed in Table 3.1. These ingots are then melted in a silicon carbide crucible of a 40-kg capacity using an electrical resistance furnace. The melting temperature was maintained at 740 ± 5°C. Calculated amounts of Mg, Si, and Fe were subsequently added in accordance with the balance of weight obtained and required to reach the target composition in each case. Silicon and magnesium were added next in their pure form, while iron and beryllium were added in the form of Al-25%Fe and Al-5% Be master alloys, respectively. Melt treatment was effectuated by adding a combination of Ti and B to the melt in the form of Al-5%Ti-1%B master alloy rods for the purposes of grain refinement. The Sr-modified alloys were obtained through the addition of 200 ppm Sr to the as-received alloys in the form of an Al-10%Sr master alloy; the melts were then degassed and stirred for 15 minutes after the addition was made. The degassing process was carried out using pure dry argon injected into the molten metal at a constant rate of 30 ft^3/h by means of a rotary graphite impeller. Once the degassing process was completed, the melt was carefully skimmed so as to remove the oxide layers from the surface of the melt. Following this, samples were taken from each alloy melt for chemical analysis using a SPECTROLAB Jr. CCD Spark Analyzer in order to obtain the actual

chemical composition; and lastly, the molten metal for each composition was poured into different types of molds based on the objectives listed for the test involved.

Table 3.1 Chemical composition of the as-received 356 alloy.

Alloy	Element (wt%)							
356	Si	Fe	Cu	Mn	Mg	Ti	Sr	Al
	7.32	0.09	0.1	< 0.01	0.38	0.12	0.002	Bal

3.3 Casting Procedures

3.3.1 Thermal Analysis and Related Studies

In order to obtain the cooling curves and to identify the main reactions and corresponding temperatures occurring during the solidification of Al-7Si-Mg alloys, thermal analysis was carried out for all of the compositions prepared. The molten metal for each composition was poured into a cylindrical graphite mold of 80 mm height and 60 mm diameter which had been preheated to 600°C so as to create a slow cooling rate resembling equilibrium conditions in order to make the phase identification possible. A high sensitivity Type-K (chromel-alumel) thermocouple, which had been insulated using a double-walled ceramic tube, was attached to the centre of the graphite mold, as shown in Figure 3.1 and Figure 3.2. The temperature-time data was collected using a high speed data acquisition system linked to a computer. From this data, the cooling curves and the corresponding first derivative curves for a number of selected alloys were plotted so as to identify the main reactions occurring during solidification with the corresponding temperatures. The codes and compositions for the Be-free and Be-containing Al-7Si-xMg-yFe alloys cast in the

preheated graphite mold are provided in Table 3.2 and Table 3.3, respectively. Cylindrical specimen plates, 15 mm deep, were sectioned off at the centre of each graphite mold casting close to the thermocouple tip for all of the compositions obtained. Two samples, having the dimensions 2.5 × 2.5 cm, were machined from each plate for qualitative and quantitative analysis purposes; one sample was classified as 'as-cast' while the other was coded 'after heat treatment'.
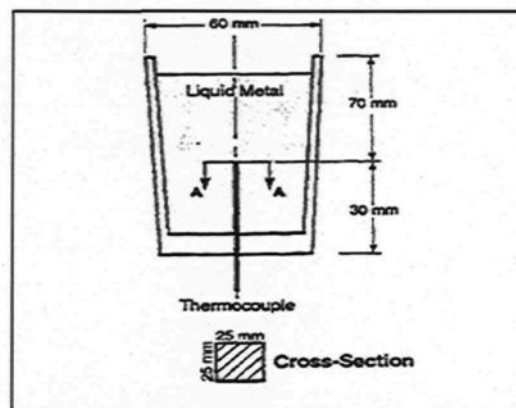
Figure 3.1 Schematic drawing showing the graphite mold used for thermal analysis.
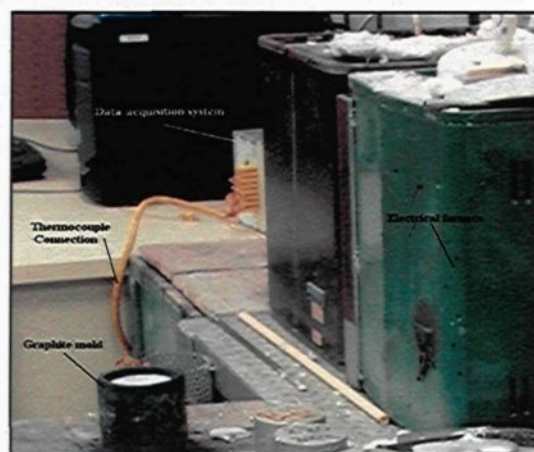
Figure 3.2 Thermal analysis set-up.

Table 3.2 Chemical composition of the 356 and 357 alloys used in this study.

356 Alloy Codes	Element (wt%)							
	Si	Fe	Mg	Mn	Cu	Ti	Sr	Al
1A	7.22	0.10	0.42	0.00	0.02	0.12	0.00	Bal.
2A	7.04	0.25	0.41	0.02	0.10	0.11	0.00	Bal.
3A	7.16	0.46	0.41	0.03	0.11	0.09	0.00	Bal.
4A	6.90	0.64	0.41	0.02	0.11	0.11	0.00	Bal.
5A	7.09	0.83	0.39	0.03	0.11	0.16	0.00	Bal.
1AS	7.13	0.10	0.41	0.01	0.02	0.11	0.018	Bal.
2AS	6.72	0.24	0.46	0.02	0.11	0.11	0.015	Bal.
3AS	7.02	0.43	0.46	0.03	0.11	0.10	0.02	Bal.
4AS	6.77	0.55	0.43	0.03	0.10	0.10	0.014	Bal.
5AS	7.00	0.80	0.37	0.0	0.04	0.10	0.018	Bal.
357 Alloy Codes	**Element (wt%)**							
	Si	Fe	Mg	Mn	Cu	Ti	Sr	Al
6C	7.00	0.10	0.55	0.00	0.01	0.10	0.00	Bal.
7C	7.42	0.29	0.58	0.02	0.11	0.17	0.00	Bal.
8C	7.17	0.44	0.54	0.02	0.11	0.14	0.00	Bal.
9C	7.20	0.57	0.58	0.02	0.11	0.11	0.00	Bal.
10C	7.41	0.75	0.59	0.03	0.11	0.19	0.00	Bal.
6CS	7.00	0.10	0.56	0.02	0.10	0.10	0.016	Bal.
7CS	7.00	0.26	0.60	0.02	0.10	0.10	0.021	Bal.
8CS	7.00	0.40	0.60	0.02	0.10	0.10	0.021	Bal.
9CS	7.00	0.60	0.53	0.02	0.10	0.10	0.015	Bal.
10CS	7.00	0.78	0.65	0.02	0.10	0.10	0.018	Bal.
11C	7.18	0.10	0.75	0.02	0.10	0.13	0.00	Bal.
12C	7.30	0.29	0.74	0.03	0.11	0.12	0.00	Bal.
13C	7.31	0.38	0.76	0.03	0.11	0.16	0.00	Bal.
14C	7.51	0.63	0.79	0.27	0.11	0.18	0.00	Bal.
15C	7.00	0.80	0.78	0.03	0.10	0.10	0.00	Bal.
11CS	7.43	0.10	0.79	0.00	0.02	0.11	0.015	Bal.
12CS	7.20	0.29	0.78	0.02	0.10	0.14	0.018	Bal.

13CS	7.35	0.46	0.82	0.02	0.11	0.16	0.021	Bal.
14CS	7.44	0.55	0.78	0.03	0.11	0.14	0.014	Bal.
15CS	7.75	0.80	0.72	0.03	0.11	0.10	0.022	Bal.
16C	7.47	0.10	1.00	0.00	0.02	0.10	0.02	Bal.
16CS	7.16	0.10	1.00	0.00	0.00	0.10	0.017	Bal.

S: Sr-modified; A: 356 alloy; C: 357 Alloy

Table 3.3 Chemical composition of 356 and 357 alloys containing Be.

356 Alloy	Element (wt%)								
Codes	Si	Fe	Mn	Cu	Mg	Ti	Sr	Be	Al
1AB	7.06	0.11	0.02	0.20	0.36	0.10	0.003	0.055	Bal.
1ABS	6.95	0.11	0.02	0.20	0.37	0.10	0.017	0.057	Bal.
357 Alloy	Element (wt%)								
Codes	Si	Fe	Mn	Cu	Mg	Ti	Sr	Be	Al
6CB	7.07	0.11	0.02	0.10	0.62	0.10	0.003	0.045	Bal.
6CSB	6.80	0.11	0.02	0.10	0.64	0.10	0.018	0.05	Bal.
11CSB	7.32	0.92	0.016	0.1	0.77	0.1	0.018	0.05	Bal.
16CB	6.63	0.11	0.02	0.16	1.00	0.10	0.003	0.05	Bal.
16CSB	7.12	0.11	0.02	0.06	1.00	0.10	0.023	0.06	Bal.

B: Be-content; S: Sr-modified; A: 356 alloy; C: 357 Alloy

3.3.2 Solidification Rate and Related Studies

Two L-shaped steel molds with a cross-sectional area of 2.5 × 2.5 cm each were used to cast test bars made of the selected 6C and 6CS alloys for the purposes of investigating the effects of solidification rate and solution heat treatment time on the π-phase and Si-particle characteristics of 357 alloys. The first of these L-shaped steel molds had been preheated to 450°C prior to pouring, followed by cooling in atmospheric air to

promote a high cooling rate, while the second mold had been preheated to 700°C and then slowly cooled inside the furnace at 450°C in order to impose a slow cooling rate. Figure 3.3 represents the L-shaped metallic molds used for the current study. Twenty-one samples, 2.5 × 2.5 cm in dimension, were sectioned off and machined from each rectangular cast bar for each composition in such a way as to obtain 84 samples in total. These samples were coded firstly for the as-cast condition and then again after heat treatment.

Figure 3.3 L-shaped metallic molds used in the current study.

3.3.3 Mechanical Properties and Related Studies

3.3.3.1 Preparation of Bars for Tensile Testing

A certain number of alloy melts, having a composition of 6C and 6CS, were also prepared using the same procedures as in subsection 3.2 for casting bars to be used in tensile testing. The main objective from this test is to study the effects that a T6 temper with different solution treatment times would have on the tensile properties of selected 6C and 6CS alloys. As may be seen in Figure 3.4, the alloy melts were poured into an ASTM B 108 permanent metallic mold which had first been preheated to 450°C, then air cooled.

Figure 3.5 shows the standard dimensions of the tensile test bar. Each casting provided two test bars. For each alloy composition, 128 test bars were produced to obtain 256 bars in total. All of these bars were coded and grouped into lots for testing, either in the as-cast condition or after heat-treatment.

Figure 3.4 Standard ASTM B-108 permanent metallic as used in the current study.
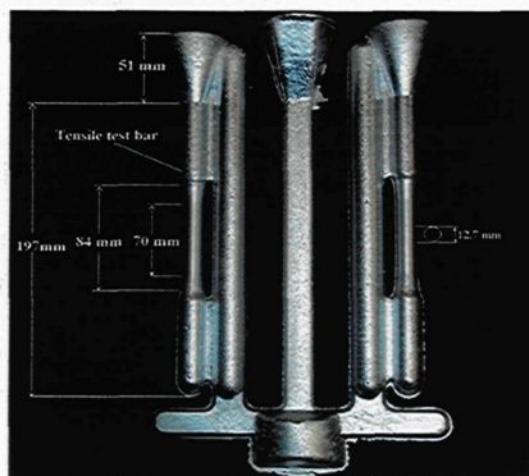
Figure 3.5 Casting showing the dimensions of a test bar obtained for this study.

3.3.3.2 Preparation of Bars for Impact Testing

A copper end-chill mold constructed of refractory materials was used in order to study the effects which two different cooling rates and a T6 temper with different solution treatment times would have on the impact properties of 6C and 6CS alloys. This end-chill mold produced a casting with a wide range of solidification times and secondary dendrite arm spacings along the height of the casting above the end-chill. The bottom portion which is close to the copper base provides the highest cooling rate whereas the upper portion provides a low cooling rate, as can be seen clearly in Figure 3.6. Each casting block was machined to obtain 2 rectangular plates having the dimensions 125 mm x 20 mm; the first plate corresponds to level 1 (SDAS = 35μm), while the second plate corresponds to level 3 (SDAS = 110μm). Each specimen plate provided five samples with standard dimensions of H = 10mm, W = 10mm, and L = 55 mm, as will be observed in Figure 3.7. For each alloy composition, 120 samples were obtained. These bars were coded for as-cast and post heat treatment conditions.

3.4   Heat Treatment

The samples obtained from the graphite mold casting were solution heat-treated at 540°C for 8 hours followed by quenching in warm water at 60°C whereas the samples obtained from the L-shaped metallic mold castings were solution heat-treated at 540°C for 19 different time periods ranging from 2 to 100 hours at 540°C followed by quenching in

warm water at 60°C. Bars for tensile and impact testing obtained from the ASTM B-108 permanent metallic mold and end-chill metallic mold castings, respectively, were subjected to solution heat treatment at 540°C for time periods ranging from 2 to 100 hours, then
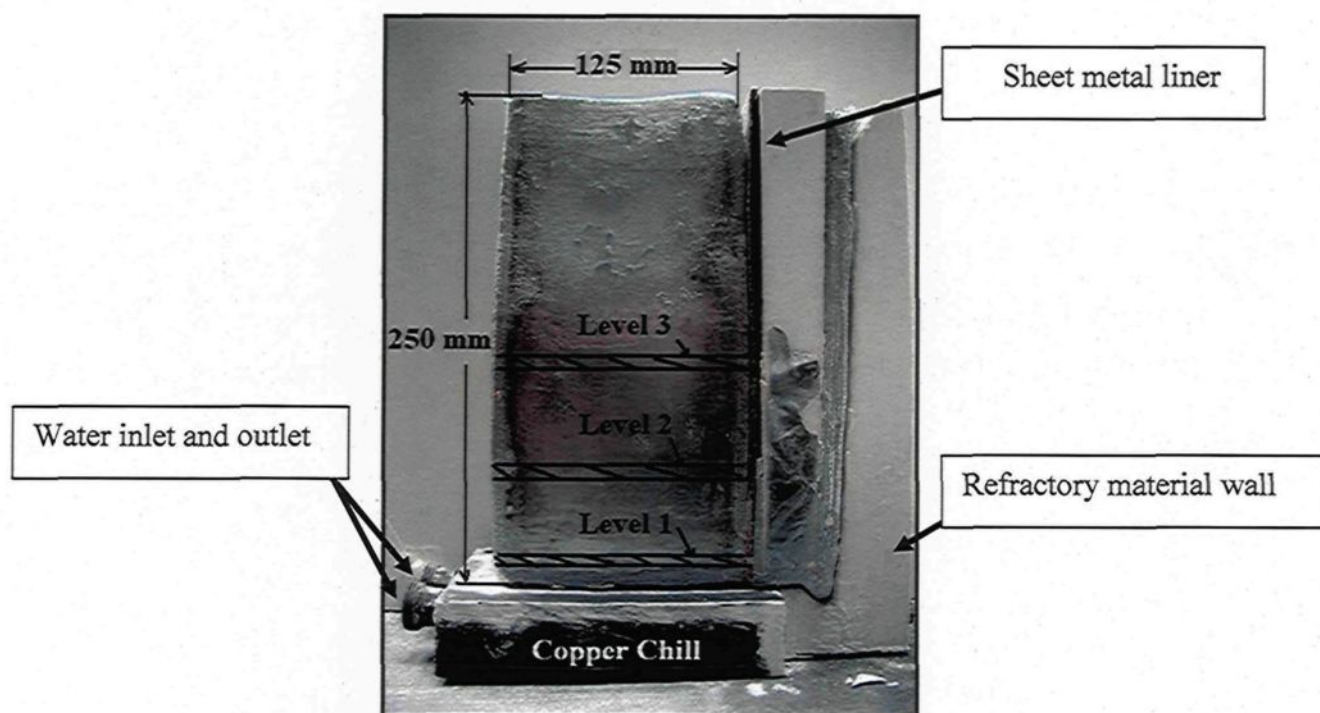
Figure 3.6 End-chill metallic mold used to prepare the casting.
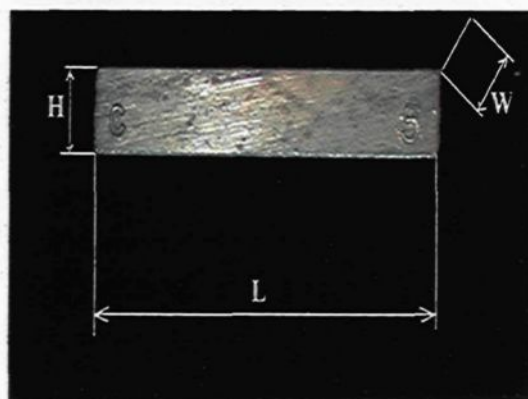
Figure 3.7 Unnotched Charpy specimen used for impact testing.

quenched in warm water at 60°C followed by artificial aging at 155°C for 5 hours. All the heat treatment processes were carried out using a Blue M forced air furnace.

3.5 Mechanical Testing

3.5.1 Tensile Testing

The as-cast and heat-treated bars for tensile testing produced from the ASTM B-108 permanent mold were pulled to failure using a Servohydraulic Mechanical Testing Machine working at a strain rate of 1.0×10^{-4}/s, as shown in Figure 3.8. The tensile test results obtained for each test specimen include elongation to fracture (%El), 0.2% offset yield strength (YS), and ultimate tensile strength (UTS). Five test bars were tested for each composition in the as-cast and T6-155°C aged condition.

3.5.2 Impact Testing

A standardized high strain-rate Charpy impact test was used to determine the amount of energy absorbed by unnotched samples during fracture at room temperature. This test was carried out using a computer-aided instrumented Charpy impact test machine, model SI- 1D3, as shown in Figure 3.9. The system consists of a drop weight impact pendulum, instrumented tup, and a data acquisition system to provide a comprehensive load and

Figure 3.8 The MTS Servohydraulic mechanical testing machine.
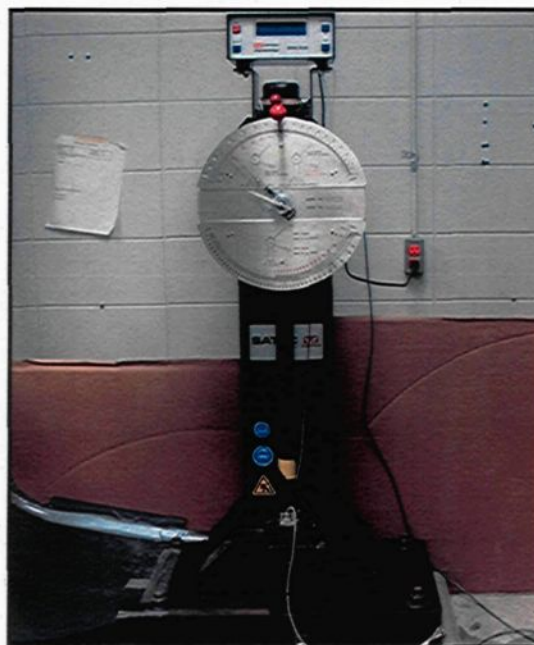
Figure 3.9 A computer-aided instrumented Charpy impact test machine, model SI- 1D3.

energy record obtained for each test. The impact values reported are the average of five test bars for as-cast and T6-155°C aged conditions.

3.6   Examination of the Microstructure

3.6.1   Preparation of Samples

The as-cast and heat treated samples for metallographic examination were mounted in bakelite using a Struers Labo Press-3 mounting press. The sample surfaces were then ground and polished using a Tegra Force-5 Grinder/Polisher to obtain a satisfactory surface finish. Table 3.5 provides a list of the grinding and polishing procedures which were applied; between each intermediate stage, the samples were cleaned with a mixture of 95% alcohol and 5% soap.

Table 3.4 Grinding and polishing procedures used for sample preparation.

Stage	Abrasive	Coolant	Time (min)
1	SiC 320	Running Water	1
2	SiC 400	Running Water	1
3	SiC 600	Running Water	1
4	SiC 800	Running Water	1
5	Diamond Suspension (6μm)	Special Oil	5-6
6	Diamond Suspension(1μm)	Special Oil	5-6
7	Colloidal Silica Suspension	Special Oil	4

3.6.2   Quantitative and Qualitative Analyses

3.6.2.1 SDAS Measurements

The average secondary dendrite arm spacing (SDAS) was measured for samples obtained from the graphite and L-shaped metallic molds using a Clemex Vision PE 4.0 optical microscope equipped with an image analysis system, as shown in Figure 3.10. Thirty fields were selected to cover the entire sample surface so as to obtain accurate measurements. Table 3.5 shows the various dendrite arm spacing values obtained from the graphite and metallic mold samples.

Figure 3.10 Clemex Vision PE 4.0 optical microscope used in the current study.

3.6.2.2   Eutectic Silicon Particle Measurements

Silicon particle measurements were carried out for samples obtained from copper end-chill metallic mold castings with the aim of investigating the effects of solution heat

treatment times on the silicon particle characterization using a Clemex Vision PE 4.0 optical microscope equipped with an image analysis system. The measurements were taken at a magnification of 200x and 500x for the non-modified and Sr-modified 6C and 6CS alloys, respectively. The eutectic Si-particle characteristics, namely area, length, roundness and aspect ratio, were measured over 40 fields covering the whole sample area in a systematic manner.

Table 3.5 SDASs obtained from the graphite and metallic mold samples.

Alloy code	Mold Type	Average SDAS (μm)
6C	L- shaped mold; heated at 450°C (Furnace cooling)	110
6C	L- shaped mold; heated at 450°C (Air cooling)	35
6C and 1A	Graphite; heated at 600°C (Air cooling)	65

3.6.2.3   Iron Intermetallic Phases

Phase identification and volume fraction of iron intermetallics were carried out for selected samples obtained from the graphite mold, and L-shaped metallic mold castings in the as-cast and heat treated conditions; this involved using an Electron Probe Microanalyzer (EPMA) in conjunction with wavelength dispersive spectrometry (WDS), which incorporated a JEOL JXA-8900L WD/RD combined microanalyzer operating at 20 kV and 30 mA with an electron beam ~ 2μm in diameter for this purpose, as shown in Figure 3.11.

Figure 3.11 Electron Probe Microanalyzer (EPMA) used in the present study.

With regard to volume fraction measurement, it should be mentioned that the volume fraction of iron intermetallics was quantified on the basis of phase brightness. The brightness of each phase is a function of its average atomic number. The quantification process is based on an elimination technique wherein, by subtracting the volume fraction of the brighter phases from the total volume fraction of all the phases present within the matrix, the volume fraction of the phase in question may be determined. The volume fraction of the π-phase iron intermetallic was quantified for as-cast and heat treated samples coded in Table 3.2, and Table 3.3 which were obtained from graphite mold castings. The π-phase and β-phase volume fractions were also quantified for 6C and 6CS alloys obtained from the L-shaped metallic molds under two conditions, (i) as cast, and (ii) solution heat-treated at 540°C for different periods of time from 2 to 100 hours. For a number of selected

heat-treated samples obtained from the L-shaped metallic mold casting, line scans were taken along paths across the iron intermetallics and matrix using EPMA in order to investigate the effects of π-phase decomposition on the matrix chemistry. Readings of the concentrations, in wt%, were taken along the line scan path at intervals of 4 μm, firstly, to avoid overlapping of the analyzed zones and, secondly, to obtain a continuous scan along the path selected.

3.5.3.4   Hardening Precipitates

Field-emission gun scanning electron microscopy (FEGSEM) was used to examine the hardening precipitates for 6C and 6CS alloys obtained from tensile-tested specimens in the T6 heat-treated condition. Samples 10 mm high were sectioned off 5mm beneath the fracture surface. The procedure for preparing the samples was the same as the one used in the previous experiments, as described in subsection 3.6.1. In order to facilitate the detection of the hardening precipitates, these polished samples were subjected to a chemical micro-etching process. The etching agent used for this study was 0.5mL HF, namely 48%, *i.e.* a 0.5mL HF solution of a 48% concentration with the remaining portion constituted of 99.5mL water. This etchant was applied to the samples at room temperature for a length of time ranging from 30 to 60 sec. Figure 3.12 shows the field emission scanning electron microscope used in this study.

3.6.2.4 Fractography

An examination was carried out on the fracture surface of selected broken specimens obtained from the impact test using a Scanning Electron Microscope (SEM) equipped with an EDX system for element analysis. Samples were cut 6mm beneath the fracture surface. Another set of samples was cut from longitudinal sections passing through the fracture surface obtained from impact specimens. This examination was carried out using an optical microscopes and image analysis software throughout.
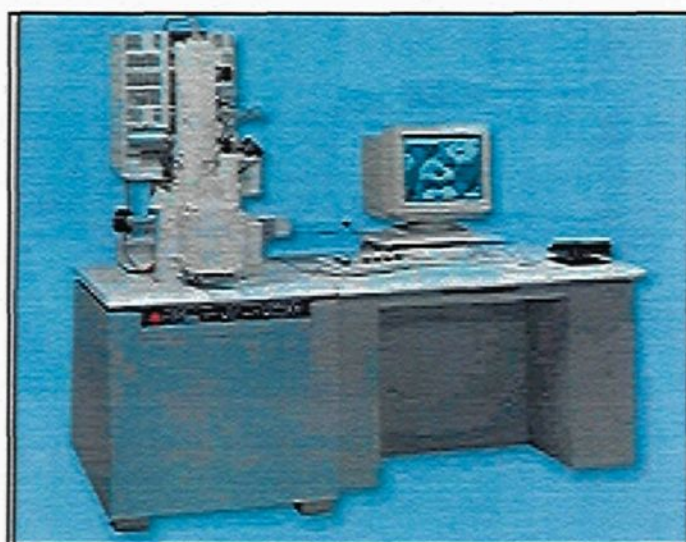
Figure 3.12 Field emission scanning electron microscope used in the current study.

CHAPTER 4

MICROSTRUCTURAL ANALYSIS

CHAPTER 4

MICROSTRUCTURAL ANALYSIS

4.1   Introduction

This chapter consists of five main sections. The first two sections present a discussion of the results obtained from studying the effects of iron, magnesium, and beryllium, both individually and in combination, on the microstructure and solidification sequences of Al-7Si-Mg alloys using the thermal analysis technique. The third section discusses the metallurgical parameters which affect the quantitative and qualitative analysis of the π-phase formed in non-modified and Sr-modified Al-7Si-xMg-yFe alloys obtained from graphite and L-shaped metallic mold castings. The parameters studied include the effects of Fe and Mg content; the effects of Be addition; the influence of solution heat treatment time; and the effects of solidification rate. The fourth section examines the impact of the decomposition of the π-phase on the matrix chemistry of 357 alloys. The last section will address the mechanism of π- to β-phase decomposition during solution heat treatment.

4.2   Microstructure Features and Phase Identification

In keeping with the precipitation sequences reported by Bäckerud et al.[15] for Al-7Si-Mg alloys, the microstructure of the as-cast Al-7Si-xMg-yFe alloy containing 0.4, 0.6, and

0.8 wt% Mg and 0.1-0.8 wt% Fe, obtained from graphite mold castings with an SDAS of ~ 65 μm reveals the following: (1) primary aluminum phase, (2a) eutectic silicon, (2b) post-eutectic β-Al$_5$FeSi phase with platelet-like morphology, (3) π-AlFeMgSi phase with scriptlike and blocklike morphology, and (4) Mg$_2$Si with black-script morphology, as shown in Figure 4.1(a). As a result of the addition of Sr, the morphology of the eutectic silicon particles undergoes a change from an acicular to a fibrous form, as may be seen from a comparison of Figure 4.1(b) and Figure 4.1(a).

With regard to the π-phase, the stoichiometry proposed by Closset et al.[21] and Bäckerud et al.,[15] namely, Al$_8$FeMg$_3$Si$_6$. In the current work, the calculated stoichiometry of the β- and π-phase iron intermetallics based on the composition obtained from WDS analyses of the as-cast samples of alloys 1A and 15C, are in the vicinity of the suggested formulas,[15] regardless of the Fe and Mg content of the alloy, as presented in Table 4.1.

Table 4.1 Chemical composition of the Fe intermetallic phases observed in 1A and 15C alloys.

Alloy	Phase	Element (at%)				Formula	
		Al	**Si**	**Fe**	**Mg**	**Calculated**	**Suggested**
1A (356) 0.4Mg-0.1Fe	π-phase	47.68	30.3	6.8	15.14	Al$_{9.4}$Fe$_{1.3}$Mg$_3$Si$_6$	Al$_8$FeMg$_3$Si$_6$
	β-phase	63.00	20.9	16.2	0	Al$_{3.9}$FeSi$_{1.2}$	Al$_5$FeSi
15C (357) 0.8Mg-0.8Fe	π-phase	47.85	26.8	6.03	19.07	Al$_{7.5}$Fe$_{0.94}$Mg$_3$Si$_{4.2}$	Al$_8$FeMg$_3$Si$_6$
	β-phase	65.5	17.6	16.6	0	Al$_{3.9}$FeSi$_{1.06}$	Al$_5$FeSi
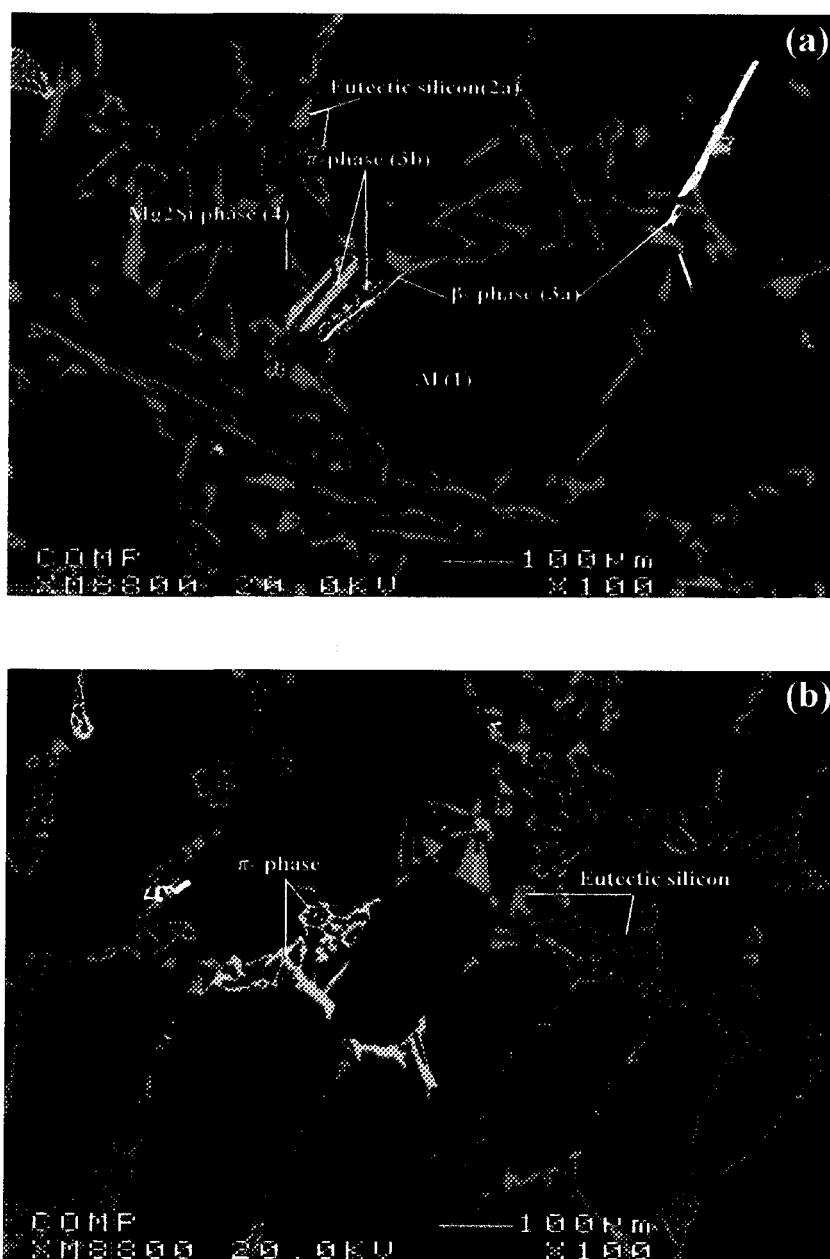
Figure 4.1 Backscattered electron images of 357 alloy in the (a) non-modified, and (b) Sr-modified conditions showing: (1) primary aluminum phase, (2a) eutectic silicon, (3a) β-Al5FeSi phase, (3b) π-AlFeMgSi phase, and (4) Mg_2Si phase.

4.3   Thermal Analysis

4.3.1   Effects of Iron and Magnesium Content

Thermal analysis was carried out in order to determine the precipitation sequence and formation temperature of the iron intermetallics observed in alloys 1AS (0.4%Mg-0.1%Fe) and 4AS (0.4%Mg-0.55wt%Fe). The reactions and corresponding temperatures obtained from the cooling curves for these alloys are listed in Table 4.2. As Figure 4.2(a) reveals, solidification of the 1AS alloy begins with the precipitation of α-aluminum (1), followed by formation of the Al-Si eutectic (2) together with the precipitation of the post-eutectic β-Al_5FeSi. It is expected that as solidification proceeds, the β-phase present will be transformed into the π-phase as a result of the peritectic reaction (3): $L+Al_5FeSi \rightarrow Al+Si+Al_8Mg_3FeSi_6$. The last reaction (4) to be detected is characterized by a wide peak, which may arise from two merged reactions. The first of these is related to the formation of Mg_2Si followed by the second reaction which corresponds to the quaternary eutectic reaction: $L \rightarrow Al+Si+Mg_2Si+Al_8Mg_3FeSi_6$. Upon comparing the first derivative curve in Figure 4.2(a) with the one shown in Figure 4.3(a) for alloys 1AS and 4AS, respectively, it will be seen that, at 0.1 wt% Fe, for alloy 1AS, the first derivative curve reveals four peaks, while at 0.55 wt% Fe, for alloy 4AS, a new peak marked as (2) may be observed before the peak for eutectic reaction, which corresponds to the formation of the pre-eutectic β-phase. Other reactions remain the same as those described on Figure 4.2(a).It has been reported [25, 99] that increasing the Fe content from 0.1 wt% to 0.55 wt% changes the solidification sequences of Al-7Si-0.4Mg alloys;

Table 4.2 Main reactions observed from thermal analysis data of alloys 1AS, 4AS, 14CS and 11CSB.

Alloy Code	Temp.($^{\circ}$C)	Reaction[15]
1AS 0.1%Fe-0.4%Mg	611 (1)	- Formation of Al-dendritic network
	570 (2)	- Precipitation of Al-Si- eutectic - Precipitation of post-eutectic β-Al$_5$FeSi phase
	560 (3)	- Transformation of β-phase into π-Al$_8$Mg$_3$FeSi$_6$ phase
	545 (4)	- Precipitation of Mg$_2$Si - Quaternary eutectic reaction*
4AS 0.55%Fe-0.43%Mg	611 (1)	- Formation of Al-dendritic network
	577 (2)	- Formation of pre-eutectic β-Al$_5$FeSi phase
	570 (3)	- Precipitation of Al-Si-eutectic - Precipitation of post-eutectic β-Al$_5$FeSi phase
	553 (4)	-Transformation of β-phase into π-Al$_8$Mg$_3$FeSi$_6$ phase
	543 (5)	- Precipitation of Mg$_2$Si - Quaternary eutectic reaction*
14CS(357) 0.55%Fe-0.78%Mg	610 (1)	- Formation of Al-dendritic network
	570 (2)	- Formation of pre-eutectic β-Al$_5$FeSi phase
	560 (3)	- Precipitation of Al-Si eutectic - Precipitation of post-eutectic β-Al$_5$FeSi phase
	551 (4)	-Transformation of β-phase into π-Al$_8$Mg$_3$FeSi$_6$ phase - Precipitation of Mg$_2$Si
	539 (5)	- Quaternary eutectic reaction*
11CSB(357) 0.1%Fe-0.77%Mg-0.05Be	612.5 (1)	- Formation of Al-dendritic network
	610 (2)	- Formation of Be-Fe phase
	558.7 (3)	- Precipitation of Al-SI-eutectic - Precipitation of post-eutectic β-Al$_5$FeSi phase
	550 (4)	-Transformation of β-phase into π-Al$_8$Mg$_3$FeSi$_6$ phase - Precipitation of Mg$_2$Si
	539 (5)	- Quaternary eutectic reaction*

* Quaternary eutectic reaction: L $\rightarrow$ Al+Si+Mg$_2$Si+Al$_8$Mg$_3$FeSi$_6$

Figure 4.2 (a) Temperature-time cooling curve and its first derivative obtained from the Sr-modified 356 alloy 1AS, and (b) the corresponding microstructure showing the small size of the β-phase and the π-phase particles.

this is thoroughly supported by the current thermal analysis. At 0.1 wt% Fe, the β-phase precipitates at low temperatures together with the Al-Si eutectic and is characterized by fine platelets in the microstructure, as shown in Figure 4.2(b). At 0.55 wt% Fe, however, most of the β-phase will precipitate at high temperatures before the Al-Si eutectic. This β-phase is characterized by its large size in the microstructure, as shown in Figure 4.3(b). Consequently, increasing the Fe content will increase the quantity and size of the β-phase in the microstructure, which is not favourable to the mechanical properties.

In order to arrive at a clearer understanding of the effect of magnesium on the precipitation sequence and reaction temperature, the Mg content in alloy 4AS was increased to 0.8 wt%, creating alloy 14CS. Two separate peaks were identified corresponding to reactions (4) and (5), as shown in Figure 4.4. The reactions and corresponding temperatures which occur during solidification of alloys 14CS and 4AS, containing high and low Mg levels, respectively are listed in Table 4.2 for comparison purposes. There is a significant reduction in the eutectic temperature by ~10°C in the higher Mg-containing alloy (14CS), compared to the low Mg-containing alloy (4AS), this is in agreement with published findings.[2,100] The same authors[100] reported that this reduction in eutectic temperature affects the modification of the eutectic Si particles.

Upon examination of the microstructure, the π-Al$_8$FeMg$_3$Si$_6$ phase is often observed to be in close contact with β-Al$_5$FeSi phase platelets. The inset in Figure 4.2(b) reveals that the interface between the β- and π-phase is seamlessly fused together, which may lead to the reasonable assumption that the β-Al$_5$FeSi phase will precipitate as a first step, followed

by the growth of the π-Al$_8$FeMg$_3$Si$_6$ phase from the surface of the β-Al$_5$FeSi thereafter, according to the L+Al$_5$FeSi $\rightarrow$ Al+Si+Al$_8$Mg$_3$FeSi$_6$ reaction.[15]
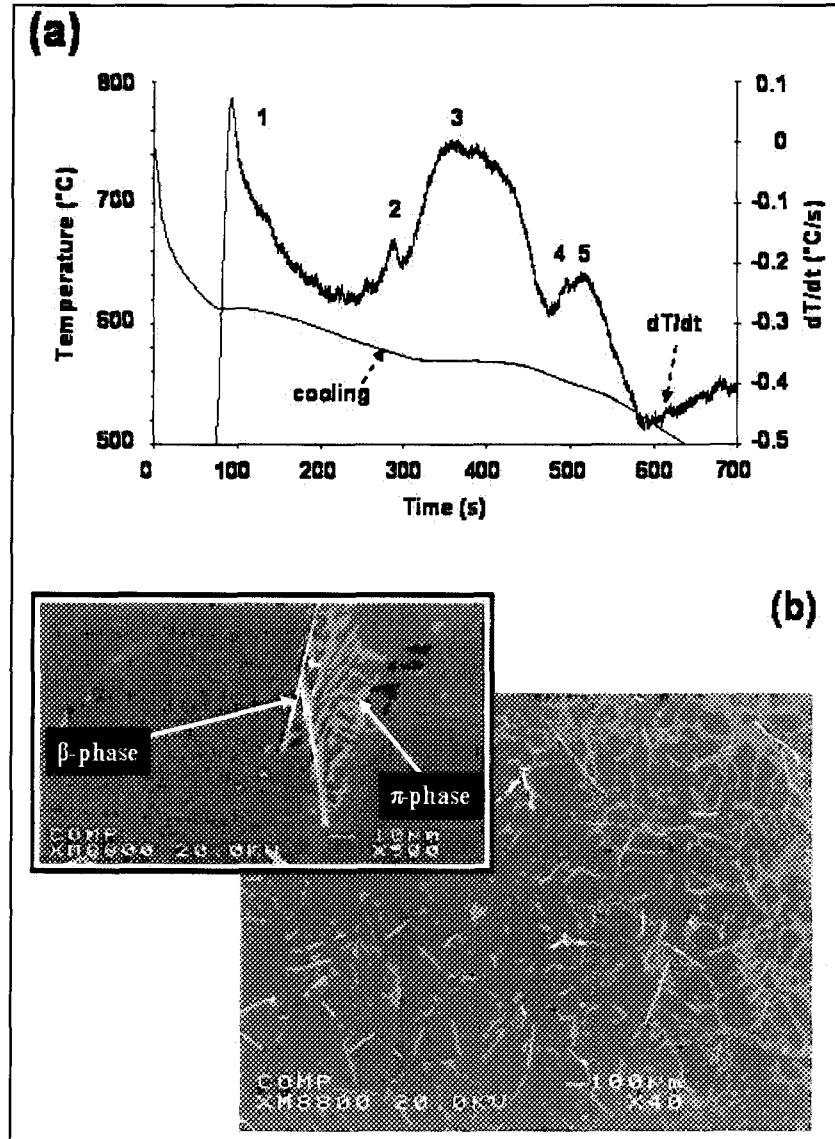
Figure 4.3   (a) Temperature-time cooling curve and its first derivative obtained from the Sr-modified 356 alloy 4AS; and (b) the corresponding microstructure showing the large size of the β-phase and the π-phase particles.
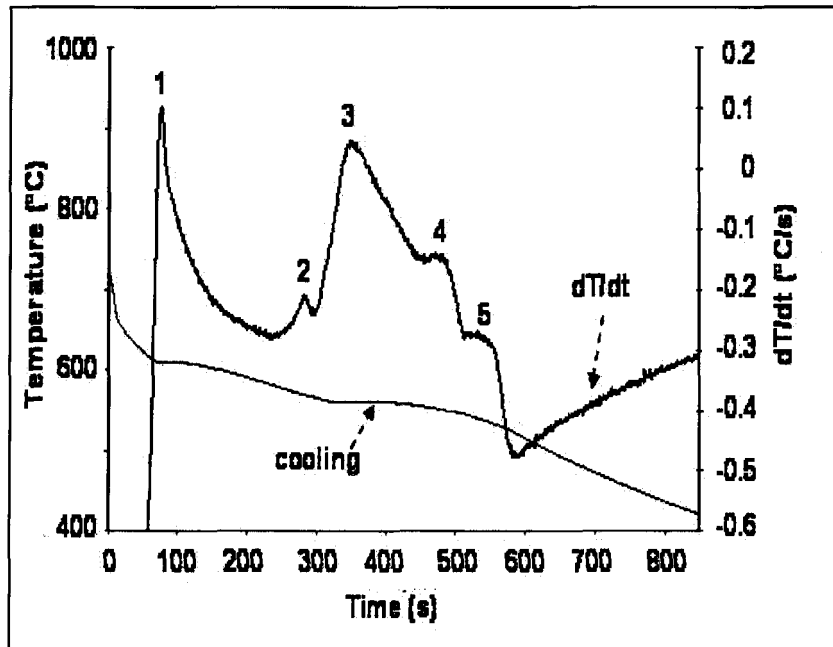
Figure 4.4 Temperature-time cooling curve and its first derivative obtained from the Sr-modified 357 alloy 14CS.

4.3.2 Effects of Beryllium Addition

The morphology of iron intermetallics illustrates the fact that there are several differences between Be-containing and Be-free alloys. The iron intermetallics observed in the optical microstructure of the Al-7Si-0.77Mg-0.92Fe-0.05Be alloy, coded 11CSB, and obtained from a graphite mold casting are (i) the nodular Fe-Si-Al phase with a composition close to Al_8Fe_2Si, and (ii) the Be-Fe phase with a script like morphology, as may be seen in Figure 4.5(a). This microstructure observation is in agreement with the reported literature concerning the microstructure of Be-containing 357 alloys.[101,96] It will be seen clearly from the microstructure in Figure 4.5(a) that the Be-Fe phase exists inside primary α-Al dendrites; this agrees with the corresponding thermal analysis results
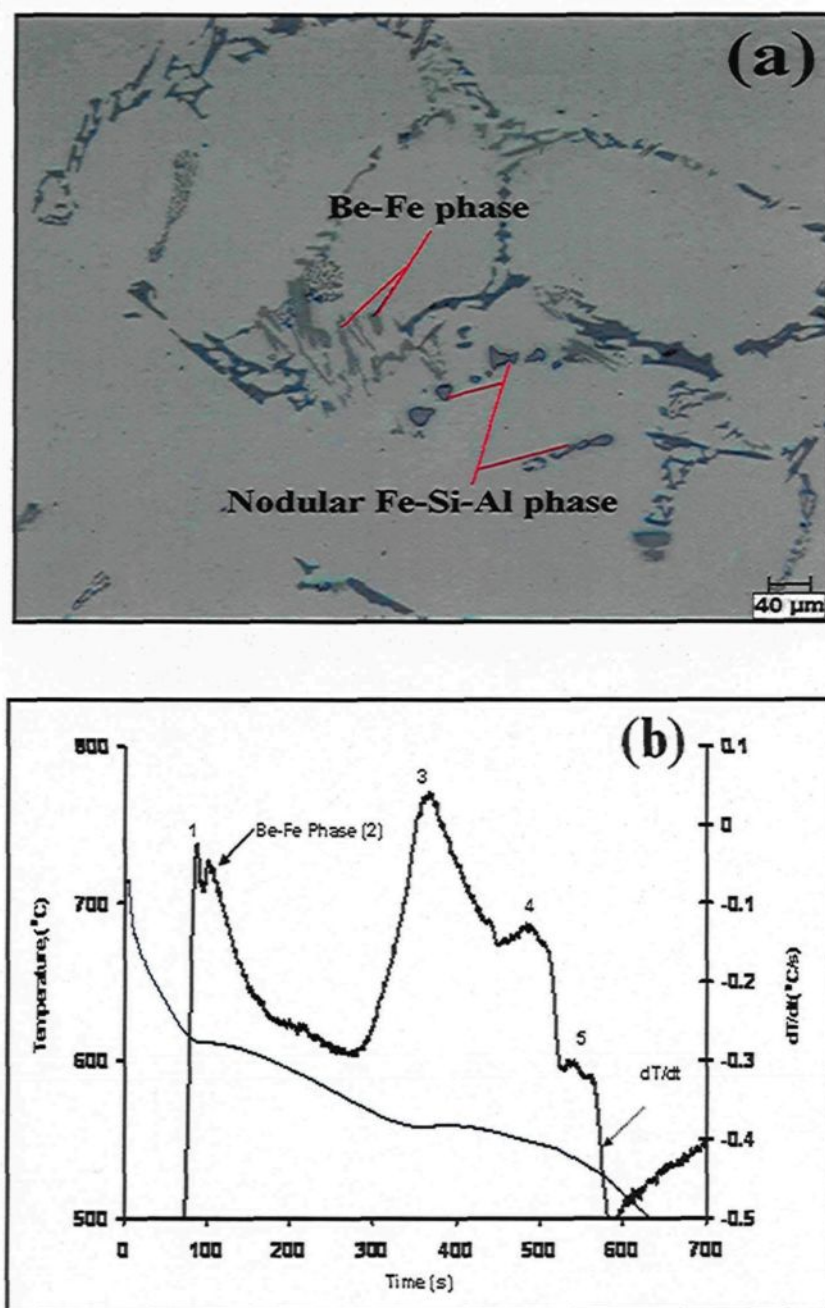
Figure 4.5 (a) Optical microstructure showing the Be-Fe phase formed inside the α-Al dendrite, and (b) the corresponding temperature-time cooling curve and its first derivative obtained from the Sr-modified Be-containing 357 alloy 11CSB.

obtained from the same alloy in which a reaction marked as peak (2) as detected, and presented in Figure 4.5 (b).The formation temperature of this reaction is about 610°C which is close to the formation temperature of α-Al. Also, this temperature is higher than the formation temperature of the pre-eutectic β-Al$_5$FeSi phase marked as peak (2) in Table 4.2 for the Be-free 4CS, as seen in Figure 4.4.

Based on observation of the microstructure and the corresponding thermal analysis data, the addition of Be results in a change in the precipitation sequence of the iron intermetallic whereby peak (2) in Figure 4.5 (b) show corresponds to the formation of the Be-Fe phase. In support of this observation, Murali et $al.$[97] carried out an interrupted quenching experiment to detect the formation temperature of the Be-Fe phase; they found that the Be-Fe phase exists in the microstructure at the point where the melt quenched from the liquid temperature at 607°C implying that the formation temperature of the Be-Fe phase must be higher than this temperature. The precipitation sequence and the corresponding temperatures for Sr-modified Be-containing Al-7Si-0.79Mg-0.1Fe alloy may be found in Table 4.2.

4.4   Qualitative and Quantitative Analyses

The following subsections will cover a qualitative and quantitative analysis of the π-phase formed in non-modified and Sr-modified Al-7Si-Mg alloys in terms of the various metallurgical parameters affecting its formation in said alloys.

4.4.1 Effects of Iron and Magnesium Content

Figure 4.6 illustrates the effects of Fe and Mg content on the volume fraction of the π-phase in non-modified and Sr-modified Al-7Si-xMg-yFe alloy samples obtained from graphite mold castings, (SDAS ~ 65μm), in the as-cast and solution heat-treated conditions. As the Fe content increases from 0.1 wt% to 0.8 wt%, the π-phase volume fraction increases by varying degrees in the non-modified and Sr-modified alloys at all levels of Mg content, as can be seen in Figures 4.6(a) and (b), respectively. Figure 4.6(b) demonstrates how the addition of 0.02 wt% Sr to Al-7Si-xMg-yFe alloys results in slight increases in the volume fraction of the π-phase, compared to Figure 4.6 (a). This may be explained in terms of the presence of Sr which results in breaking up β-phase platelets as reported by Samuel et al.,[70] thereby reducing the length and increasing the density of β-phase platelets. The authors claim that Sr was absorbed by the β-phase platelets leading to their destabilization, and hence, to their fragmentation. This may contribute to an increase in the number of β-platelets available for the peritectic reaction to occur thereby forming further amounts of π-phase.

Figure 4.6 also demonstrates the effects of solution heat treatment at 540°C/8hr on the π-phase volume fraction in non-modified and Sr-modified Al-7Si-xMg-yFe alloys. In non-modified Al-7Si-0.4Mg-yFe alloys, as shown in Figure 4.6(a), the π-phase is almost completely dissolved at all Fe levels after solution heat treatment. The non-modified Al-7Si-0.4Mg-0.1Fe alloy microstructures shown in Figures 4.7(a) and (b) support this
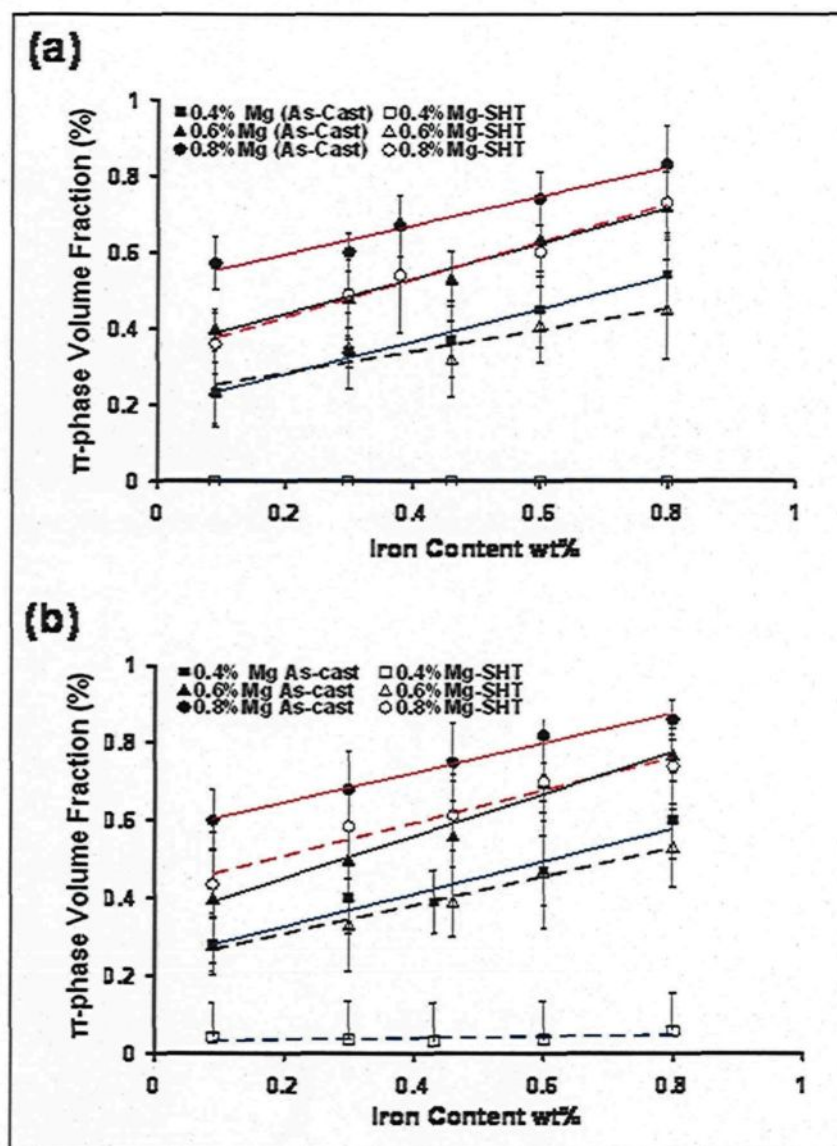
Figure 4.6 Effects of Fe and Mg content on the volume fraction of the π-phase intermetallic in Al-7Si-xMg-yFe alloys (SDAS = 65 µm) in the as-cast and solution heat-treated (540°C/8h) conditions: (a) non-modified alloys, and (b) Sr-modified alloys.
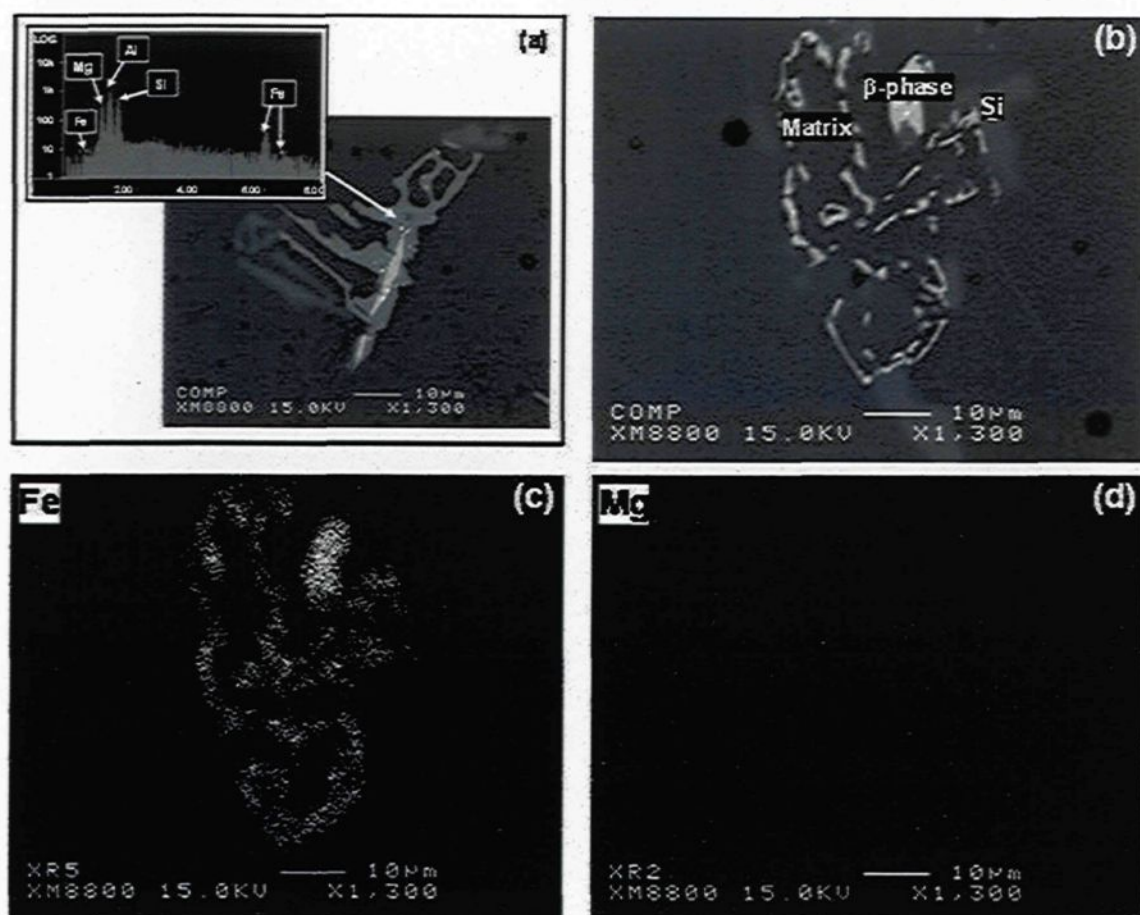
Figure 4.7   (a,b) Backscattered electron images of non-modified 356 alloy coded 1A in: the (a) as-cast condition, showing π-phase and β-phase particles, (b) after solution heat treatment (540°C/8hrs), showing complete decomposition of the π-Al$_8$Mg$_3$FeSi$_6$ phase into fine β-Al$_5$FeSi needles; (c,d) show X-ray images (c) Fe and (b) Mg corresponding to (b).

observation. Figure 4.7(a) shows the π-phase in the as-cast condition, while Figure 4.7 (b) reveals the presence of fine needles in the microstructure after solution heat treatment. The X-ray images of the Mg and Fe distribution within these fine needles are presented in Figures 4.7(c) and (d), respectively, and support the claim that the fine needles are indeed β-phase needles. This observation suggests that, during solution heat treatment, the π-phase in the 356 alloy having 0.4 wt% Mg is completely dissolved and decomposed into fine β-phase needles as a result of the presence of Mg which diffuses out from the π-phase and into the surrounding aluminum matrix. This observation confirms the findings of Taylor et $al.$[10] who reported that, at 0.3-0.4 wt% Mg, the as-cast Chinese-script in 356 alloys π-phase is reduced as a result of its transformation into clusters of fine β-phase needles.

On the other hand, in the solution heat-treated Sr-modified Al-7Si-0.4Mg-yFe alloys, the π-phase is not completely decomposed after solution heat treatment, may be seen from Figure 4.6 (b). This observation is supported by the microstructures of the solution heat-treated Sr-modified Al-7Si-0.4Mg-0.1Fe alloy in Figures 4.8(a) and (b), where Figure 4.8(a) shows the as-cast microstructure and Figure 4.8(b) reveals fine needles accompanied by small spheroidized π-phase particles. These spheroidized particles are expected to reveal the process of decomposition of the π-phase into β-phase needles. The X-ray images corresponding to the backscattered image of Figure 4.8(b), and showing the distribution of Fe and Mg in the decomposed π-phase, namely Figures 4.8(c) and 4.8(d), confirm this observation. Based on the latter, it may be suggested that the incomplete decomposition of the π-phase into β-phase needles in solution heat-treated Sr-modified Al-
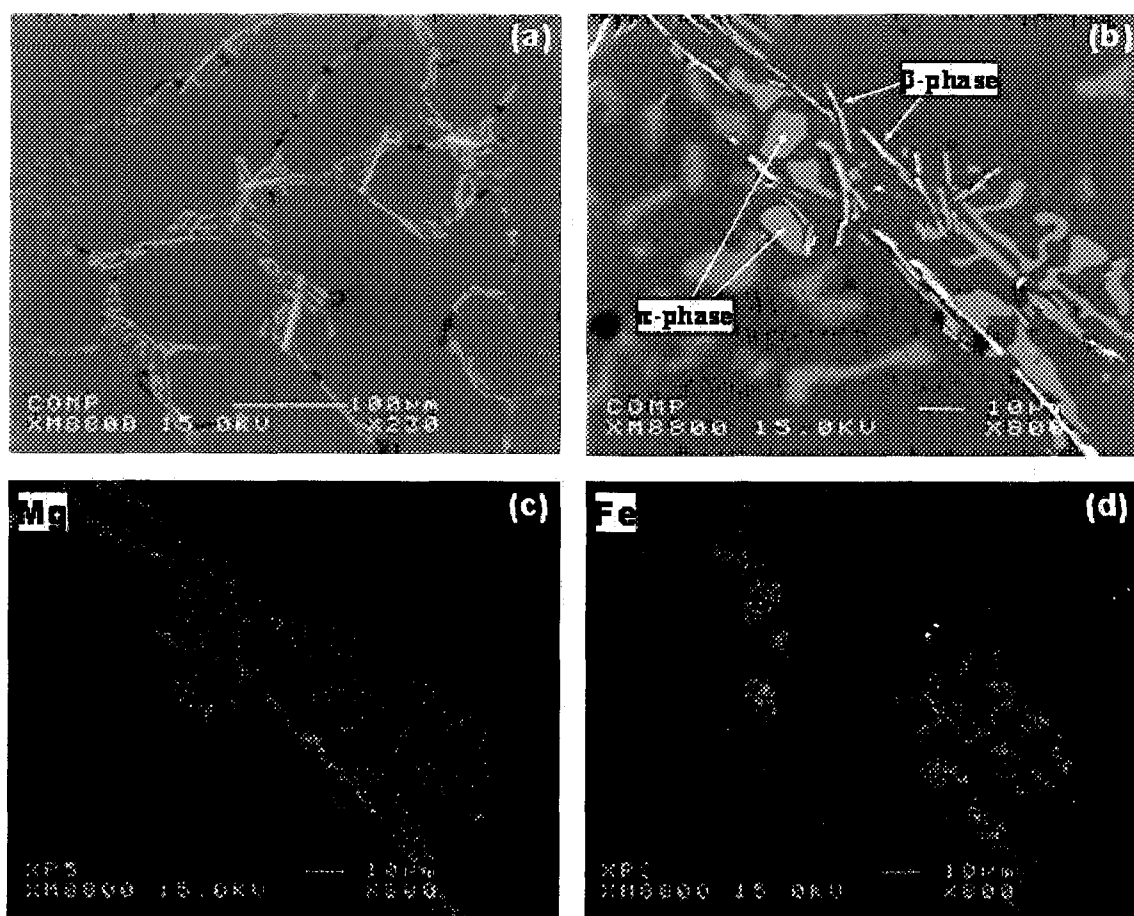
Figure 4.8 (a) and (b) show backscattered electron images of a Sr-modified 356 alloy coded 1AS in the (a) as-cast condition, showing π-phase and β-phase, (b) after solution treatment (540°C/8hrs) showing partial decomposition of π-$Al_8Mg_3FeSi_6$ into fine β-Al_5FeSi needles; (c) and (d) show X-ray images of Fe and Mg corresponding to (b).

7Si-0.4Mg-0.1Fe alloys is most likely related to the existence of moderately large π-phase

particles for which a longer solution heat treatment time of more than 8 hours may be

required to achieve complete decomposition of the π-phase. It will also be observed from

Figures 4.6(a) and 4.6(b) that when the Mg content in Al-7Si-xMg-yFe alloys is higher than

0.4 wt%, there is an increase in the resistance of the π-phase to decompose completely into

β-phase needles after 8hr of solution heat treatment in both the non-modified and Sr-

modified alloys compared to 0.4 wt% Mg alloys. This observation is supported by the

microstructures of the solution heat-treated non-modified Al-7Si-0.75Mg-0.1Fe alloy, as

shown in Figure 4.9. Figure 4.9(a) corresponds to the as-cast microstructure; Figure 4.9(b)

shows a small amount of the π-phase particles decomposed into fine β-phase needles, while

the remaining particles display fragmentation and spheroidization. The chemical

composition of the π-phase as obtained by WDS analysis of the as-cast and solution heat-

treated samples in the Al-7Si-0.8Mg-0.1Fe alloy, as listed in Table 4.3, reveals that there is

almost no change in the composition of π-phase in both conditions. It will be seen that the

calculated stoichiometry of the π-phase in both conditions approaches the suggested

formula of $Al_8FeMg_3Si_6$.[15]

Table 4.3 Chemical composition of the π-phase formed in the Al-7Si-0.8Mg-0.1Fe alloy before and after heat treatment.

.Alloy	Phase	Element (at%)				Formula	
		Al	Si	Fe	Mg	Calculated	Suggested[15]
Al-7Si-0.8Mg-0.1Fe (As-cast)	π-phase	48.3	27.0	5.88	18.57	$Al_{7.8}Fe_{0.95}Mg_3Si_{4.4}$	$Al_8FeMg_3Si_6$
Al-7Si-0.8Mg-0.1Fe (Solution heat treated)	π-phase	48.4	26.7	5.33	18.5	$Al_{7.8}Fe_{0.86}Mg_3Si_{4.3}$	$Al_8FeMg_3Si_6$
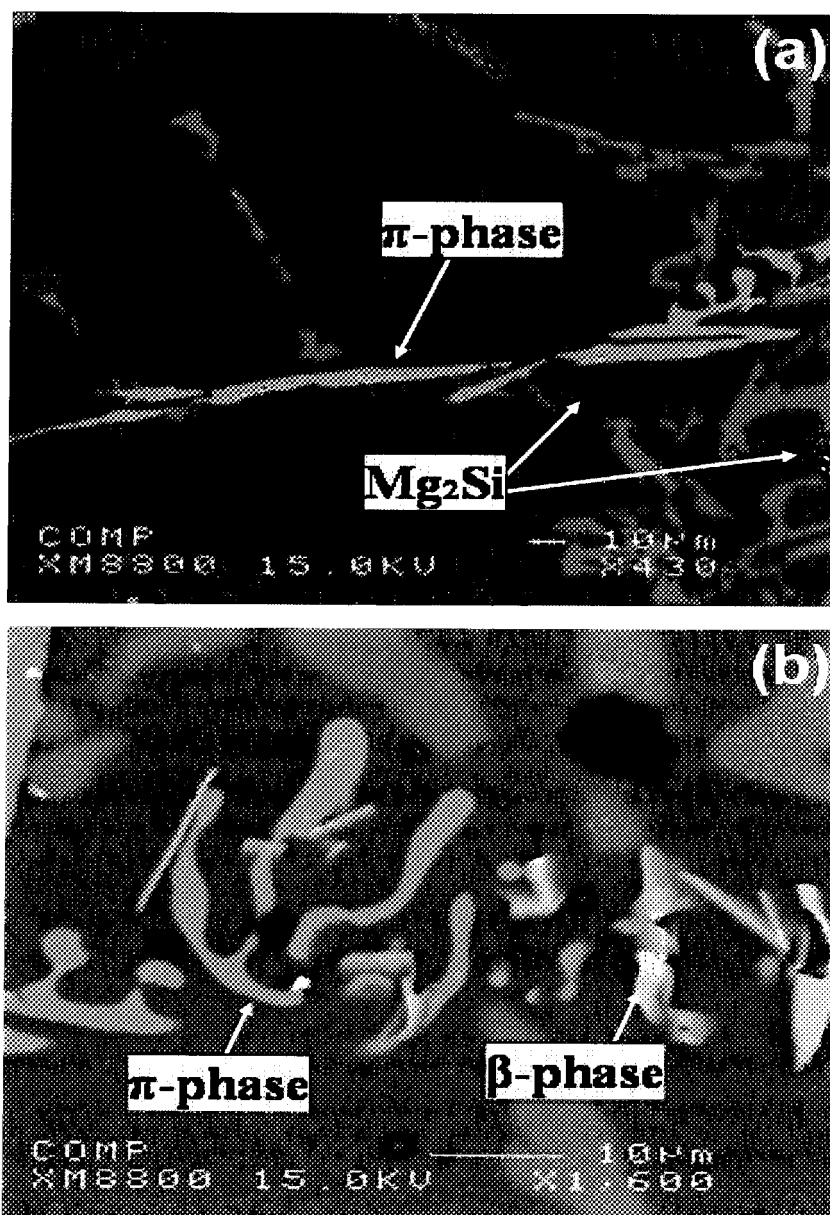
Figure 4.9   Backscattered electron images of a non-modified 357 alloy coded 11C in; (a) the as-cast condition, and (b) after solution heat treatment (540°C/8h), showing partial decomposition of the π-phase into fine β-phase needles.

It is apparent from Figure 4.6 that the lowest amount of π-phase volume fraction at all Mg levels occurs at 0.1 wt% Fe. The use of Al-7Si-xMg alloys containing low amounts of Fe is thus to be recommended from a practical viewpoint. Consequently, in this study, the effects of the other two parameters involved, namely the effects of beryllium addition and solution treatment time, will be examined mainly in the light of primary Al-7Si-xMg alloys containing a low iron content (~0.1wt%).

4.4.2 Effects of Beryllium Addition

The addition of 500 ppm Be to Al-Si-xMg-0.1Fe alloys containing 0.4, 0.6, and 1.0 wt% Mg, for samples obtained from graphite mold castings, has the potential for decreasing the amount of the volume fraction of the π-phase intermetallic in both non-modified and Sr-modified alloys, as shown in Figure 4.10(a) and (b), respectively. This reduction may be ascribed to two factors: (a) the effect of Be addition to Al-7Si-Mg alloys in transforming the β-phase into a Chinese-script α-AlFeSi iron intermetallic phase, as shown in Figure 4.11 with a stoichiometry of $Al_{6.9}Fe_2Si_{1.4}$ as determined by WDS analysis, approaching Al_8Fe_2Si, noted in the literature;[102] and (b) the formation of Be-Fe phases with script morphology in Be-containing Al-7Si-0.6Mg alloys, as shown in the BSE image of Figure 4.12. These Be-Fe phases form at higher temperatures than those of the pre-eutectic β-phase, as shown earlier in the cooling curves of Figures 4.5(a) and (b), thereby reducing the Fe available to form the π-phase at the end of the solidification sequences.
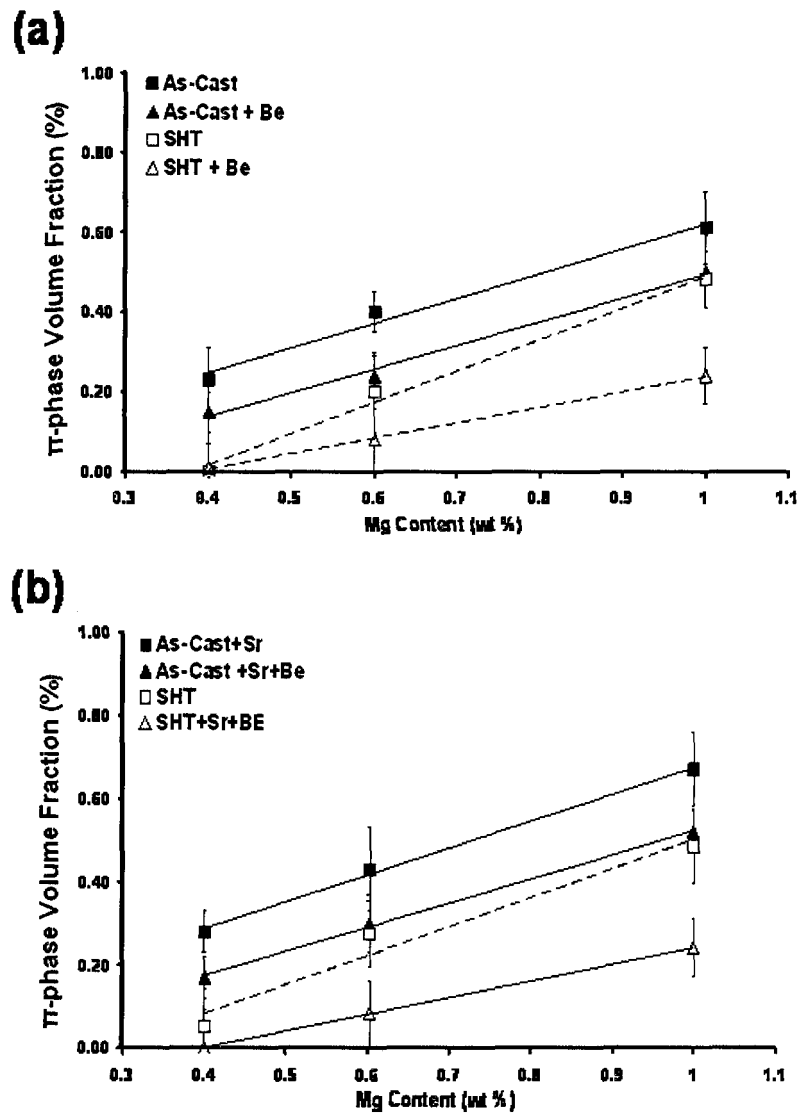
Figure 4.10 Effects of Be addation on the volume fraction of the π-phase in Al-7Si-xMg-0.1Fe Be-containing alloys: (a) non-modified alloys and (b) Sr-modified alloys.

Figure 4.11   Backscattered electron image of Be-containing 357 alloy 6CB in the as-cast condition, showing the α-Al$_8$Fe$_2$Si iron intermetallic phase.
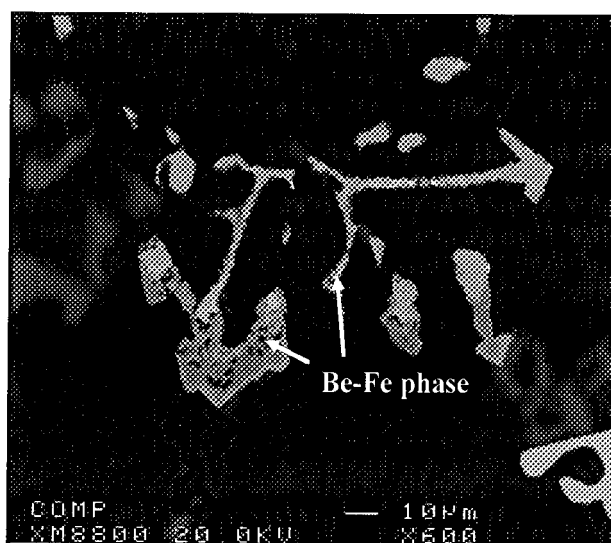
Figure 4.12   Backscattered electron image of Be-containing 357 alloy 6CBS in the as-cast condition, showing the Be-Fe phase.

A decrease in the π-phase volume fraction with respect to an increase in Mg content from 0.4 to 1.0 wt% was also observed after solution heat treatment in the non-modified and Sr-modified Be-containing Al-7Si-xMg-0.1Fe alloys, as shown in Figures 4.10(a) and (b), respectively. At 0.4 wt% Mg and after solution heat treatment, the π-phase is observed to have completely decomposed in both the non-modified and Sr-modified Be-containing alloys, while at 0.6 wt% Mg, the π-phase is seen to have only partially decomposed. This observation is supported by the Be-containing Al-7Si-0.6Mg-0.1Fe alloy microstructures, presented in Figure 4.13. Figure 4.13(a) shows the π-phase in the as-cast condition while Figure 4.13(b) reveals the decomposition of the π-phase into small β-phase particles after 8 hours of solution heat treatment at 540°C.

In order to acquire a clearer understanding of the role of Be in conjunction with a high amount of Mg, the Mg content in the Al-7Si-xMg-0.1Fe alloy was increased to 1.0 wt%. Figure 4.14(a) shows the microstructure of the as-cast Be-free Al-7Si-1.0Mg-0.1Fe alloy, while Figure 4.14(b) shows a large π-phase particle, seen on the right and small fragments of the spheroidized π-phase, seen on the left in a microstructure of the same alloy after 8hours of solution heat treatment at 540°C. The X-ray image in Figure 4.14(c) shows the distribution of Mg, confirming this to be the π-phase.

The addition of 500 ppm Be to the same Al-7Si-1.0Mg-0.1Fe alloy, on the other hand, results in the creation of small bright particles around the π-phase after solution heat treatment, as shown in the backscattered electron image of Figure 4.15(a). Figures 4.15(b),
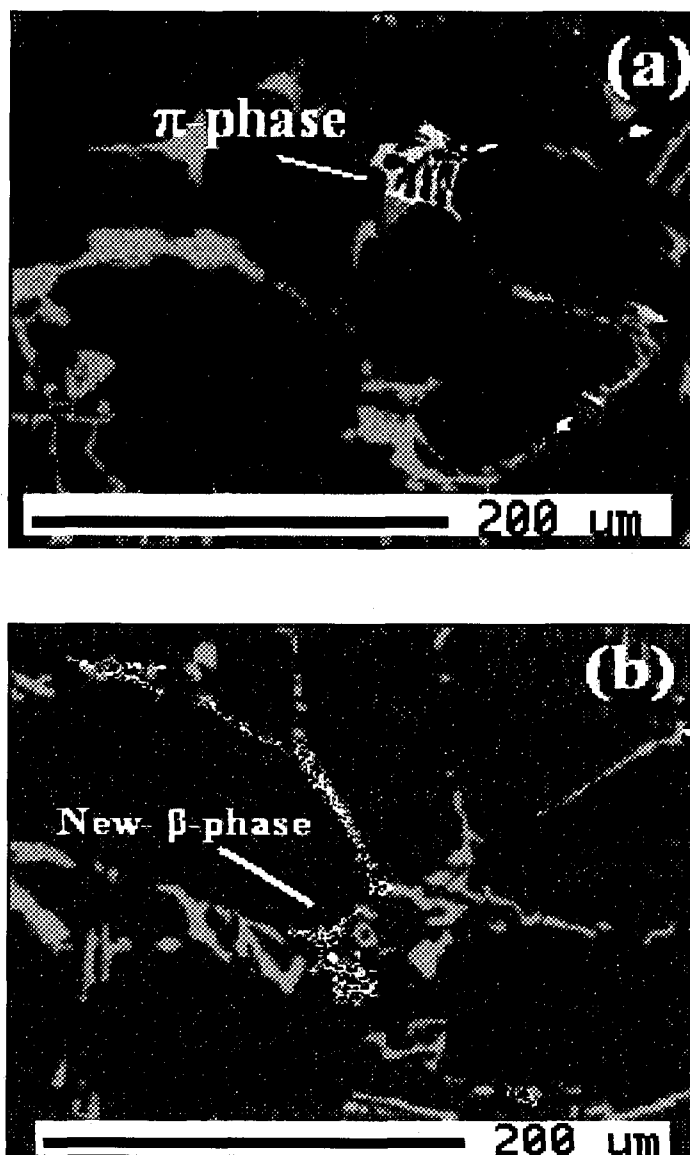
Figure 4.13   Backscattered electron images of Be-containing 357 alloy 6CB in the (a) as-cast condition, showing the π-phase intermetallic, and (b) after solution heat treatment (540°C/8hrs), showing the decomposition of π-phase into β-phase particles.
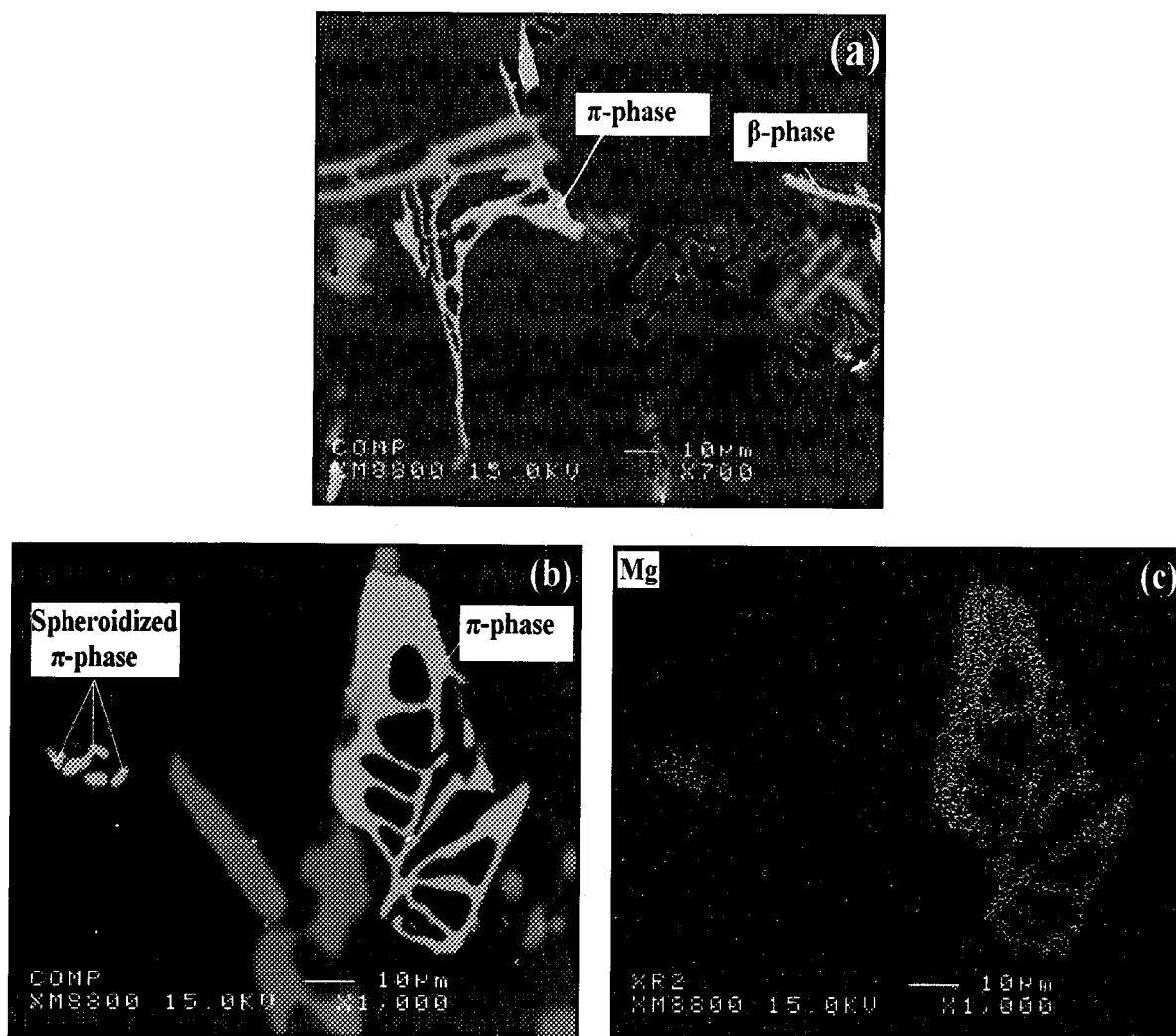
Figure 4.14 Backscattered electron images of Be-free Al-7Si-1.0Mg-0.1Fe alloy 16C in: (a) the as-cast condition, showing π- and β-phase particles, (b) after solution heat treatment (540°C/8h), showing the fragmentation of the π-Al$_8$Mg$_3$FeSi$_5$ phase; (c) X-ray image of Mg corresponding to (b).
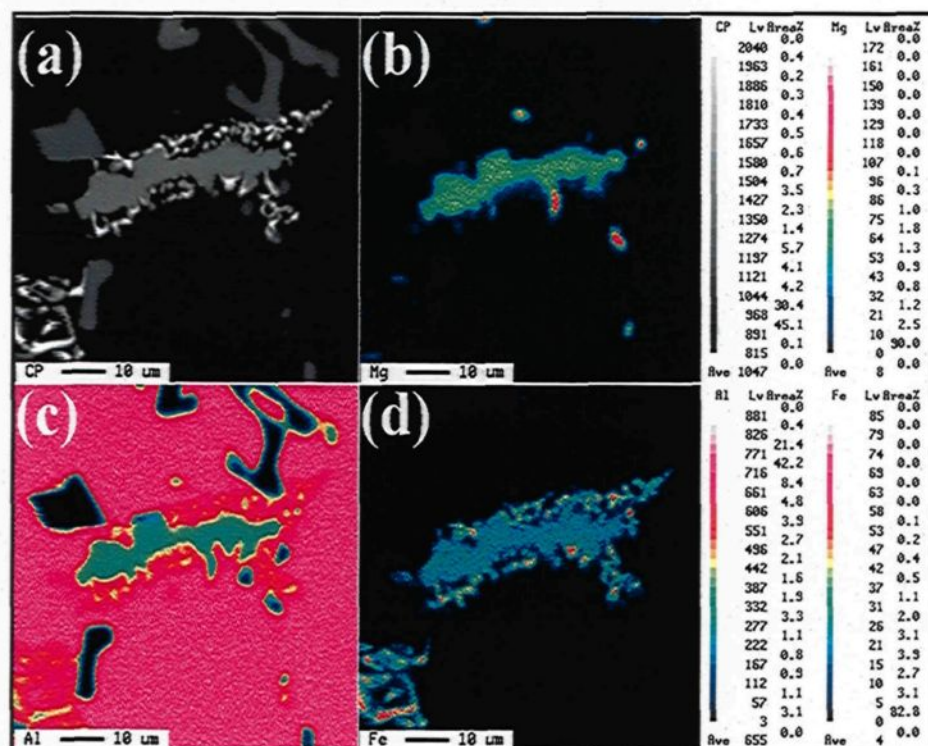
Figure 4.15 (a) Backscattered electron image obtained from Be-containing Al-7Si-1.0Mg-0.1Fe alloy 16CB after solution heat treatment (540°C/8hrs), showing the decomposed π-phase, and corresponding X-ray images of Mg (b), Al (c) and Fe (d).

4.15(c), and 4.15(d) depict the corresponding X-ray images of Mg, Al, and Fe, respectively, in the decomposed π-phase, supporting the assertion that the bright particles around the π-phase are new β-phase particles. According to this observation, it may be suggested that the addition of Be in amounts of 500 ppm to Al-7Si-xMg-0.1Fe alloys results in reducing the size and amount of the π-phase which facilitates its decomposition into β-phase particles during solution heat treatment, especially at high Mg levels, compared to Be-free alloys.

It has been reported[57] that the maximum solubility of Mg in Al-7Si-Mg alloys at 540°C is ~ 0.6 wt% Mg. Accordingly, based on the observations of the π- to β-phase

decomposition in Al-7Si-xMg-0.1Fe alloys, it may be suggested that the extent of the decomposition would depend on how far removed the Mg content of the alloy is from the solubility limit at 0.6 wt%; this implies that, in the alloys containing Mg levels higher than 0.6 wt%, the π-phase is likely to undergo only partial decomposition into β-phase needles even after long periods of solution treatment. On the other hand, for alloys containing less than 0.6 wt% Mg, it is to be expected that the π-phase will decompose almost completely into β-phase needles after a solution heat treatment of more than 8hours. In support of the latter suggestion, it was observed that an elevated quality index (Q) can be obtained in Al-7Si-Mg alloys with Mg contents of between 0.4 and 0.5 wt % which is less than the solubility limit in Al-matrix, and it was also observed that this is a range where the π-phase can decompose to a large extent into β-phase needles.[10] A gain in the Q may be expected if the π-to β-phase decomposition in Al-7Si-0.6Mg alloys is susceptible to being enhanced by solution heat treatments longer than 8hours. The following sections will thus focus on studying the effects of extended periods of solution treatment time and cooling rate on the decomposition of the π-phase in selected non-modified and Sr-modified Al-7Si-0.55Mg-0.1Fe alloys in order to understand the phenomenon of the π- to β-phase decomposition and how it affects the chemistry of the matrix and the mechanical properties.

4.4.3   Effects of Solution Heat Treatment Time

At any particular solidification rate, the resistance of the π-phase particles to undergoing complete decomposition into fine β-phase needles after standard heat treatment in selected Al-7Si-0.55Mg-0.1Fe 357 type alloys seems to be dependent on both of the

solution treatment parameters, namely, temperature and time. No attempt has been made so far to determine which one of these parameters is more effective in decreasing the resistance of the π-phase in these 357 alloys so as to bring about its complete decomposition into fine β-phase needles. It has been speculated that increasing the solution treatment temperature may decrease the resistance of the π-phase to undergoing complete transformation into fine β-phase needles in the 357 alloys containing more than 0.4wt% Mg.[10] Since the solution treatment temperature for this type of alloy is restricted to 540° ± 5°C to avoid localized melting at the grain boundaries,[57, 103] solution treatment time appears to be the only parameter available for regulating the extent of π- to β-phase decomposition.

Figures 4.16(a) and 4.16(b) show the variation in volume fraction of the π-$Al_8FeMg_3Si_6$ iron intermetallic phase as a function of solution treatment time and cooling rate, for the non-modified and Sr-modified Al-7Si-0.55Mg-0.1Fe alloys, respectively. These samples were obtained from two L-shaped metallic mold castings, one of them providing an SDAS of ~ 110µm while the other, an SDAS of ~ 35µm. The data appears to follow an exponential trend illustrating the decrease in volume fraction of the π-phase with increasing solution time of up to 100 hours for both non-modified and Sr-modified alloy samples obtained at the two cooling rates.
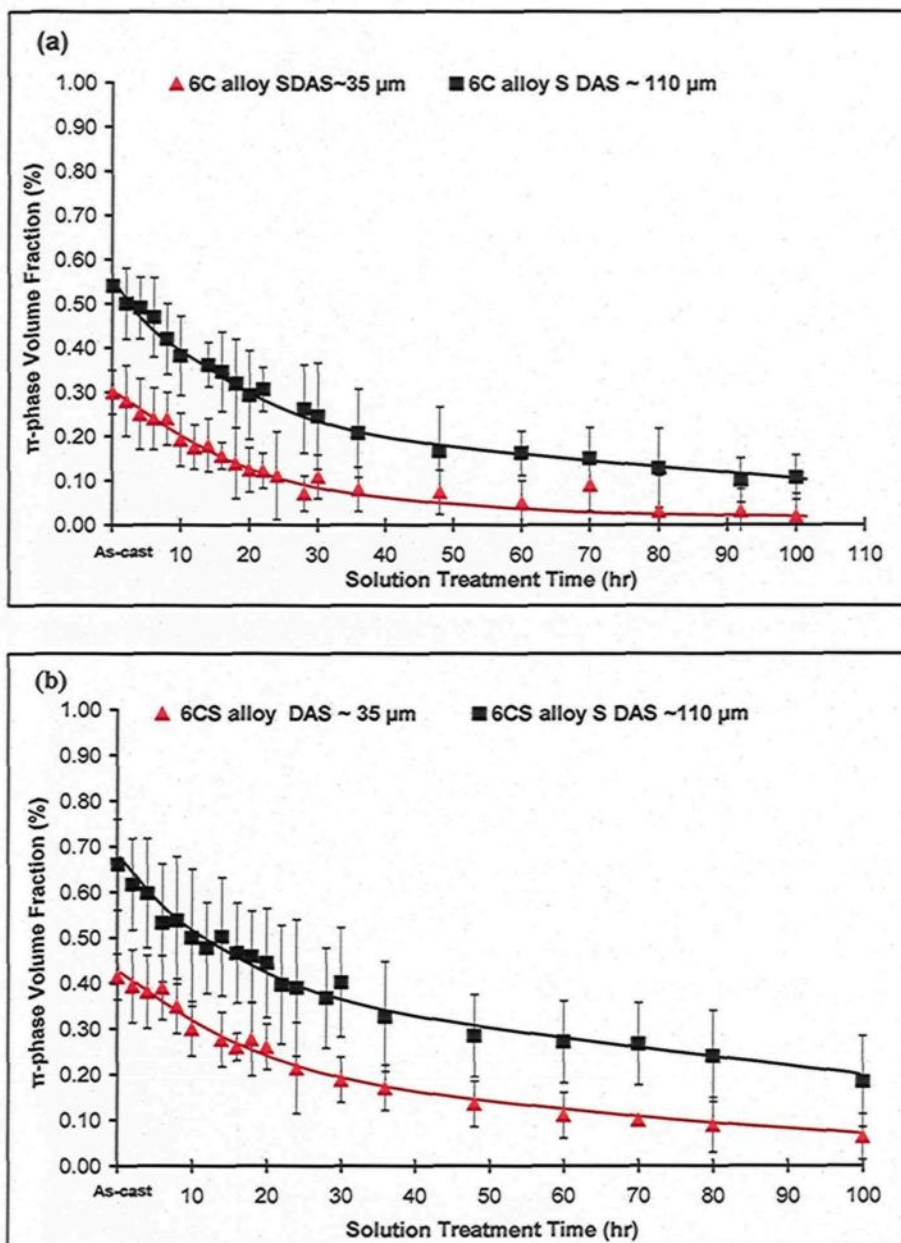
Figure 4.16. Effects of solution heat treatment time at 540°C on the volume fraction of the π-phase in Al-7Si-0.55Mg-0.1Fe alloy samples obtained at high and low cooling rates (SDASs of 35 μm and 110 μm) for (a) non-modified alloys, and (b) Sr-modified alloys.

It was also observed that the as-cast and solution-treated Sr-modified samples had a general tendency to exhibit a slightly higher π-phase volume fraction compared to the non-modified samples, especially at low cooling rates, that is to say at an SDAS of ~110 µm, as may be seen from a comparison of Figures 4.16(a) and (b). This observation corroborates the data presented in Figure 4.6(b), subsection 4.4.1. The high standard deviation in Figure 4.16 (b) is not considered an error in reading, but refers, rather, to the existence of large π-phase particles to be found in some areas away from the eutectic silicon regions in the microstructure of the Sr-modified samples, as will be substantiated by the backscattered electron image shown in Figure 4.1(b) when compared to Figure 4.1(a). The information which may be inferred from Figure 4.1(b) is in full agreement with the findings of Pennors et al.,[73] which reveal that the addition of Sr leads to local segregation of iron in certain areas, thereby favoring the precipitation of iron intermetallics. The segregation of the π-phase in Sr-modified as-cast and solution heat-treated samples can be reduced by using a high cooling rate, namely an SDAS of ~35 µm, as may be seen in Figures 4.16 (a) and (b).

The optical microstructures of the Sr-modified Al-7Si-0.55Mg-0.1Fe alloy shown in Figure 4.17 reveal the progress of π- to β-phase decomposition with the increase in solution time for two π-phase particles which are dissimilar in size. Figure 4.17(a) illustrates the as-cast microstructure showing a small blocklike π-phase particle marked "a" and a large scriptlike particle marked "b". After 16 hr of solution treatment, the π-phase particles "a" and "b" are broken down to varying degrees into small fragments and partially decomposed into β-phase needles, as shown in Figure 4.17(b). Upon increasing the solution treatment to
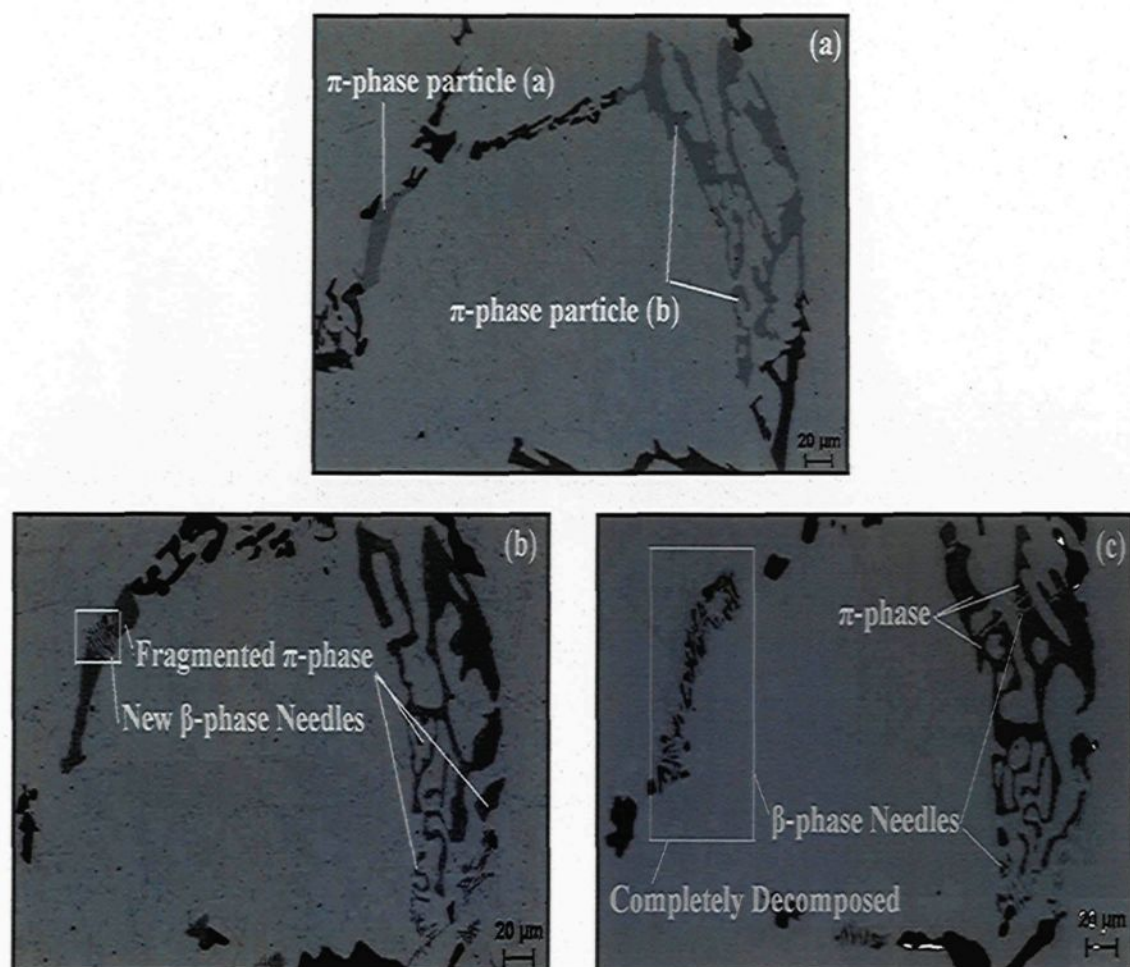
Figure 4.17 Optical microstructures showing the progress of decomposition of π- to β-phase in Sr-modified Al-7Si-0.55Mg-0.1Fe (SDAS~110 µm) in the (a) as-cast, (b) 540°C/16h ,and (c) 540°C/48h solution heat-treated conditions.

48 hrs, the fragmented π-phase particle "a" is completely decomposed into small β-phase needles, while particle "b" is still in the process of decomposition, as may be observed in Figure 4.17(c). It will be seen clearly that the π-phase particles show varying stages of decomposition into β-phase needles within the same sample. The time during which a π-phase particle starts and ends its decomposition differs from one particle to another within the same microstructure. In general, however, the π- to β-phase decomposition during solution heat treatment for times of up to 100 hours leads to a reduction in the π-phase volume fraction. This reduction is, as expected, accompanied by an increase in the newly formed β-phase volume fraction with respect to the solution treatment time, as may be observed from Figure 4.18.
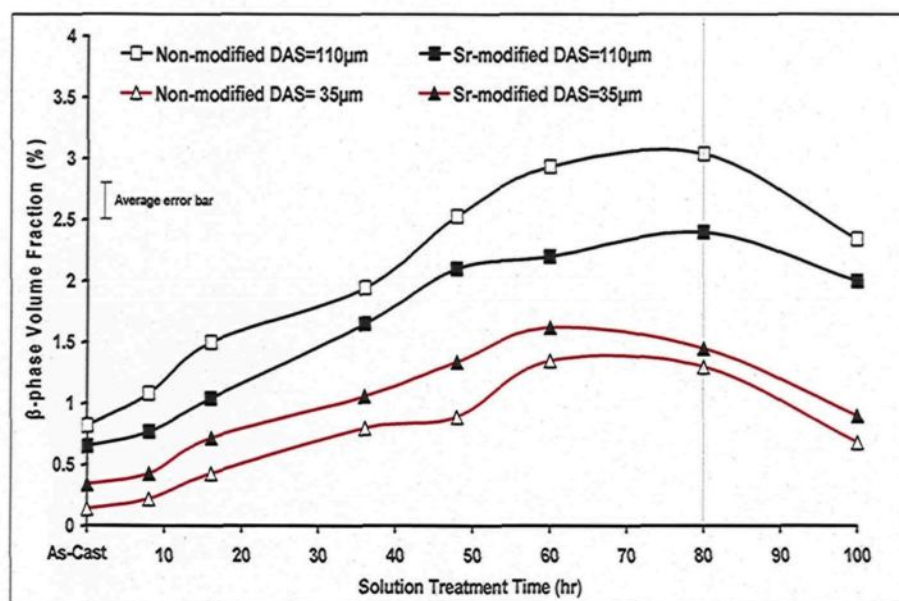
Figure 4.18 Effects of solution heat treatment time at 540°C on the volume fraction of the β-phase observed in non-modified and Sr-modified Al-7Si-0.55Mg-0.1Fe alloy samples obtained at two cooling rates, with SDASs of 35 μm and 110 μm.

In Figure 4.18, irrespective of the cooling rate, the volume fraction of the β-phase particles increases as the solution treatment time increases, in both non-modified and Sr-modified alloys; then, beyond 80 hours, it starts to decrease. The reason for this reduction in volume fraction may be attributed to the new β-phase needles which are formed during the early solution treatment period of 2 to 48 hours, such a needles become ultrafine by dissolution[85] making them difficult to measure even at a high magnification of 1000x after a prolonged solution treatment of over 80 hours.

On the other hand, the results show that there is no significant difference in the volume fraction of β-phase particles formed during solidification in the as-cast non-modified and Sr-modified samples for both low and high cooling rates, as can be seen from Figure 4.18. At the low cooling rate (SDAS ~110μm), however, the volume fraction of the new β-phase formed during the solution treatment of non-modified alloys is slightly higher than it is for the Sr-modified alloys. This slight increase in the newly formed β-phase needles may be related solely to the size of the π-phase in Sr-modified alloys as characterized by its large size, thus the number of the new β-phase needles formed during solution treatment as a result of π- to β-phase decomposition is expected to be less than it is for the non-modified alloy to a certain extent. At the high cooling rate (SDAS of ~35μm), no noticeable difference is to be observed in the newly formed β-phase volume fraction upon comparing non-modified and Sr-modified solution heat-treated samples.

The data presented in Figures 4.16(a) and (b) were replotted in the form of a log scale, as shown in Figure 4.19, in order to demonstrate the variation in the π- to β-phase

decomposition rate with respect to solution treatment time. As will be seen, the rate of π- to β-phase decomposition initially appears to be slow in the early part of the 8 hr solution treatment. For an extended period of 10 hours or longer, however, the π-phase decomposition rate accelerates. This variation in the decomposition rate with respect to solution heat treatment time may lead to the assumption that this π- to β-phase decomposition is a diffusion-controlled process which depends on the differences in concentration of the alloying elements, Mg and Si, with regard to the π-phase particles and the Al matrix, as well as solution treatment time.
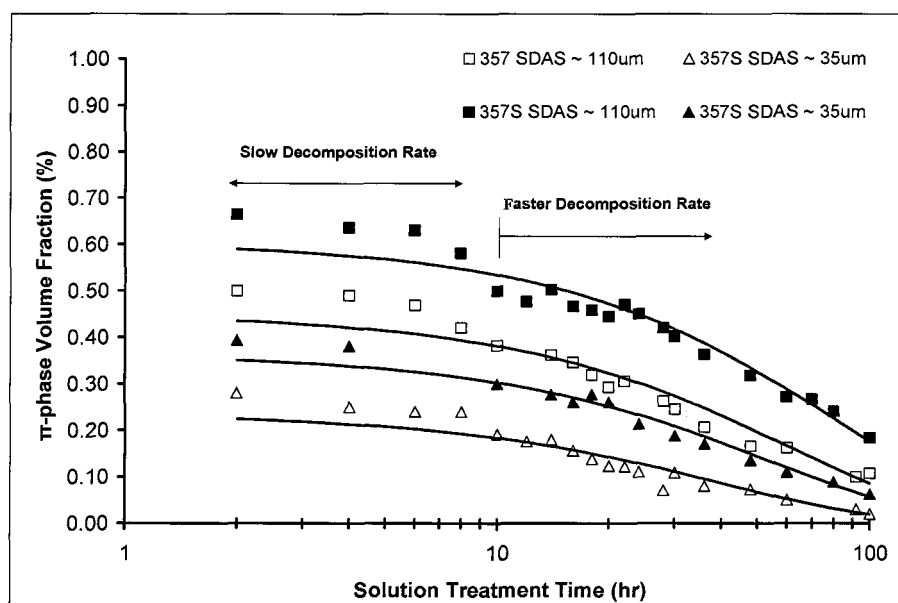
Figure 4.19 Effects of solution heat treatment time at 540°C on the volume fraction of the π-phase in Al-7Si-0.55Mg-0.1Fe alloy samples showing the variation in the π- to β-phase decomposition rate with respect to solution treatment time.

Line scans were carried out using electron probe microanalysis for Sr-modified samples which had been solution heat treated for 2 hours and 60 hours in order to

determine the distribution of the Fe and Mg concentrations along the lines AB passing through the iron intermetallic and the Al matrix, as shown in Figures 4.20(a) and (b), respectively.

Figure 4.21(a) reveals that the lowest concentration of Mg and Fe levels occurs at each of the two ends of the curves corresponding to the matrix, whereas large values for Mg and Fe concentrations may be noted when the path passes through the iron intermetallic particles. The high Mg reflections observable here together with the corresponding Fe reflections belong to the π-phase, while the strong Fe reflection refers to the point on the path where small bright particles of the new β-phase may be observed, as shown in the area marked by the small rectangle in Figure 4.20(a). Accordingly, the reason why the decomposition rate is slow within the time period of 2 to 8 hours may be attributed to the fact that the decomposition rate in this particular period is controlled by the formation of these bright particles or sites which are essential for forming the new β-phase needles during the decomposition process; this is well supported by the data provided in Figure 4.18 which reveals that there is no significant increase in the volume fraction of the newly formed β-phase needles in the early stages of the 8 hour solution treatment compared to that available in the as-cast condition.
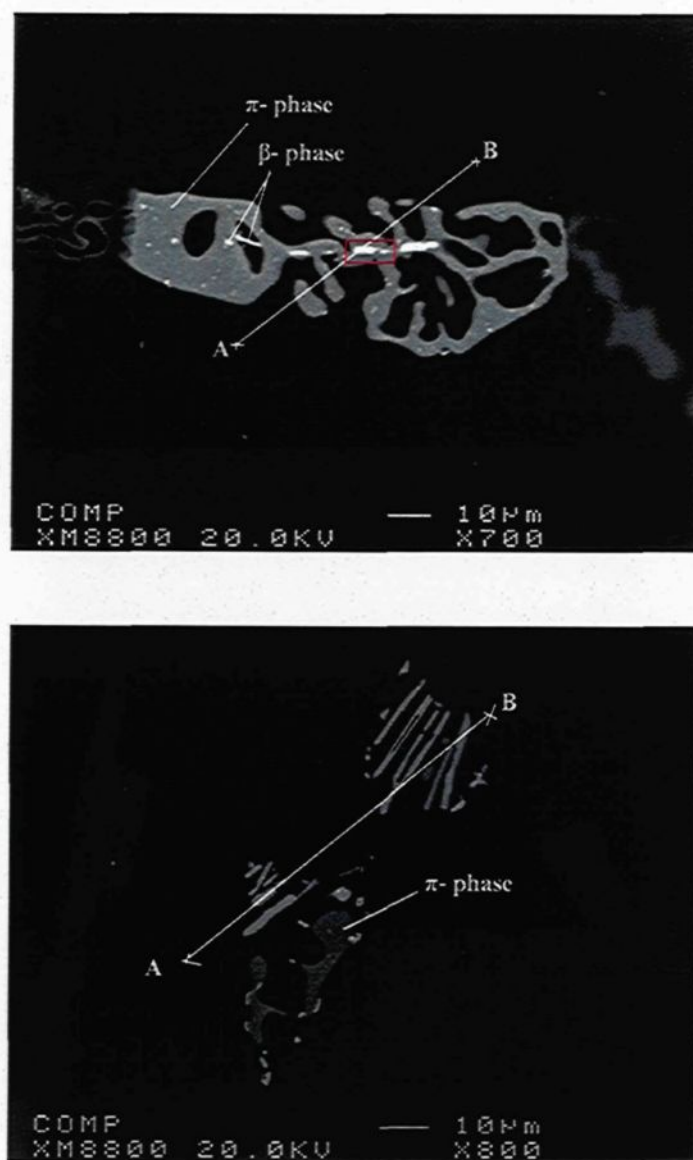
Figure 4.20 Backscattered electron images of iron intermetallics observed in the Sr-modified Al-7Si-0.55Mg alloy (SDAS=110μm): (a) 540°C/2h solution heat-treated sample, showing the β-Al$_5$FeSi phase particles with spheroidized π-Al$_8$Mg$_3$FeSi$_6$ phase particles; and (b) 540°C/60h solution heat-treated sample, showing the new fine β-Al$_5$FeSi needles.
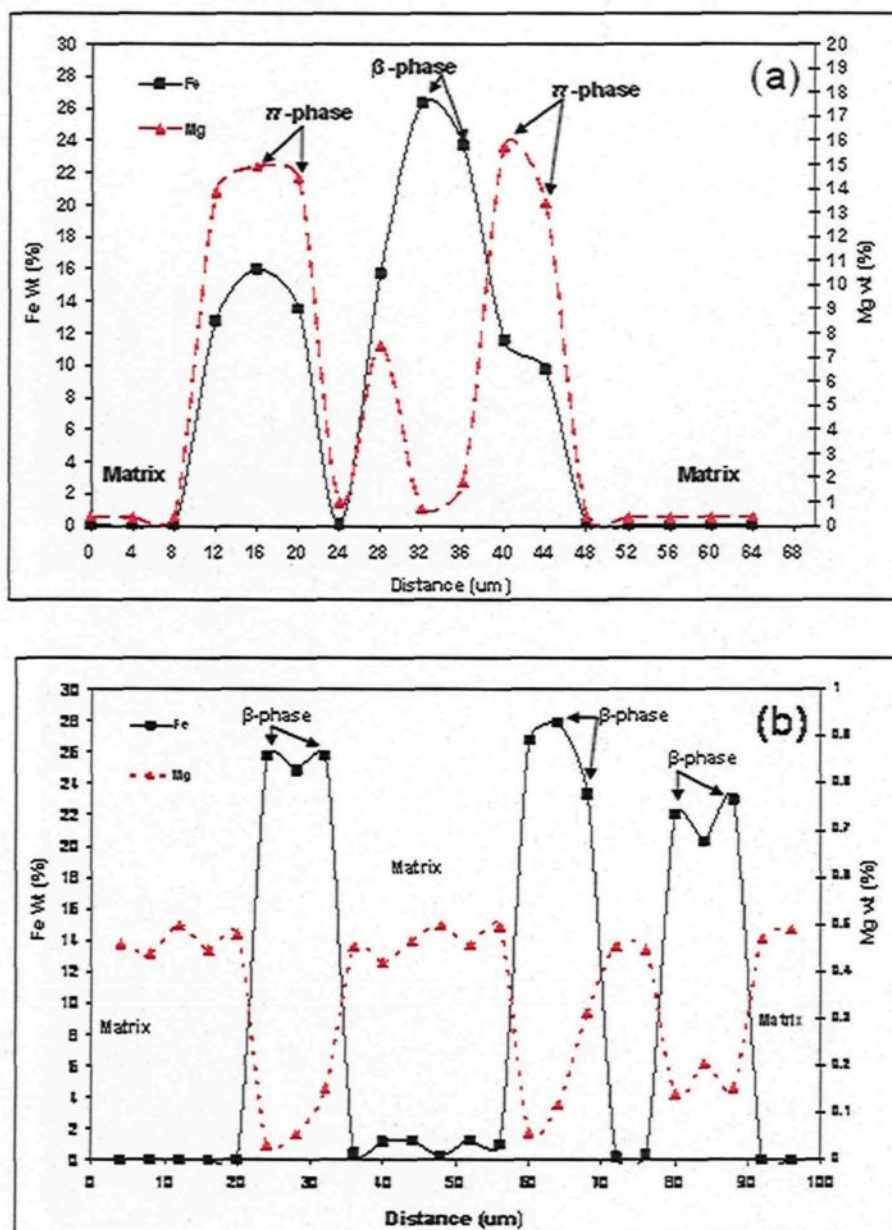
Figure 4.21 Line scans across the paths AB shown in Figure 14.20(a) and (b) for Sr-modified Al-7Si-0.55Mg-0.1Fe alloy showing the distribution of Fe and Mg in (a) 540°C/2h, and (b) 540°C/60h solution-treated samples. Note the difference in Mg content (scale) for the two cases.

With an increase in solution treatment time, the diffusive mass transport of Mg, which is the key element involved in the decomposition of the π-phase to the β-phase, is induced by the high Mg concentration gradient between the π-phase particles and the matrix, as may be noted in the line scan from Figure 4.21(a), causing these small bright particles or sites to start growing in size thereby forming new β-phase needles, and accelerating the rate of π- to β-phase decomposition. The greater the extent to which the π-phase particles will decompose into β-phase needles with increasing solution treatment time, the more the Mg content of the matrix will increase to a value which, in all probability, will approach the maximum Al-matrix solubility limits. This increase in the Mg content of the matrix creates the driving force for the decomposition to lessen, thus at 60 hours of solution treatment, or more, as may be seen from Figures 4.16(a) and (b), no noticeable change in the π-phase volume fraction values may be observed in any or all of the solution heat-treated alloy samples studied.

The preceding assertions are supported by the line scans shown in Figure 4.21(b) for the Sr-modified samples which had been solution heat treated for 60 hours in order to determine the distribution of the Fe and Mg concentrations along the line AB passing through the iron intermetallic and the Al matrix, as shown in Figure 4.20(b). As may be seen from Figure 4.21(b), the Mg content of the matrix increases from 0.35, as shown in Figure 4.21(a), to 0.47 wt%, which is close to the maximum solubility limit for Mg in the Al matrix at 540°C. The strong Fe reflection together with an extremely weak Mg reflection supports the observation that the needles or particles in Figure 4.20(b) indeed belong to the new β-phase.

4.4.4 Effects of Cooling Rate

It has been reported that applying a high cooling rate produces fine microstructural constituents and suppresses the formation of iron intermetallics by minimizing their .nucleation and eventual growth. [39,104] Increasing the cooling rate i.e; lowering the SDAS from ~110 μm to an SDAS of ~35 μm has a noticeable effect in reducing the volume fraction of the β-phase in the as-cast non-modified and Sr-modified alloys, as shown in Figure 4.18. Consequently, the π-phase formed as a result of the peritectic reaction which occurs during solidification in the as-cast samples (see peak 3 in Figure 4.2), is expected to decrease at the higher cooling rate.

Since the π-phase volume fraction in the as-cast alloy obtained at the high cooling rate is lower than the one observed at the low cooling rate, the volume fraction of the remaining undecomposed π-phase particles in the solution heat-treated samples at the high cooling rate will also be lower than the one observed at the low cooling rate, as will be seen in Figures 4.16(a) and (b). The volume fraction of the new β-phase needles will thus display lower values at the high cooling rate rather than at the low cooling rate for both non-modified and Sr-modified alloys, as shown in Figure 4.18.

In the as-cast Sr-modified alloy samples, results reveal that the amount of the Mg retained in the matrix at the high cooling rate (SDAS ~35μm) is, on average, 0.32 wt% which is higher than the average value of 0.21 wt% Mg observed at the low cooling rate where the sample SDAS is ~110μm. Consequently, the π-phase volume fraction formed in

the as-cast samples at the high cooling rate is lower than it is at the low cooling rate. The Mg measurements were taken at random positions throughout the matrix away from any intermetallic particles and was averaged over 5 such measurement readings.

4.5   Impact of π- to β-Phase Decomposition on Matrix Chemistry

Most of the dissolution and decomposition processes of intermetallics in Al-Si-Mg alloys during heat treatment are governed by the diffusion of alloying elements. The diffusion of Fe, Si, and Mg inside the Al-matrix occurs through the vacancy mechanism. Each of the alloying elements has a certain diffusion coefficient which depends on the temperature in accordance with the Arrhenius equation.[105] At 540°C, the diffusion coefficient of Fe is very low ($5.70 *10^{-15}$ m^2/s) when compared to the diffusion coefficients of Mg and Si.[106]

Figure 4.22 shows the Si/Fe ratios of the π-phase and β-phase in the Sr-modified as-cast and solution heat treated samples as a function of solution treatment time, where the π-phase displays a higher Si/Fe ratio than the β-phase; this may suggest that, since Fe has low solubility in the Al matrix,[107] it would be the Si that diffuses out of the π-phase, providing a new Si/Fe ratio which is the β-phase, having a new atomic arrangement. The Si/Fe ratio of the β-phase and that of the π-phase appears to be constant throughout the solution treatment which may imply that the stoichiometries of these two intermetallics did not undergo any change during the solution treatment process.
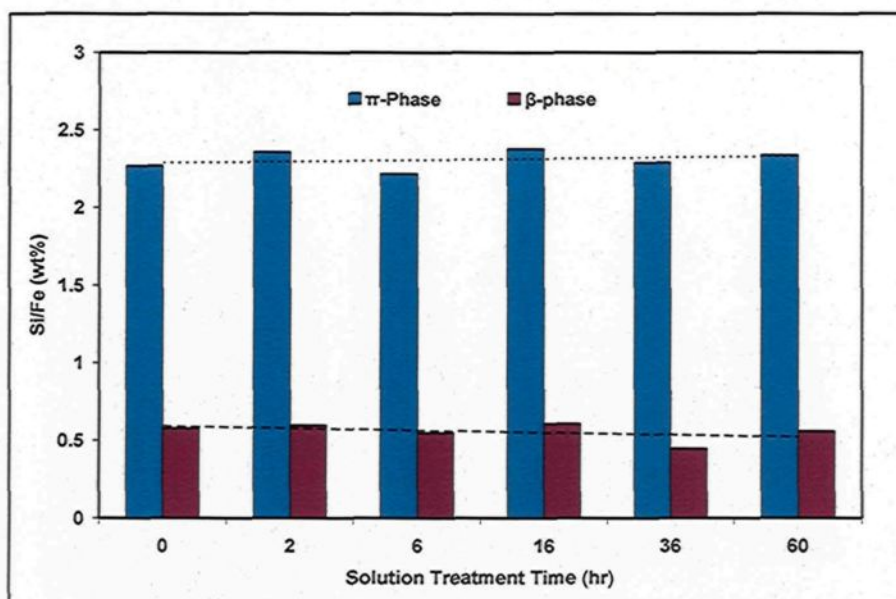
Figure 4.22 Si/Fe ratios of π- phase and β-phase observed in the as-cast and solution heat treated samples of the Al-7Si-0.55Mg-0.1Fe alloy at 540°C for up to 60 hrs.

It is evident from the above discussion that, for the π-phase to dissolve partially and decompose into fine β-phase needles particles during solution heat treatment, the Al, Mg, and Si must diffuse from the π-phase intermetallic particles in varying degrees so as to dissolve in the Al-matrix; this process is expected to occur as follows:

$$Al_8FeMg_3Si_6 \rightarrow Al_5FeSi + 3Al + 3Mg + 5Si$$
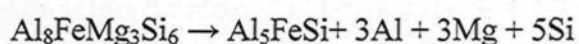
The main outcome of π- to β-phase decomposition during solution treatment is based on how this decomposition affects the Mg content in the matrix, thereby representing a significant factor in enhancing the mechanical properties of Al-7Si-Mg alloys during aging. Table 4.4 shows the composition of Fe, Si, and Mg in the matrix of non-modified and Sr-modified Al-7Si-0.55Mg-0.1Fe alloy samples (SDAS~110μm) before and after

solution treatment, as obtained by WDS analysis averaged over 10 readings per sample. In the Sr-modified alloy, the Mg content in the as-cast matrix is 0.21 wt%, while the Mg content in the bulk alloy is 0.55 wt%, hence the remaining 0.34 wt% Mg should be tied up in the Mg_2Si and the π-phases. After 2 hours of solution treatment, the Mg value increases to 0.35 wt%. According to data obtained from a study carried out by Rometsch et al.,[108] the dissolution of the Mg_2Si phase in the A357 alloy can be expected to occur in less than 2 hours, hence the increase in the Mg content observed in the matrix after 2 hours solution treatment must therefore come from the dissolution of large amounts of Mg_2Si and from the partial decomposition of small amounts of the π-phase.

Increasing the solution time to 20 hours has an observable effect on the Mg content of the matrix, increasing it from 0.35 to 0.42 wt%. This increase originates in the decomposition of a large amount of π-phase. The increase of solution time from 20 to 60 hours appears to contribute little to increasing the Mg content in the matrix from 0.42 to 0.47 wt%. After 60 hours solution treatment, however, this Mg content is found not to be equal to the bulk Mg content in the alloy, namely 0.55 wt%, the remainder, therefore still existing in the undecomposed π-phase. The reason for which the Mg content in the matrix did not attain the bulk Mg content of the alloys may be related to the possibility that the matrix reached its maximum Mg solubility limit since the Al-7Si-0.55Mg-0.1Fe alloy used cannot be deemed a ternary alloy; thus the π-phase particles in the current study are not completely decomposed even after a solution treatment of up to 100 hours at 540°C.

Table 4.4   Average composition of Si, Fe, and Mg in the matrix of non-modified and Sr-modified alloy samples in the as-cast and solution heat treated conditions.

Alloy Code	Condition	Matrix Composition wt (%)					
		Si		**Fe**		**Mg**	
		Av	**SD**	**Av.**	**SD**	**Av.**	**SD**
6C	As-cast	0.98	0.2	0.03	0.01	0.22	0.01
6CS	As-cast	0.94	0.17	0.02	0.02	0.21	0.03
6C	540°C/ 2h	1.02	0.01	0.04	0.016	0.33	0.02
6CS	540°C/ 2h	1.1	0.01	0.03	0.014	0.35	0.01
6C	540°C / 20h	1.14	0.01	0.06	0.01	0.45	0.01
6CS	540°C / 20h	1.16	0.06	0.05	0.01	0.42	0.01
6C	540°C / 60h	1.4	0.05	0.04	0.01	0.48	0.02
6CS	540°C / 60h	1.41	0.07	0.07	0.019	0.47	0.01

As was expected, the results in Table 4.4 show that there is no significant change in the Fe content of the matrix between the as-cast and solution heat treated samples. The data presented in Table 4.4 also reveals that the average Si content of the matrix is in the range of 0.94 wt% in the as-cast Sr-modified sample. The remaining 6.06 %wt % of silicon content is present in the form of eutectic silicon particles, Mg_2Si, as well as in the π- and β-phase iron intermetallics. In the solution heat-treated Sr-modified samples, there is a slight change to be observed in the Si content of the matrix after 2 and 20 hours of solution treatment compared to the as-cast condition. In their study, by Taylor et al.,[109] did not report any change in the Si content of the 357 alloy matrix after 16 hours of solution treatment; their measurements, however, were based on randomly selected dendrite centres,

claiming that the silicon content of the matrix depends, not on the solution time, but on the solution treatment temperature.

As the maximum Si solubility limit in the Al-Si-Mg alloys is 0.9 wt% at 540°C.[57] the results obtained reveal an unexpected increase in the Si content of the matrix for the sample solution heat treated for 60 hours, as shown in Table 4.4. These results, however, are based on measuring the Si, Fe, and Mg content of the matrix using WDS analysis. These measurements are close to the iron intermetallics in the interdendritic region within a range of 10 to 15 μm from each of the sides with the possibility of probe interaction with any close Si particle. Results reveal that there is no variation between the Mg, Fe, and Si contents of the matrix, between non-modified and Sr-modified as-cast and solution-treated samples.

4.6   Mechanism of π-to β-Phase Decomposition

Figures 4.23(a) and (b) are backscattered images showing the decomposition of π-phase particles during solution heat treatment. Figure 4.23(a) shows a π-phase particle in an alloy sample after solution treatment of 10 hours. Small bright fragmented β-phase particles are to be observed at the π-phase/Al-matrix interface; also, some of these small particles exist inside the bulk of the π-phase particle. It would appear that these small particles act as nuclei around which the new β-phase needles start to grow during the process of decomposition.
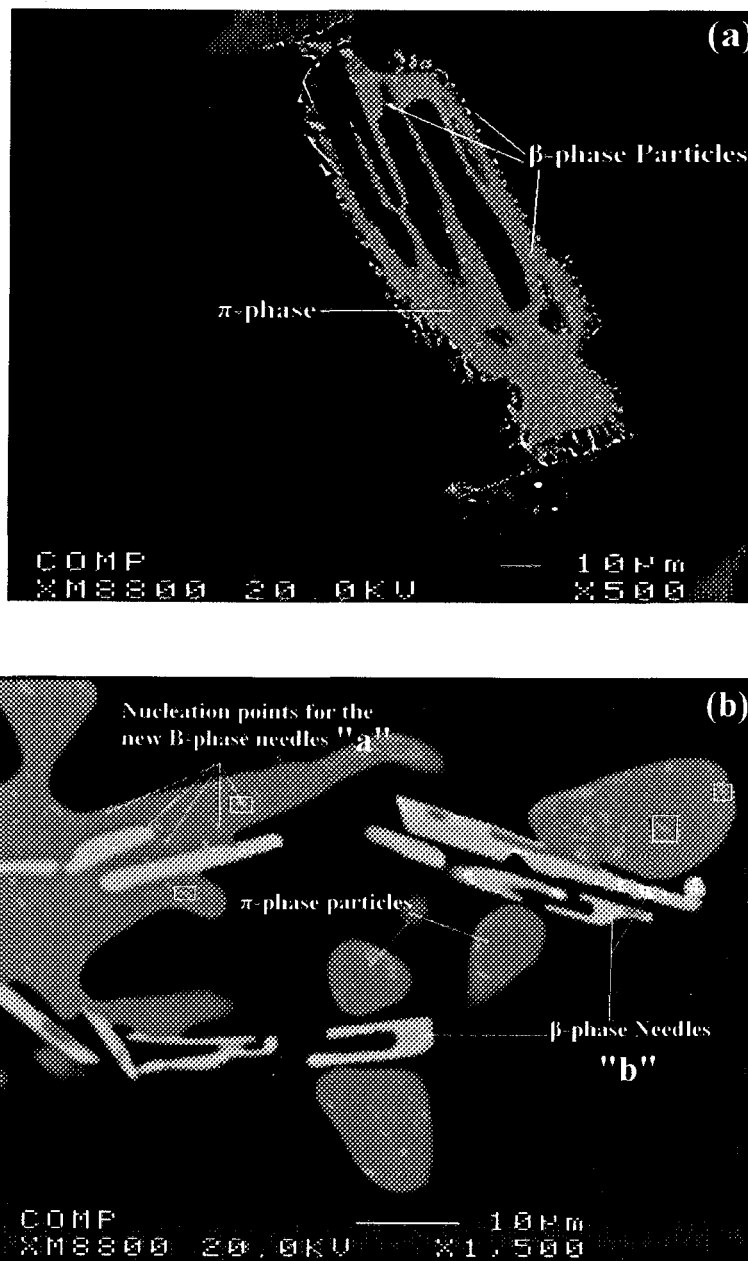
Figure 4.23 Backscattered electron images showing the mechanism of π- to β-phase decomposition in Al-7Si-0.55Mg-0.1Fe alloy samples (SDAS ~110μm): (a) solution heat-treated (540°C/10h) sample showing small, bright β-phase particles around and inside the π-phase particle; and (b) solution heat-treated (540°C/36h) ample showing breakdown of π-phase particles and growth of β-phase needles.

With an increase in the solution treatment time to 36 hours, as shown in Figure 4.23(b), the small nuclei start to grow in size (see boxed area on the π-phase particle marked "a") forming complete β-phase needles (see particles marked "b"), causing the breakdown of the π-phase particles into smaller, spheroidized fragments. Upon increasing the solution treatment time, the fragmented π-phase particles start to dissolve partially and decompose completely into a new set of small β-phase needles in the same manner as occurred earlier, until all the π-phase particles are consumed. Strontium modification has no effect whatsoever on the mechanism by which the π-phase decomposes into fine β-phase needles during solution treatment

4.7   Conclusions

Based on an analysis of the results presented in this chapter, the following conclusions may be drawn.

1- Analysis of the Al-7Si alloys with varying amounts of Mg and Fe indicates that the amount of the π-phase increases as the wt% of both elements is increased.

2- After the standard 8 hour solution treatment, the Chinese-script π-phase is completely decomposed into fine needles of the β-phase at 0.4 wt% Mg, but appears to be only partially decomposed at higher Mg contents, namely 0.6 - 0.8 wt%.

3- Qualitative and quantitative analyses of solution heat treated Al-7Si-xMg-0.1Fe alloy samples reveal that the optimum Mg levels at which the π-phase shows a high

degree of decomposition into the β-phase is in the range 0.4 -0.6 wt% Mg for all solution heat treated samples studied.

4- The addition of 500 ppm Be reduces the amount of the π-phase formed in Al-7Si-xMg-0.1Fe alloys, such additions also facilitate the decomposition of the π-phase into the β-phase, particularly at higher levels of Mg content, that is to say, 1.0 wt%.

5- In all the Al-7Si-0.55Mg-0.1Fe type alloys studied, long solution treatment times lead to a significant reduction in the volume fraction of the π-phase through the dissolution and decomposition of the π-phase into fine β-phase needles. Not all π-phase particles, however, undergo complete decomposition even after 100 hours of solution treatment.

6- During solution heat treatment, the π-phase shows partial dissolution before or during its decomposition into the β-phase needles. The decomposition starts at certain localized points appearing as a bright spots at the interface between the π-phase and the Al-matrix, as well as inside the bulk of the π-phase particles. Strontium modification seems has no effect on the mechanism by which the π-phase decomposes into fine β-phase needles.

7- The rate of π- to β-phase decomposition from 2 to 8 hours of solution treatment is slow, whereas it accelerates at 10 hours or longer treatment times. The decomposition rate is also dependent on the initial size of the π-phase particles in the as-cast sample.

8- At low cooling rates (SDAS ~110 μm), Sr modification leads to an increase in the size and a lowering of the number of π-phase particles compared to the non-

modified alloy. It is thus recommended that the lowest permissible amount of Sr addition be used for melt treatment. Also, a high cooling rate is preferable for obtaining small amounts of β- and π-phase iron intermetallics.

9- Using solution treatment times of up to 60 hours improves the π-phase decomposition to a large extent and increases the concentration of Mg in the matrix to the highest level compared to the as-cast condition; large amounts of Mg_2Si will thus be expected to precipitate during the aging of these solution treated samples.

CHAPTER 5

MECHANICAL PROPERTIES

CHAPTER 5

MECHANICAL PROPERTIES

5.1   Introduction

The mechanical properties of Al-Si-Mg alloy castings are controlled mainly by their microstructure, in particular, by the SDAS, the morphology of Si particles, the Mg_2Si precipitation, and the nature of the iron intermetallics.[34, 110, 111] In the present chapter, an attempt will be made to provide a greater understanding of the link between the decomposition of the π-phase during solution heat treatment, as discussed in chapter 4 and the mechanical properties of the same selected non-modified and Sr-modified Al-7Si-0.5Mg-0.09Fe alloys. The discussion of the results obtained will be presented in three main subsections, namely, pertaining to the silicon particle characteristics, the impact properties, and the tensile properties.

5.2   Silicon Particle Characterization

The shape and size of the silicon particles formed during the solidification of Al-7Si-Mg alloys have a significant effect on the mechanical properties of the castings, and must, therefore, be controlled so as to obtain the desired properties. The cooling rate, Sr-

modification, and heat treatment are considered to be the three most thoroughly reported-upon parameters for controlling Si-particle shape and size with a view to obtaining optimum mechanical properties. In this study, the alloys selected for Si particle characterization were the 6C and 6CS alloys in the as-cast and heat-treated conditions. The heat-treated alloys were solution treated for time periods ranging from 2 to 100 hours at 540°C, followed by quenching in warm water at 60°C and then aging at 155°C for 5 hours. The silicon particle characteristics were measured using an optical microscope-an image analyzer system. The parameters characterizing silicon particles were the average Si particle area (μm^2); then average Si particle length (μm); roundness ratio (%), and aspect ratio.

Figure 5.1(a) shows the Si average particle area (μm^2) for non-modified 6C and Sr-modified 6CS alloy samples solidified at a low cooling rate and solution heat treated for times of up to 100 hours. In the non-modified as-cast samples, the Si particles were acicular in form, with an average area of 62.5 μm^2 and 44.8 μm^2 for low cooling rate and high cooling rate samples, respectively. During the first 6 hours of solution treatment, the average area of the Si particles for both cooling rates reduced. As the solution time increases, the particle area begins to increase in a gradual manner up to 20 hours, beyond which it becomes more or less constant until it reaches the 48 hour mark and then increases slightly until it reaches a maximum value at 100 hours. Figure 5.1(b) shows the average particle length for the same 6C alloy at different cooling rates as a function of solution treatment time; the plot displays the same trend as the average particle area. During the first six hours, there is a reduction in the average Si-particle length; as the solution treatment
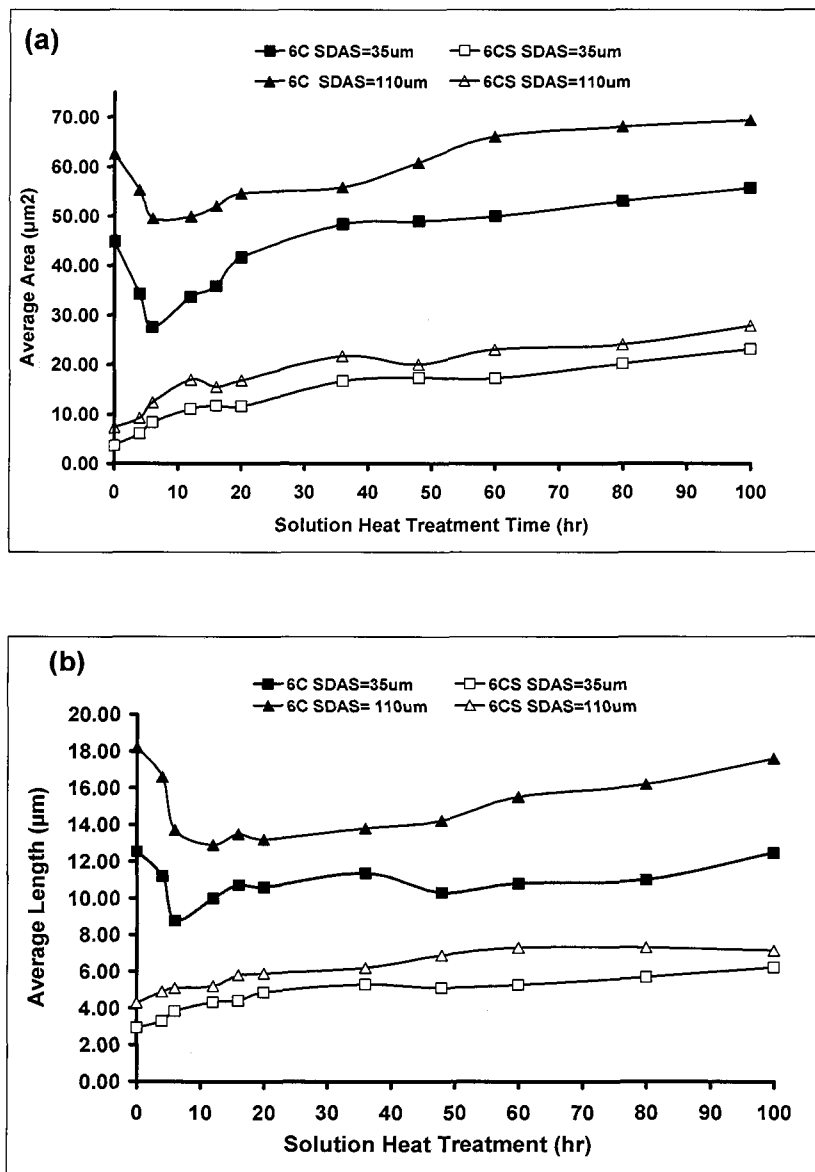
Figure 5.1 Effects of solution heat treatment time and cooling rate on: (a) average Si particle area, and (b) average Si particle length, for non-modified 6C and Sr-modified 6CS alloys

time is increased, the average length also increases until it reaches a maximum value at 100 hours.

Based on the data presented in Figures 5.1(a) and (b), for non-modified and Sr-modifed alloys, the reduction in the average particle area and length in the early portion of the allotted period of six hours for both low and high cooling rates indicates the process of fragmentation occurring in the silicon particles. This process is triggered by the instability of the interface between the silicon particles and the aluminum matrix; it is driven by a reduction in the total interfacial energy.[111] During this stage, the large silicon particles undergo necking and break down into a series of particles having smaller lengths than the as-cast particles. These fragmented particles gradually begin to spheroidize and increase in size (area and length) with increase in the solution treatment time. Prolonged solution treatment leads to Si-particle coarsening. Cooling rate also contributes significantly to reducing the average area and length in the as-cast and heat-treated non-modified alloy samples.

In Sr-modified castings, Sr addition results in a depression in the nucleation temperature of the eutectic Si and also changes the growth morphology of this eutectic Si from coarse acicular needles to a fibrous form, particularly in the structures obtained at low cooling rate.[112] As a result, the 6CS alloys exhibit reduced values of average area and length in the as-cast samples compared to the non-modified 6C alloys, as may be seen from Figure 5.1(a). As the solution treatment time is increased to12 hours, a direct increase is

observed in the average area and length of the Si particles when compared to the non-modified alloys, as may be seen in Figures 5.1(a) and (b).

This direct increase in area and length is explained by the fact that the as-cast Si particles in the modified alloys are relatively smaller in size than the non-modified case; there are thus no large particles to undergo fragmentation, so that the Si particles are susceptible to spheroidization more easily and directly, as well as in a shorter period of time, compared to the non-modified samples. Complete spheroidization and coarsening is thus expected to occur in the 12-20 hour range. Obviously, a prolonged solution treatment time of up to 100 hours would lead to further coarsening of the Si particles. As can be seen in Figures 5.1, with regard to the Sr-modified alloys, both low and high cooling rate samples display an appreciably similar average particle area over the entire range of solution treatment times. The effect of decreasing the SDAS from 110μm to 35μm, however, is more significant in reducing the average particle area and length in the non-modified alloys.

Figures 5.2 (a) and (b) show the variation in average Si particle roundness and aspect ratio as a function of solution treatment time at 540°C for non-modified 6C and Sr-modified 6CS alloys at the two cooling rates. With regard to non-modified alloys, Figure 5.2(a) shows that the roundness of the silicon particles increases from 37% and 30% in the as-cast condition to 54% and 47% after 20 hours of solution treatment for the samples corresponding to SDASs of 35μm and 110μm, respectively. The roundness increases gradually as the solution time increases, reaching a maximum at 20 hours after which it
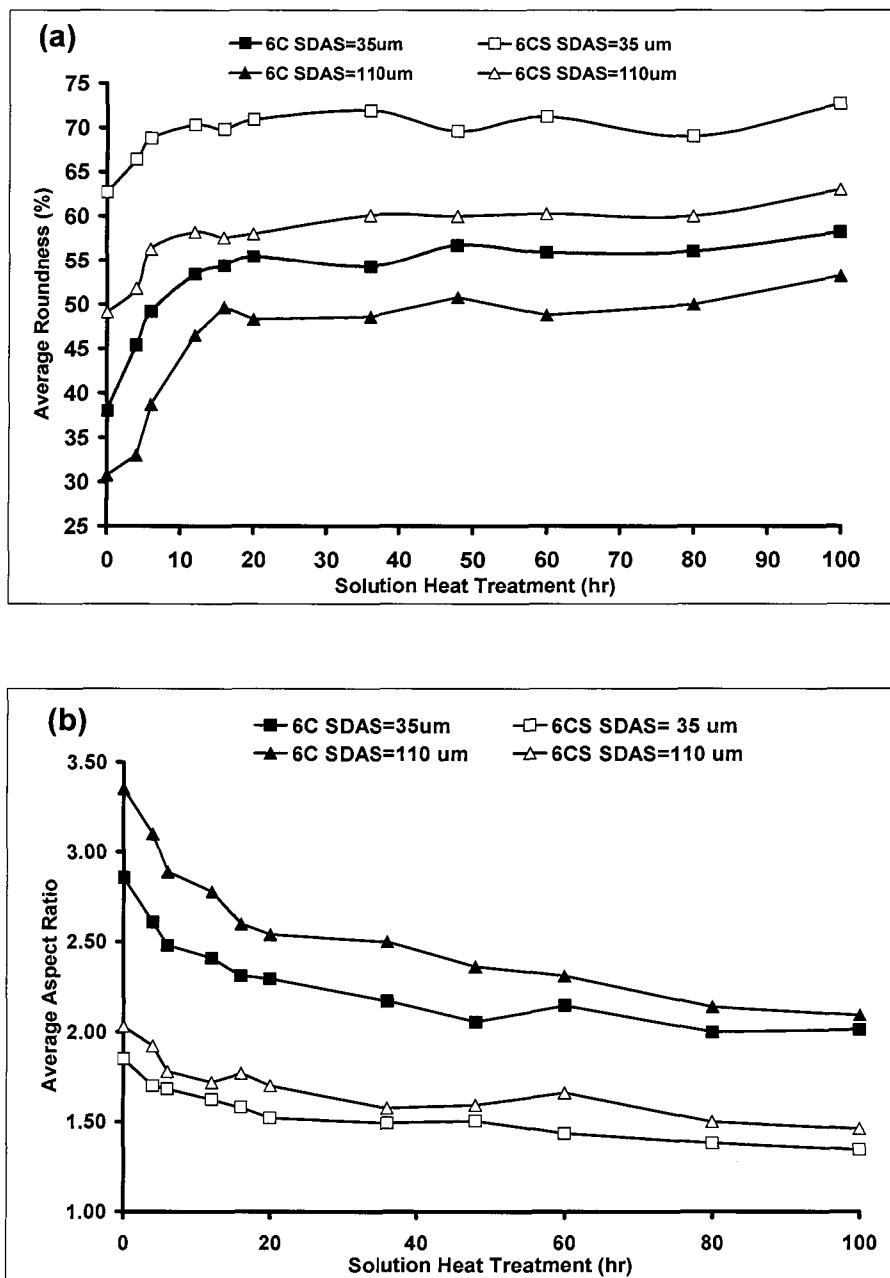
Figure 5.2 Effects of solution heat treatment time and cooling rate on: (a) average Si particle roundness, and (b) average Si particle aspect ratio, for non-modified 6C and Sr-modified 6CS alloys.

remains more or less constant up to the 100 hour mark. Figure 5.2(b) shows the average aspect ratio values displayed by the same alloys. Starting at a higher value in the as-cast condition for all cases, the aspect ratio begins to decrease with an increase in the solution treatment time right up to 100 hours. Zhu et al.[113] proposed that the decrease observed in the aspect ratio and the increase observed in the roundness ratio of the Si particles in non-modified alloys with the increase in solution treatment time are all a result of the dissolution, separation and spheroidization of the Si particles during the solution heat treatment processes.

Thirugnanam et al.[114] asserted that the eutectic structure which forms at a high cooling rate is fine and uniform because of the fact that the high cooling rate prevailing during solidification divides the eutectic liquid into many small pockets rather than into large eutectic regions such as the ones present in low cooling rate structures. Thus, the as-cast and heat-treated 6C alloy samples obtained at the high cooling rate, show greater improvement in roundness and aspect ratio than those obtained at the low cooling rate.

The roundness and aspect ratio of the Sr-modified 6CS alloy samples are plotted in Figures 5.2(a) and (b), respectively, as a function of solution treatment time. In comparison to the non-modified alloys, the as cast 6CS alloys show much higher roundness ratios, 62% and 49%, corresponding to the high and low cooling rates, respectively. With increase in solution treatment time, roundness attains its maximum value after 12 hours of solution treatment, after which the values remain more or less the same at both cooling rates with

further increase in the solution heat treatment time. These results confirm the claim that Sr modification reduces the time required for attaining maximum spheroidization.

Shivkumar et al.[4] observed that the silicon particles in modified alloys attain a high degree of spheroidization after 12 hours of solution treatment, whereas in non-modified alloys even after that length of time, coarse needles of Si particles may still be observed. The non-modified eutectic structure is resistant to spheroidization; consequently, a higher rate of this process may be observed in the modified samples. As expected, the 6CS alloys display a lower aspect ratio in the as-cast condition compared to the as-cast 6C alloys, as shown in Figure 5.2(b).The aspect ratio is reduced further during the first 12 hours of solution treatment, indicative of the ongoing improvement in the spherodization of the Si particles with increase in solution treatment.

The optical micrograph shown in Figure 5.3(a) reveals the acicular morphology of the Si particles in the as-cast non-modified 6C alloy. Figure 5.3(b) illustrates the effects of an 8 hour solution treatment at 540°C on the Si-particle characteristics, showing the fragmentation process of Si particles through necking and then separation into smaller particles. The start of spheroidization of a number of these particles and the rounding of sharp corners of certain other Si particles may also be noted. After prolonged solution heat treatment of up to 100 hours, as shown in Figure 5.3(c), the Si particles appear larger in size, as a result of coarsening; however, a number of particles may still be observed in the process of fragmentation. It will be seen clearly that these optical micrographs support the data presented in Figures 5.1 and 5.2.
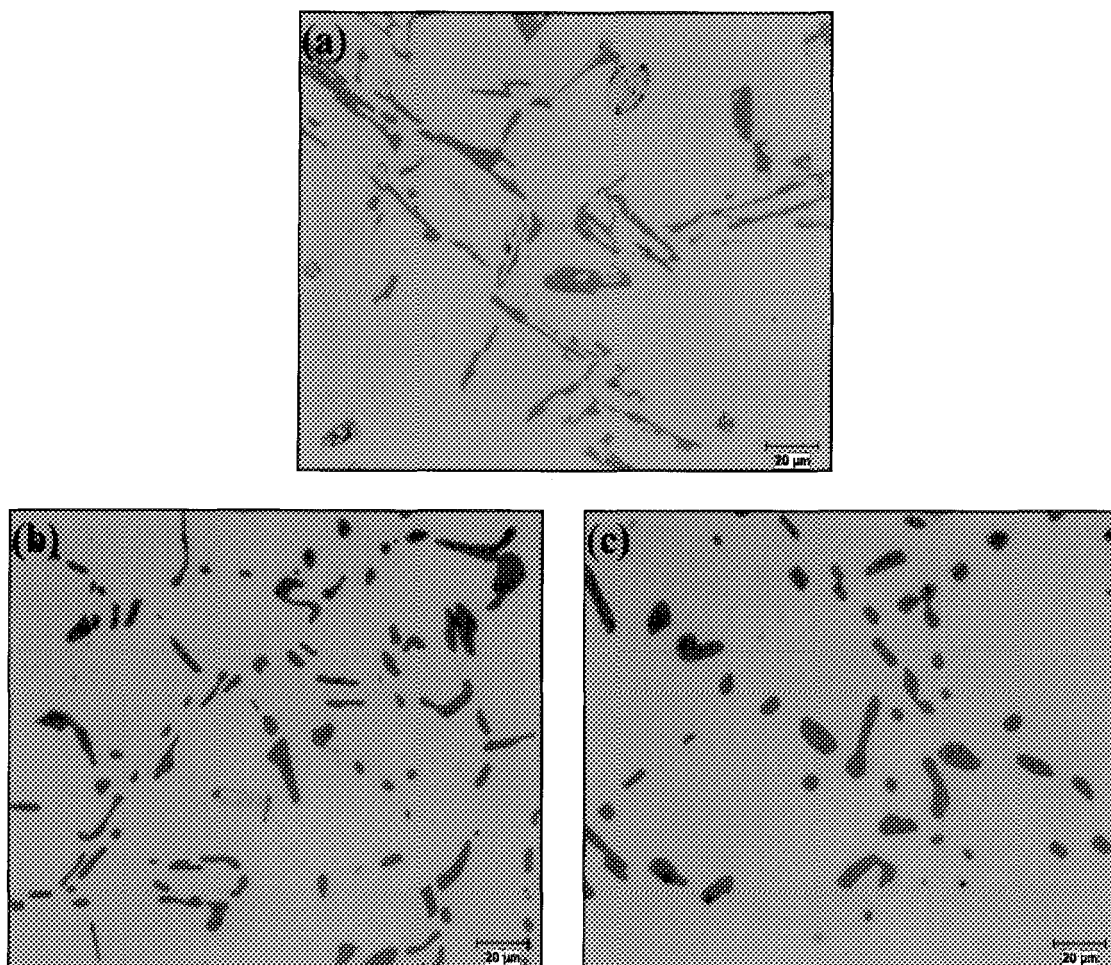
Figure 5.3 Optical micrographs showing the Si particle morphology in non-modified 6C alloy in (a) the as-cast condition, and after solution treatment at 540oC for (b) 8hrs, and (c) 80 hrs.

Figure 5.4 shows the dual effect of solution heat treatment and modification on the morphology of the eutectic Si particles. Figure 5.4(a) display the optical micrograph of the as-cast 6CS alloy sample obtained at the high cooling rate (SDAS ~ 35μm); showing a well modified eutectic structure compared to the acicular form shown in Figure 5.3(a).In this case, as Figure 5.4(b) shows, after 8 hours of solution treatment at 540°C, the Si particles appear to be completely rounded, in the absence of any fragmentation process. A comparison of Figure 5.4(b) and Figure 5.3(b) indicates that in Sr-modified structures, a major fraction of the Si particles become spheroidized after 8 hours of solution treatment. In non-modified alloys, however, this is not the case, and the extent of spheroidization is very small. After prolonged solution treatment of up to 100 hours, the Si particles grow and coarsen, as may be seen in Figure 5.4(c), resulting in an increase in the interparticle distance.
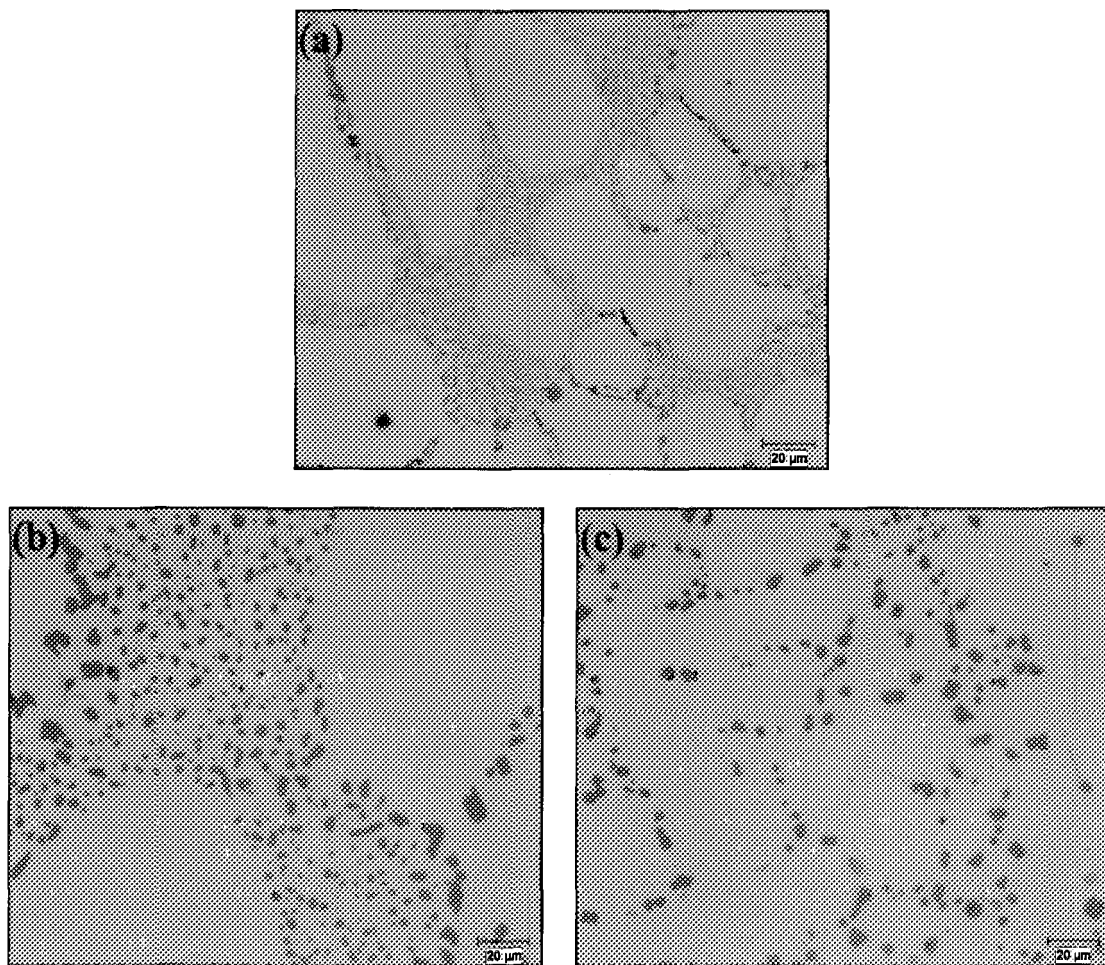
Figure 5.4 Optical micrographs showing the Si particle morphology in Sr-modified 6C alloy in (a) the as-cast condition, and after solution treatment at 540oC for (b) 8hrs, and (c) 80 hrs.

5.3   Impact Test Results

Impact testing was carried out on the samples obtained from specimen blanks sectioned from the end-chilled mold castings at two levels, namely 10 mm and 100 mm above the end-chill, corresponding to SDAS values of 110μm and 35μm, respectively. An instrumented impact testing machine was used to generate load-and-energy deflection time curves for each set of tested specimens, an example of which is shown in Figure 5.5. The energy obtained at maximum load is representative of the fracture initiation energy, E_I, while the energy required for the propagation of the crack, Ep, can be calculated by subtracting E_I from the total absorbed impact energy, E_T.
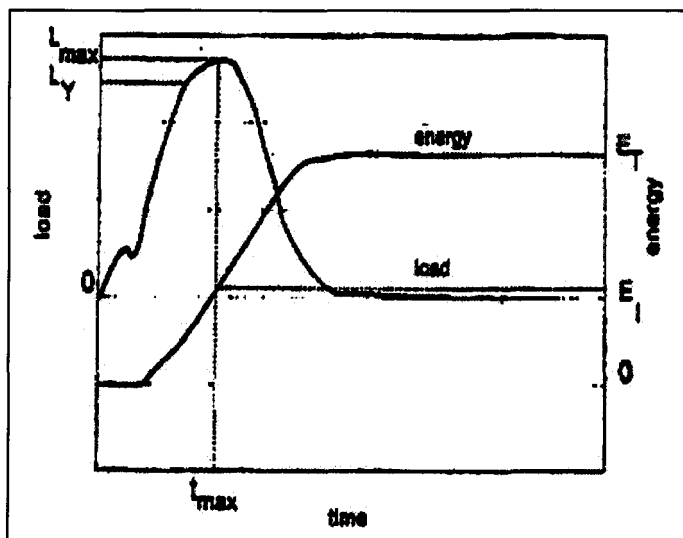
Figure 5.5 Typical load-time curve obtained using the data acquisition system.

The total absorbed energy, however, does not provide much information about the details of the fracture behaviour of a material, which is why dividing the energy into its two component parts is essential. A high strength brittle material will have large crack initiation

energy, and a small crack propagation energy. Conversely, a low strength ductile material will exhibit a small Ei and large Ep values. Therefore, even if the Charpy impact energy for the two materials were to be the same, their fracture behaviour would be noticeably different. The total absorbed energy value, E_T, is strongly dependent on the test technique and shape of the specimen.[89] Consequently, The charpy impact tests in this study were performed on unnotched specimens in order to place greater emphasis on the effects of the microstructural constituents on the impact energy than that the notch geometry.[111]

Figure 5.6 shows the total impact energy values at room temperature for the as-cast and T6 heat-treated 6C and 6CS alloys solidified at the two cooling rates, as a functioning time. For the as-cast alloys solidified at the low cooling rate, (SDAS ~110µm), Sr modification increases the impact energy from 7.7 J to 15.25 J. Similarly, for the as-cast alloys solidified at the high cooling rate,(SDAS of 35µm), the total impact energy increases from 12.9 J to 22 J in the modified alloy.

Figures 5.7(a) and (b) show the average crack initiation and propagation energies, respectively, for as-cast and T6 heat-treated 6C and 6CS alloys as a function of cooling rate and solution heat treatment time. A comparison of Figures 5.7(a) and Figure 5.7(b), clearly shows that Sr modification plays a far more significant role in improving the crack initiation energy than in the propagation energy alloy samples for all conditions studied.

These observations are in full agreement with a study carried out by Hafiz and Tobayashi[115] concerning the effects of Sr-modification on the Charpy Impact Test energy
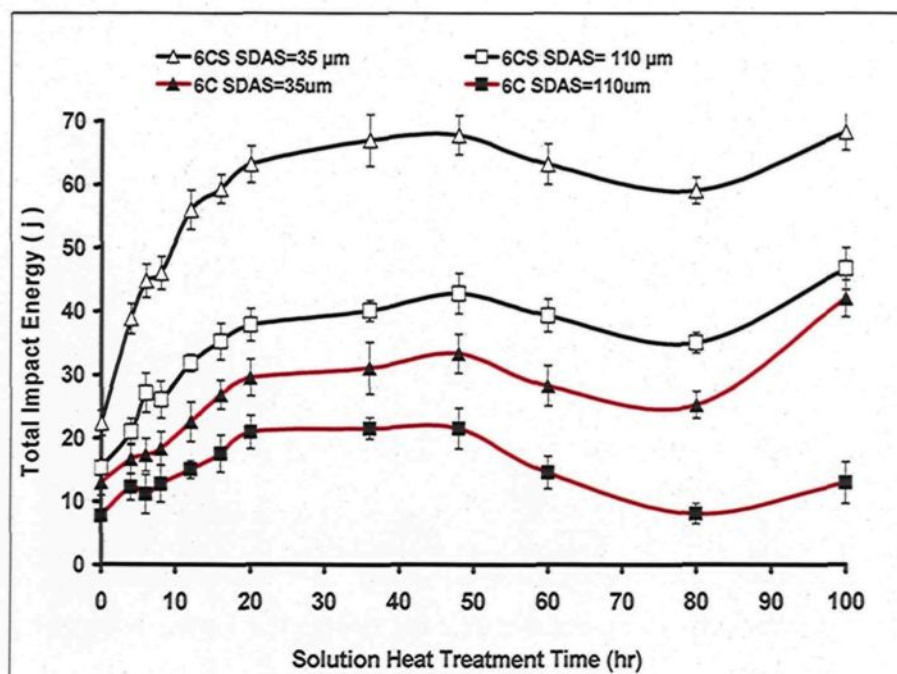
Figure 5.6 Effects of solution treatment time at 540°C on the total impact energy of 6CS-T6 and 6C-T6 alloys obtained at high and low cooling rates (SDASs of 35 μm and 110 μm, respectively).

of A356 alloys. They reported significant improvements of 101% and 440% respectively, in the impact energy of Sr-modified sand mold and water-cooled copper mold castings, when compared to the non-modified castings.

In non-modified as-cast alloys, the high stress concentration at the sharp edges of the acicular silicon particles which display a high aspect ratio and poor sphericity causes the formation of large voids in the eutectic region during loading. These large voids facilitate crack initiation and link up at a high speed with low propagation energies.[114, 116] As mentioned in the previous section, strontium modification leads to a change in the morphology of the eutectic silicon from acicular to finely distributed fibrous particles
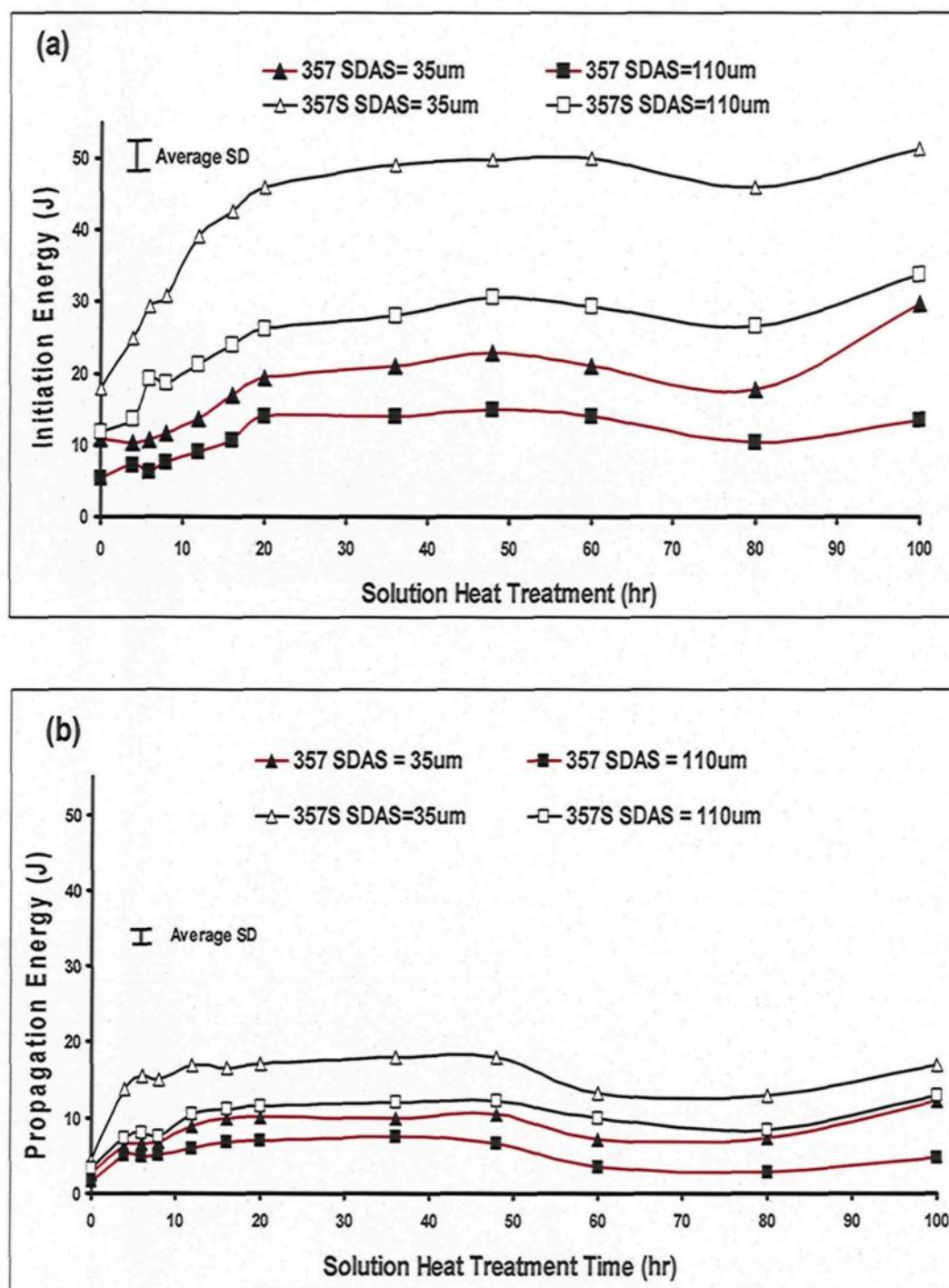
Figure 5.7 Effects of solution treatment time at 540°C on the crack initiation and crack propagation energy of (a) 6C-T6 and (b) 6CS-T6 alloys obtained at high and low cooling rates (SDASs of 35 μm and 110 μm, respectively).

having a much lower aspect ratio. Strontium modification is thus seen to improve the initiation energy radically as a result of a reduction in the crack initiation sites; this might explain why such modification makes an appreciable contribution to the improvement observed in the crack initiation and crack propagation energies of the as-cast 6CS alloys studied.

The results shown in Figure 5.6 also indicate that the as-cast 6C and 6CS samples obtained at the high cooling rate, display some improvement in the total impact energy values compared to those obtained at the low cooling rate. Increasing the cooling rate has a greater effect in improving the crack initiation energy of 6C and 6CS alloys than in improving crack propagation energy, as shown in Figures 5.7(a) and (b). These results may lead to the conclusion that the behavior of the alloys studied under impact loading is the result of the refinement of the iron intermetallics and the morphology and size of the Si particles brought about by applying the high cooling rate.

This conclusion is supported by the results[117] reported and the data presented earlier in Figures 4.16, 4.18, 5.1 and 5.2. The results shown in Figures 5.1 and 5.2 reveal that using a high cooling rate produces a significant improvement in the Si particles characteristics, i.e., length, roundness, and aspect ratio of the as-cast 6C and 6CS alloys over those obtained when the same alloys are solidified at a low cooling rate.

Decreasing the SDAS from 110μm to 35μm i.e. increasing the cooling rate, has a significant effect in that it reduces the volume fraction of the π-phase and β-phase iron

intermetallics in the as-cast 6C and 6CS alloys, as previously presented in Figures 4.16 and 4.18, respectively. Based on the above discussion, it will clearly be seen that the number of crack initiation sites is expected to decrease upon increasing the cooling rate, and consequently the average total energy of the as-cast alloys studied will also be enhanced.

Upon increasing the solution treatment time in the heat-treated samples, all the 6C and 6CS alloys studied began to show higher E_i and Ep values than the corresponding as-cast values, as shown in Figure 5.7. As will be observed from Figure 5.7, all the four conditions studied follow nearly the same trend with an increase in the solution treatment time. After 20 hours of solution treatment, all the heat-treated alloys studied attained almost maximum improvement in Ei, Ep and the corresponding total impact energy (Et) values, as shown in Figure 5.6.

As may be seen in Figures 5.7(a) and (b), after 20 hours of solution treatment the crack initiation energy, E_I, increases to 223% and 108%, respectively, for non-modified and Sr-modified alloys obtained at the high cooling rate, compared to the corresponding as-cast alloys; on the other hand, at the low cooling rate, the improvement in the crack initiation energy, E_I, was 86% and 170% for unmodified and Sr-modified alloys, respectively, compared to the as-cast alloys. With regard to the propagation energy, E_P, improvements of 150% and 280% were obtained for non-modified and Sr-modified alloys, respectively, after 20 hours of solution treatment. In comparison, at high cooling rates, the improvement observed was 230% for non-modified alloys, and 290% for Sr-modified alloys.

These results point to the fact that it is important to take into account the changes occurring in the Si particle characteristics and in the iron intermetallics as a result of heat treatment in order to explain the improvements observed in the absorbed impact energy of the heat-treated alloys studied. With regard to such Si particle characterization, the maximum improvement in Si particle roundness of all the heat-treated alloys studied was attained after 20 hours of solution treatment, as will be seen in Figures 5.2(a) and (b). Similarly for the aspect ratio, maximum improvement was also observed after 20 hours of solution treatment for all the heat-treated alloys studied. Such results lead to the deduction that, the improvements which may be observed in the average impact energy in this 20-hour period of solution treatment are directly related to the changes *viz*, improvements in the silicon particle characteristics, brought about in the same period of solution treatment time.

The improvements in the impact energy obtained after 20 hours of solution treatment in non-modified alloys are due to the fragmentation and gradual spheroidization of the Si particles, wherby the sharp edges of these particles become rounded thereby promoting fracture resistance.[90] The direct and rapid spheroidization of the eutectic Si in Sr-modified alloys with respect to the solution treatment time results in reducing the angularity and increasing the spacing between the brittle Si particles.[119] Consequently, the amount of ductile α-Al increases thereby providing additional resistance to crack initiation, which may explain the role of Si particles in improving the impact energy of all the heat-treated Sr-modified alloys studied.

Based on the results obtained from the quantitative analysis of the iron intermetallics, as shown in Figures 4.16 and 4.18, increasing the solution treatment time from 2 to 20 hours leads to two possible effects. The first effect is a decrease in the amount of the π-phase iron intermetallic through dissolution and decomposition into the newly-formed β-phase needles. The second effect is the diffusion of the Mg into the matrix as a result of the dissolution of Mg_2Si and decomposition of the π-phase; the amount of Mg in the matrix available for strengthening is thus expected to increase.

The presence of newly formed β-phase needles and the strengthening of the matrix through the formation of Mg_2Si precipitation upon aging will contribute negatively to the impact energy values of the heat-treated samples. According to the results shown in Figures 5.6 and 5.7, it would appear that the improvement in impact energy resulting from changes in the Si particle parameters occurring in the first 20-hr period of solution treatment can compensate for the losses in impact energy arising from the presence of the π-phase, the newly formed β-phase needles, and the strengthening of the Al-matrix.

Upon increasing the solution treatment time from 20 hours to 48 hours, the results shown in Figure 5.6 reveal that there is no significant increase in the total energy, which is unexpected. In this period of time, there are two competing changes affecting the impact results. The increase in the Si particle length and area result in a high degree of spheroidization and coarsening, consequently the density of these particles decreases, resulting in fewer sites being available for crack initiation thereby leading to an overall increase in ductility. On the other hand, the increase in the number of newly-formed β-

needles and in the amount of Mg in the Al-matrix as a result of further decomposition of the π-phase leads to a reduction in ductility. It would appear from Figure 5.6 that these two opposite effects are in balance and result in the stabilization of the average impact values between 20 and 48 hours of solution treatment.

After prolonged solution treatment time, as shown in Figures 4.16 and 4.18, the volume fraction of the π-phase reaches a minimum value. Consequently, the new β-phase needles reach maximum volume fraction between 60 and 80 hours from the outset of the solution treatment. The drop observed on the impact energy resulting from the fact that the β-phase needles reached the maximum volume fraction value attainable in conjunction with the strengthening of the Al matrix through the formation of more Mg_2Si tends to compensate for the improvement deriving from the changes occurring in the Si particle morphology within this period of time. Thus there is an unexpected drop in initiation and propagation energies between 60 and 80 hours of solution heat treatment, as shown in Figure 5.7. Once the newly formed β-needles start to dissolve at solution times beyond 80 hours, as shown in Figure 4.18, the impact energy will begin to improve again at the 100 hour mark to values close to the maximum values. This explanation has been further supported by fracture analysis which will be discussed in greater detail in the next subsection.

A study was carried out by Shivkumar et al. [118] on the effects of solution treatment time with regard to the impact properties of non-modified and Sr-modified A356-T6 castings solidified at two different cooling rates corresponding to SDASs of 48 μm and 24

μm, respectively. The authors observed that the average Charpy impact energy values increased with increase in the solution treatment time. It should be noted that the study in question concentrated on 356 alloys which contain ~ 0.38 Mg. According to data presented in the current study and the data reported in the literature,[10] the amount of π-phase is noticeably small at this level of Mg, in addition to the fact that it is completely dissolved and decomposed in the early portion of the 8 hours of solution treatment; the newly formed β-phase needles do not thus exist in the microstructure for any extended period of time, which may explain why the authors did not report any reduction in the impact energy values for any solution treatment time.

It has been suggested that when Sr modification in combination with a high cooling rate, a tougher material is produced.[119] This suggestion is in agreement with the current results presented in Figures 5.6 and 5.7, where the as-cast and heat-treated 6CS samples which solidified at the high cooling rate display superior improvement in total energy values compared to the other alloys. Also, it was reported that Sr-modification may be used to lower solution treatment time durations.[120] As can be seen from Figure 5.6, the total impact energy values obtained for the non-modified alloy samples after 20 hours of solution treatment may also be obtained with a solution treatment of only 4 hours if the alloys are chemically modified with Sr, providing a cost- effective means of achieving the same level of impact toughness.

5.4 Fractography

Fractography involves the detailed analysis of a fracture surface of tested samples, so as to determine the cause of the fracture and the relationship of the fracture mode to the microstructure of the sample material itself. Fractography examination may be carried out using an optical microscope, or a scanning electron microscope. A knowledge of fracture behavior is of crucial importance when upgrading material specifications and improving product design.

5.4.1 SEM Analysis of Fracture Surfaces

The fracture surfaces of a certain number of selected impact tested-samples of 6C and 6CS alloys in the as-cast and heat-treated conditions were examined using a scanning electron microscope. Backscattered electron (BSE) images and secondary electron (SE) images were taken of the fractured surface with a view to investigating the role of Si particles and iron intermetallics in fracture behavior. The backscattered electron images provide information regarding the fracture surface morphology where the image contrast is sensitive to the atomic mass of the material. Secondary electron images, on the other hand, provide information about the topography of the fracture surface and are not sensitive to the atomic mass of the material.[121]

Figure 5.8 displays the fracture surface of as-cast 6C and 6CS alloy samples solidified at a low cooling rate (SDAS of 110μm). Figures 5.8(a) and (b) show, respectively, the secondary electron and backscattered images of the fracture surface of the

non-modified 6C alloy revealing that a crack is triggered and how it propagates through the cleavage fracture of coarse Si particles, as may be seen in the plates of cracked Si particles. The EDX spectrum presented in Figure 5.8(c), corresponding to the circled regions in Figure 5.8(b), confirms that the crack initiates through splitting of the π-phase iron intermetallic. The smooth surface of the π-phase and the shearing of the dendrite cell, both confirm the brittle nature of this alloy. Accordingly, this alloy displays the lowest impact energy of all the as-cast alloys studied. The secondary electron and backscattered images of the Sr-modified 6CS as-cast alloys, as shown in Figures 5.8(d) and (e), reveal a dimpled fracture surface and secondary cracks which propagate through the interdendritic region. The nature of the fracture surface indicates that the alloy is more ductile when compared to non-modified alloy.

Decreasing the SDAS from 110μm to 35μm has the effect of increasing the ductility of the non-modified and Sr-modified alloys, as indicated by the SEM fractographs provided in Figure 5.9. For non-modified alloys, the secondary electron and backscattered images shown in Figures 5.9(a) and (b), respectively, reveal that the crack passes through the eutectic region in which acicular Si particles may be observed.
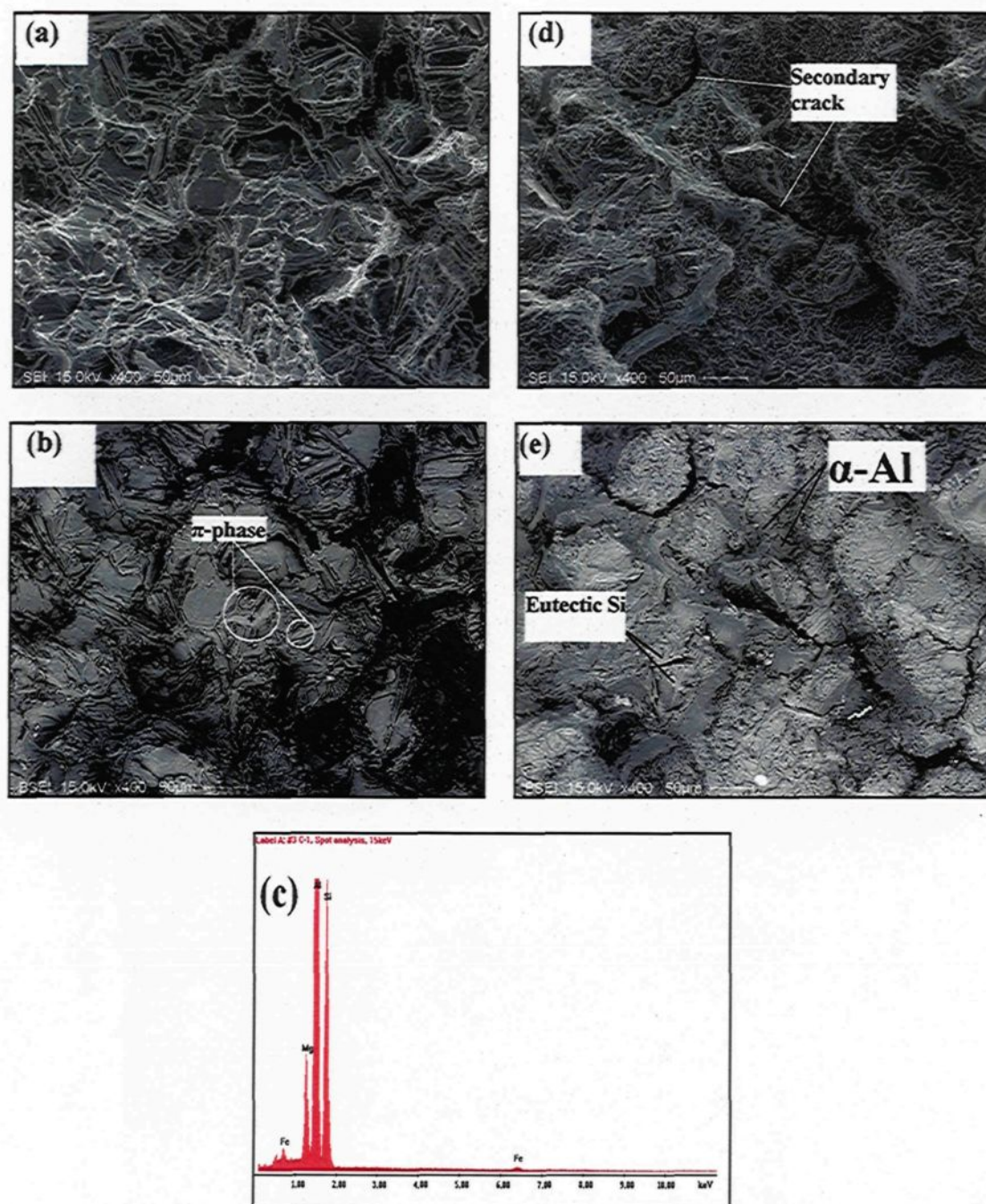
Figure 5.8 (a,b) Fracture surface of non-modified 6C alloy sample in the as-cast condition: (a) SE image; (b) BSE image; (c) EDX spectrum taken from the marked area in (b) revealing the presence of the π-phase. (d , e) Fracture surface of 6CS alloy in the as-cast condition: (d) SE image; and (e) BSE image, (samples were obtained at the low cooling rate).

The fracture surface also shows areas containing cleaved Si particles. The EDX spectrum shown in Figure 5.9(c) was taken from the marked area in Figure 5.9(b) and reveals a strong Si peak which supports the fact that the plates shown in the marked area are indeed Si particles. The combination of Sr modification and a high cooling rate results in extremely fine Si particles. The appearance of the fracture surface will thus consist of a massive dimpled area[122] as shown in the BSE and SE images of Figures 5.9(d) and (e), respectively, and may explain the presence of the highest impact energy value displayed by this alloy among all the as-cast alloys studied.

After 8 hours of solution heat treatment, a brittle fracture mode was observed in the non-modified 6C alloy solidified at low cooling rate. The BSE and SE images shown in Figures 5.10(a) and (b), reveal that cracks initiate through the cleavage of Si particles, as evident by the presence of large-faced Si plates on the fracture surface; this alloy thus exhibits the lowest impact value of all the 8-hr solution-treated samples. The EDX spectrum of Figure 5.10(c), obtained from the circled area in Figure 5.10(b), reveals strong Fe and Mg peaks which support the presence of an undecomposed π-phase particles on the fracture surface.

An inspection of the fracture surface of the 8-hr solution-treated Sr-modified 6CS alloy sample obtained at low cooling rate as shown in Figures 5.10(d) and (e), confirms that the addition of Sr make the alloy more ductile so that fracture occurs in the ductile mode,
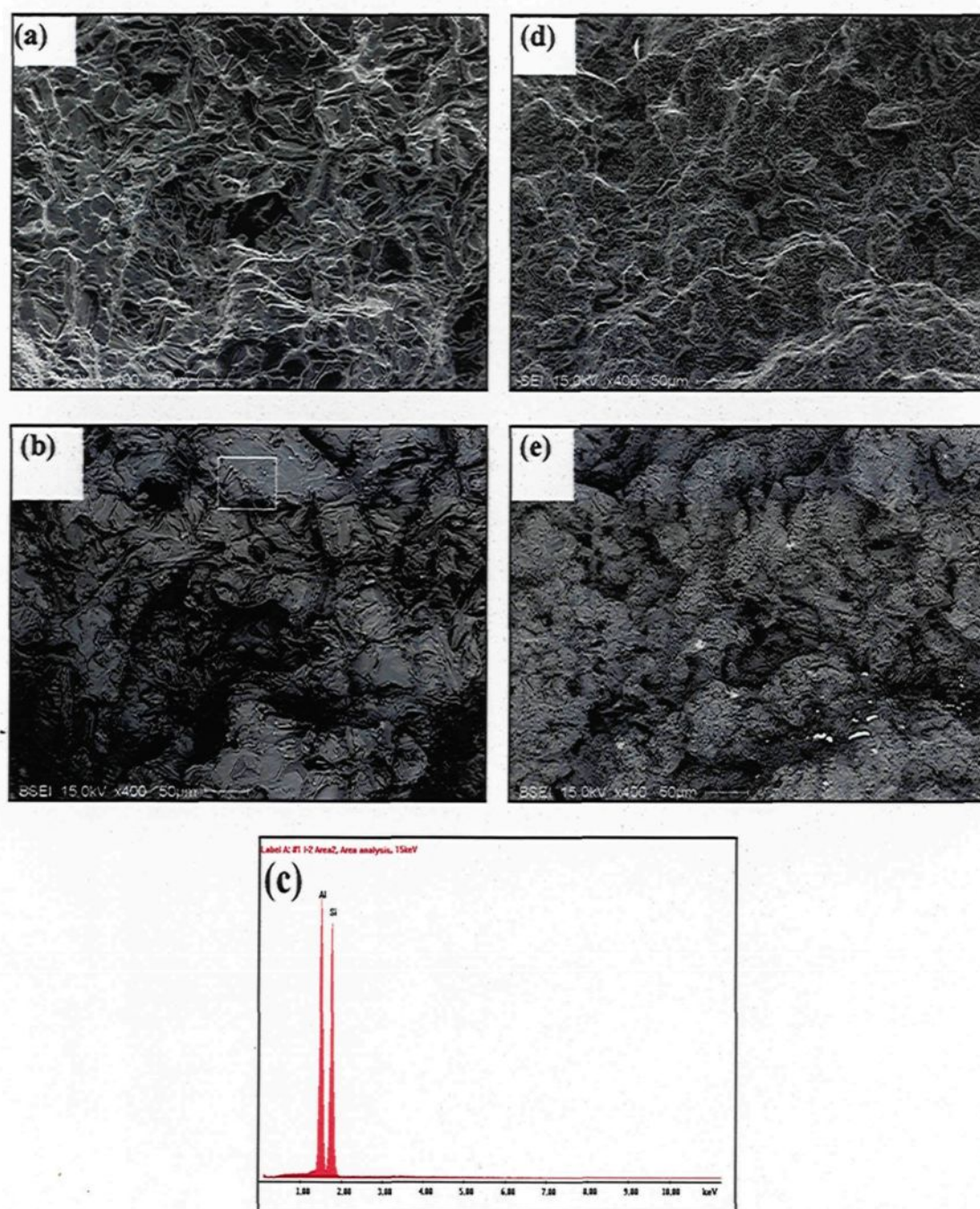
Figure 5.9 (a,b) Fracture surface of non-modified 6C alloy sample in the as-cast condition: (a) SE image; (b) BSE image; (c) EDX spectrum taken from the square area in (b) revealing a strong Si reflection. (d,e) Fracture surface of 6CS alloy in the as-cast condition: (d) SE image; and (e) BSE image, (samples were obtained at the high cooling rate)
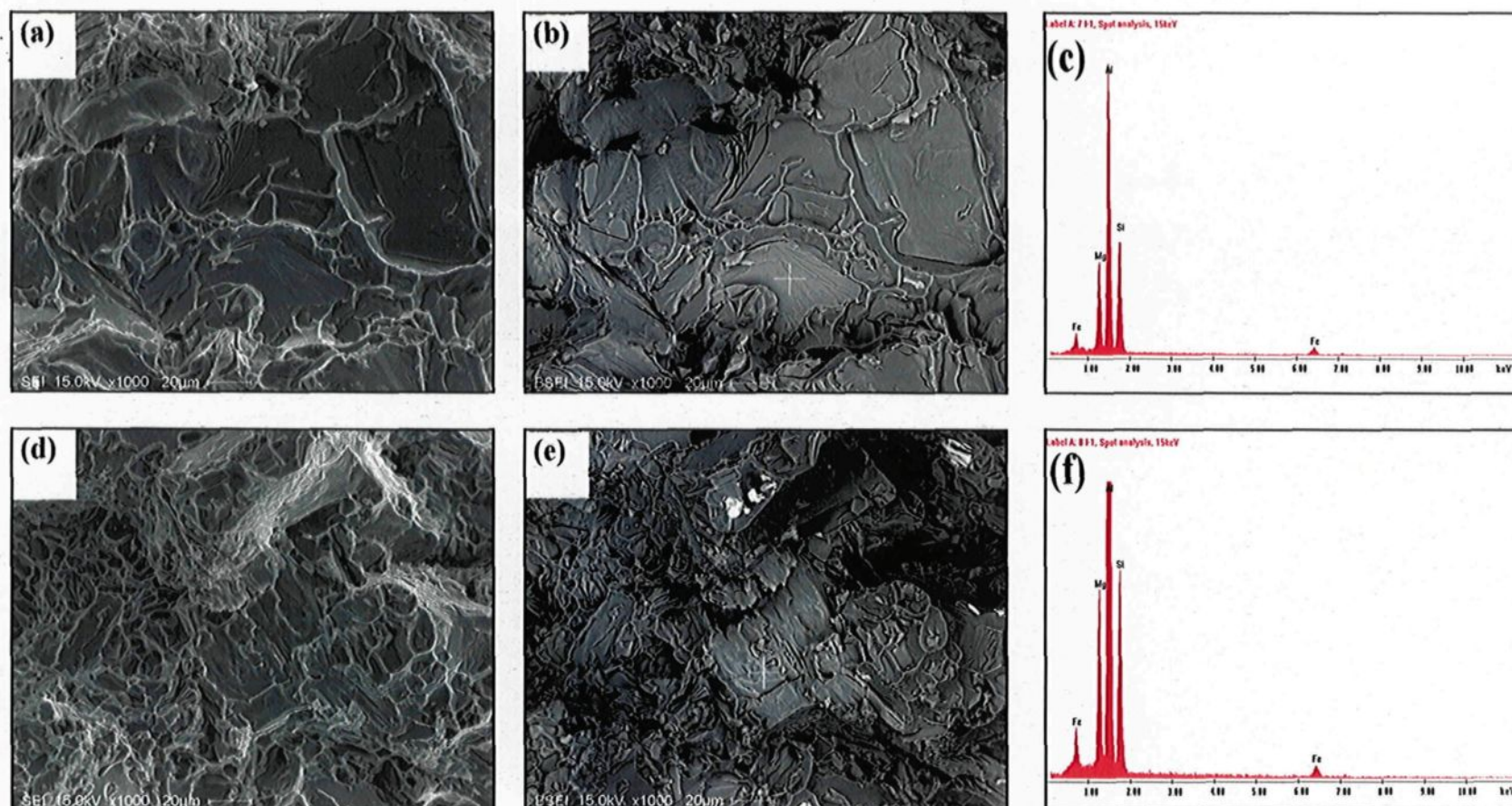
Figure 5.10 (a,b) Fracture surface of 6C alloy sample solution heat-treated for 8 hrs at 540°C: (a) SE; (b) BSE; (c) EDX spectrum taken from the marked area in (b) revealing the presence of the π-phase. Fracture surface of 6CS alloy solution heat-treated for 8hrs at 540°C: (d) SE image; (e) BSE image; (f) EDX spectrum taken from the marked area in (e) revealing the presence of the π-phase, (samples obtained at low cooling rate)

As evidenced by the dimpled nature of the fracture surface. The EDX spectrum shown in Figure 5.10(f), obtained from the area marked in Figure 5.10(e), reveals that the crack propagates through a large undecomposed π-phase particles represented by the faced plate marked by the cross. Figure 5.11 shows the secondary electron and backscattered electron images accompanied by two EDX spectra of the 8 hr solution-treated Sr-modified 6C alloy sample obtained at a high cooling rate. As will be seen from Figures 5.11(a) and (b), the fracture exhibits a mixture of brittle and ductile modes, as evidenced by initiation and propagation of the crack through the cleavage fracture of the π-phase and newly-formed β-iron intermetallic needles marked in area A and by the dimpled regions such as in area B in Figure 5.11(a). The EDX spectra shown in Figures 5.11(c) and (d) confirmed the presence of the undecomposed π-phase, (strong Fe and Mg peak) and that of the newly-formed β-needles. This observation indicates that, at the high cooling rate, the amount of π-phase formed is small compared to the alloys solidified at a low cooling rate, thus facilitating its decomposition into β-needles. The area marked B in Figure 5.11(a) reveals a ductile fracture mode as indicated by the presence of fine dimples. The 6CS alloy, however, displays ductile fracture in general, as it also displays the highest total impact energy of all the 8 hr solution-treated samples studied.

Figures 5.12(a) and (b) show the fracture surface of the 6C alloy solidified at the low cooling rate and solution heat treated for 80 hours at 540°C. Figures 5.12(a) and (b) reveal that the fracture surface still contains regions showing cleavage facets of Si particles and iron intermetallics even after prolonged solution treatment time.
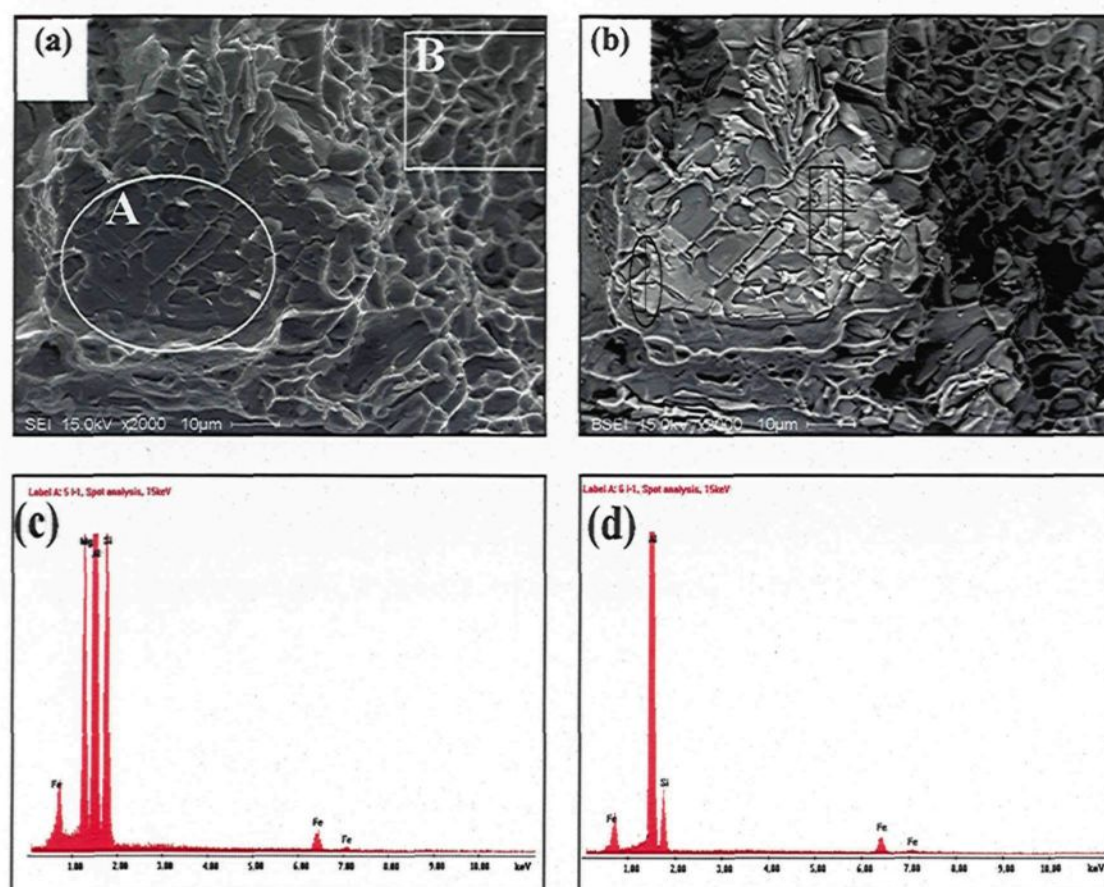
Figure 5.11 Fracture surface of 6CS alloy solution heat-treated for 8 hrs at 540°C: (a) SE Image; (b) BSE image; (c) EDX spectrum taken from oval area in (b) revealing the presence of the π-phase; (d) EDX spectrum taken from the rectangular area in (b) revealing the presence of the β-phase, (sample obtained at high cooling rate)

The EDX spectrum of Figure 5.12(c) obtained from the marked areas in Figure 5.12(b) reveals the presence of the newly-formed β-phase needles on the fracture surface. This sample displays the lowest impact energy of all the 80-hr solution-treated samples. A fine dimple structure was also observed in the 80-hr solution-treated Sr-modified 6CS alloy obtained at low cooling rate, as shown in Figures 5.12(d) and (e). Figure 5.12(f) shows the EDX spectrum obtained from the oval area marked in Figure 5.12(e) also reveals the presence of the newly-formed β-phase needles on the fracture surface.

When the 6CS alloys were solidified at the high cooling rate, and solution treated for 80 hours, this provided superior impact energy values for all the 80-hr solution heat-treated alloys, as presented earlier in Figure 5.6. This result is confirmed by the presence of an extremely fine dimpled structure and a large amount of α-Al on the fracture surface of such alloys, as shown in Figures 5.13(a) and (b). Newly-formed β-phase needles were observed on the fracture surface as confirmed by the EDX spectra presented in Figures 5.13(c) and (d) taken from the two areas marked in Figure 5.13(b). Based on such observations of the presence of the β-phase needles on the fracture surface of all 80-hr solution-treated samples studied, it becomes possible to explain the reduction in the impact energy values occurring in the samples solution heat treated for 60 to 80 hours, as shown in Figure 5.6.
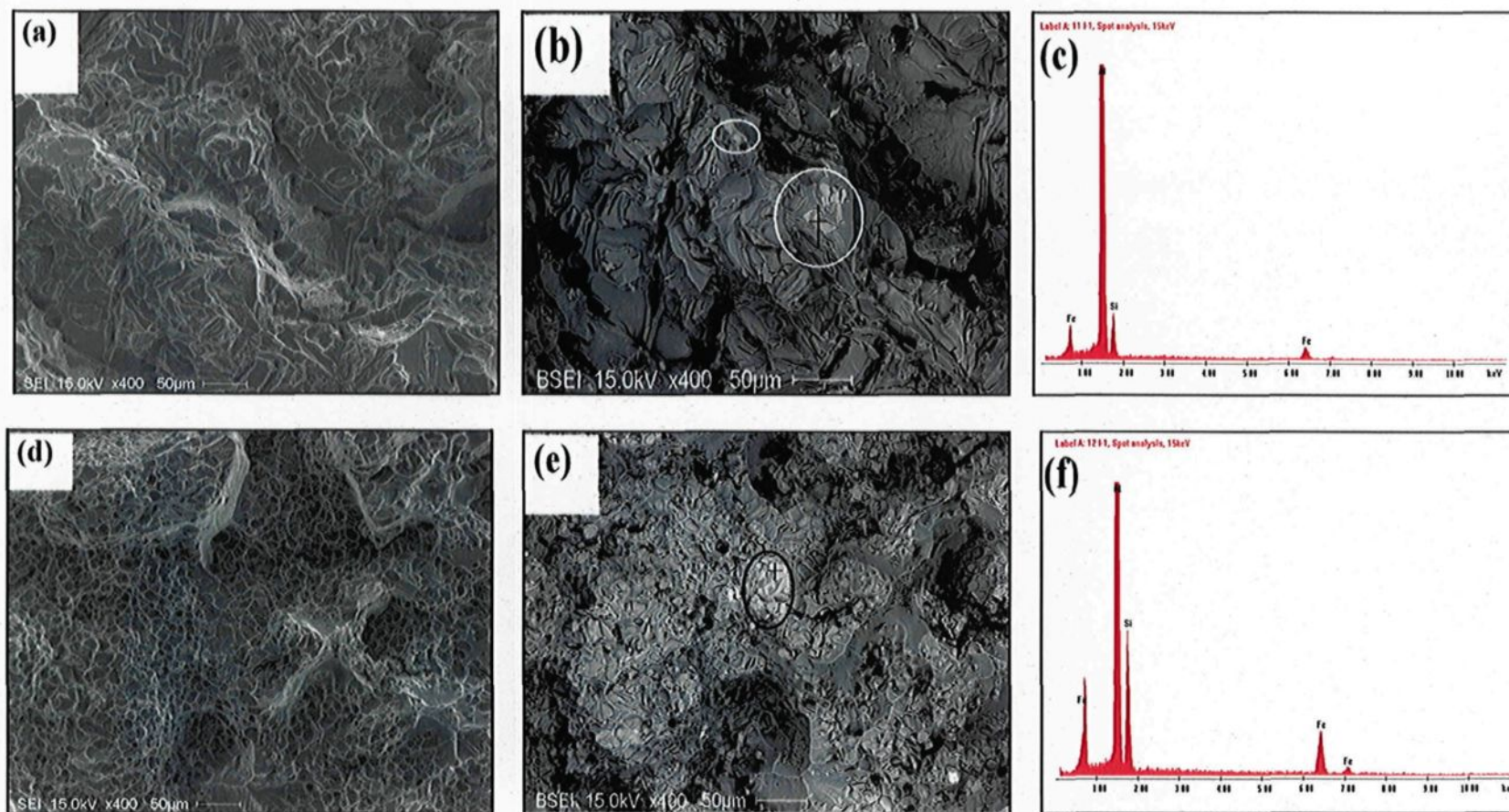
Figure 5.12 (a,b) Fracture surface of 6C alloy solution heat-treated for 80 hrs at 540°C: (a) SE image; (b) BSE image; (c) EDX spectrum taken from the marked area in (b) revealing the presence of fine β-phase needles; (d,e) Fracture surface of 6CS alloy solution heat-treated for 80 hrs at 540°C: (d) SE image; (e) BSE image; (f) EDX spectrum taken from the marked area in (e) revealing the presence of fine β-phase needles,(Samples obtaned at low cooling rate)
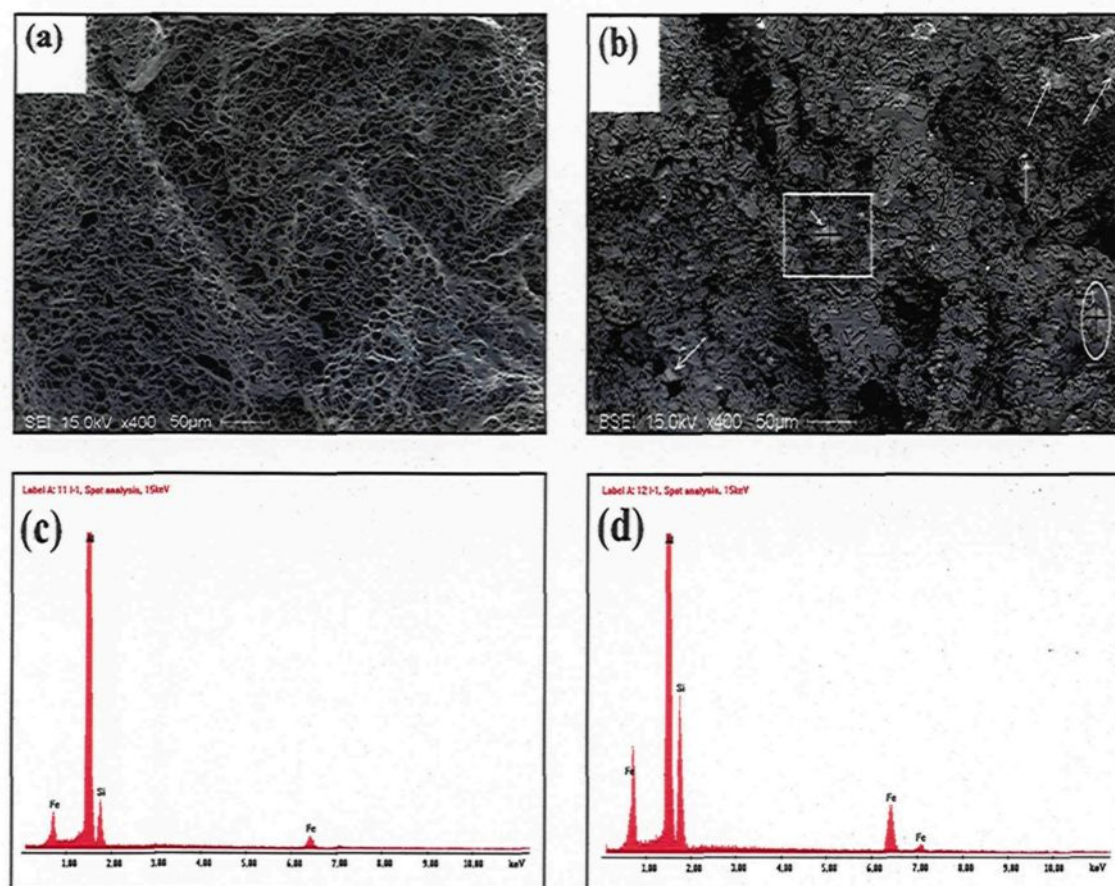
Figure 5.13 Fracture surface of 6CS alloy solution heat-treated for 80 hrs at 540°C: (a) SE image; (b) BSE image; (c) EDX spectrum taken from the marked area in (b) revealing the presence of fine β-phase needles; (d) EDX spectrum taken from the marked area in (b) revealing the presence of fine β-phase needles, (sample obtained at high cooling rate)

5.4.2 Microstructural Analysis of Fracture Profile

An examination of the fracture profile is carried out using optical microscopy on polished longitudinal sections of tested alloy samples. This facilitates identification of the microconstituents or phases beneath the fracture surface resulting from the propagation of the crack responsible for the fracture, and consequently, in the identification of the main and secondary cracks. The optical micrographs presented in Figures 5.14(a) and (b) show the fracture profiles of the as-cast 6C and 6CS tested alloy samples, respectively, solidified at low cooling rate. It is evident from these micrographs that the damage is initiated by the cracking of the eutectic Si particles and the formation of microcracks, or voids, in the eutectic region, as indicated by the arrow. Once a large number of eutectic Si particles crack, the matrix between the microcracks becomes unstable, and as a result the microcracks begin to coalesce and form a single main crack.[123] It should be noted here that not all of the microcracks which formed in the eutectic regions become part of the final fracture path as a result of the presence of the ductile α-Al although a majority of them do.[117]

The critical stress at which the microcracks start to form and propagate is controlled by the properties of the microstructure and the matrix.[34] Also, it has been reported that the internal stress induced in the eutectic Si particles as a result of the applied load depends on the eutectic Si particle aspect ratio and the SDAS of the matrix.[34] Consequently, the elongated Si particles in the 6C alloys solidified at a low cooling rate tend to generate higher
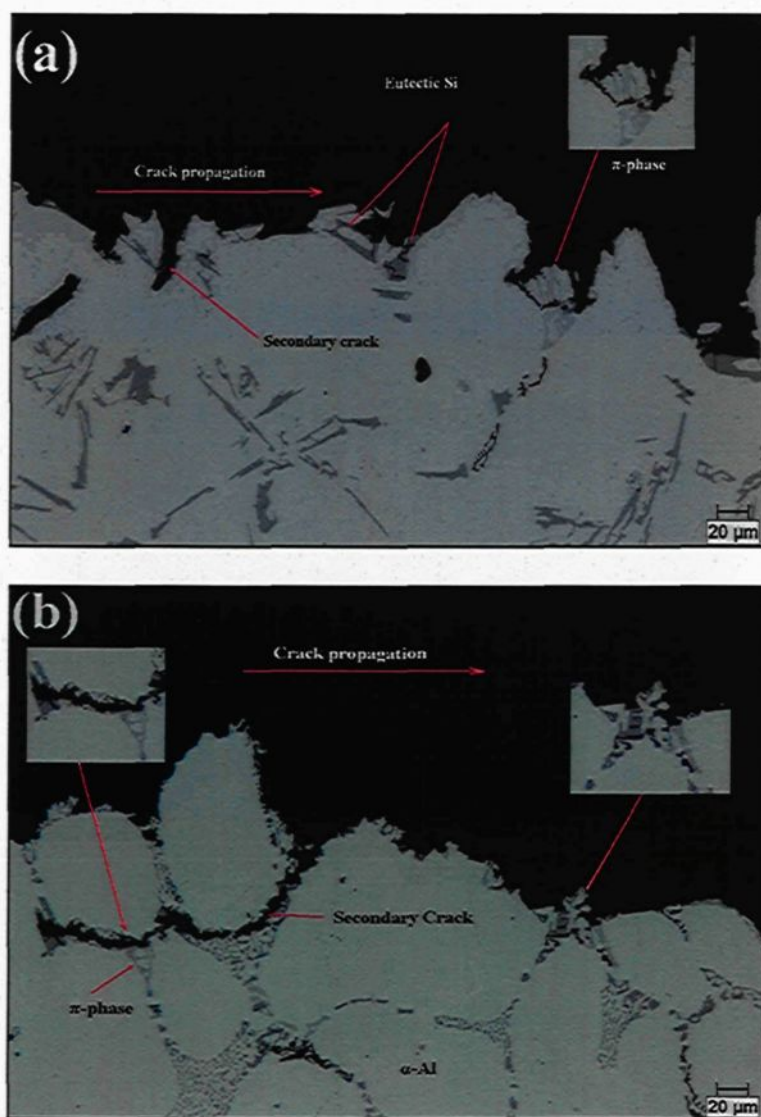
Figure 5.14 Optical micrographs obtained from longitudinal sections below the fracture surface of (a) the as-cast 6C, and (b) the as-cast 6CS alloy sample solidified at a low cooling rate,(SDAS~ 110μm)

particle stresses and in turn, have a higher probability of cracking, as will be observed from Figure 5.14(a).This figure reveals that the main crack propagates by cleavage of the long coarse Si particles, as well as the π-phase iron intermetallic particles whose brittle favors the formation of the secondary cracks underlying the primary crack. The fracture thus appears to display a mainly brittle mode and displays the lowest impact energy value among the as-cast alloys, as shown in Figure 5.6.

Figure 5.14(b) shows the fibrous morphology of eutectic Si and the segregation of the π-phase iron intermetallic as a result of Sr modification. It will be seen clearly from Figure 5.14(b) that the overall crack propagation path follows the eutectic region where hard brittle eutectic Si and π-phase iron intermetallics exist. The analysis of the fracture profile microstructure shows that the regions where the eutectic Si particles are not fully modified tend to favor crack initiation. The micrograph also shows the role of the ductile α-Al matrix in preventing the secondary crack from propagating by releasing the high stress concentration at the tip of the crack, as indicated by the inset on the left-hand side of the micrograph.

Figure 5.15 (a) displays the ductile rupture of the as-cast 6CS alloy sample obtained at the high cooling rate as the crack propagates through the well-modified Si eutectic region. This fracture mechanism followed the model proposed by Fat-Halla[122] as shown in Figure 5.16. The author in his model assumed that the brittle spherical Si particles represent the modified Si particles in the soft Al matrix and that the fracture path propagates across the soft Al-matrix circumventing the Si particles.
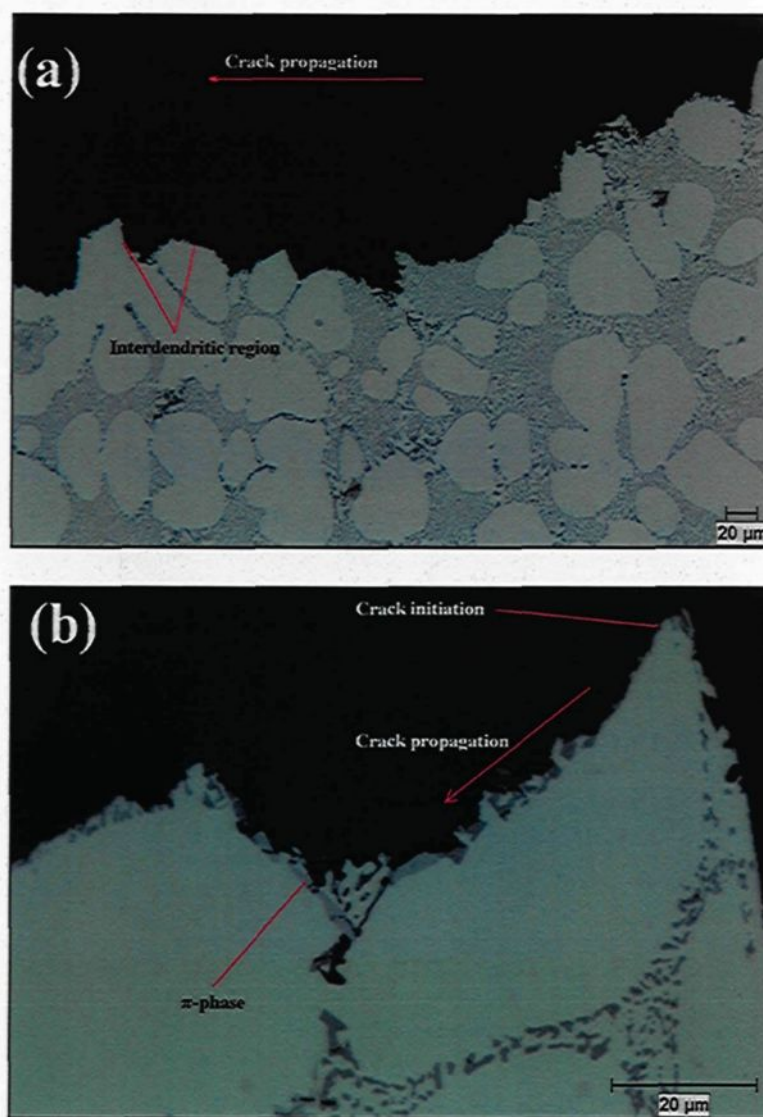
Figure 5.15 Optical micrographs obtained from longitudinal sections below the fracture surface of the as-cast 6CS alloy sample solidified at the high cooling rate(SDAS~ 35μm) showing (a) the fracture path through the eutectic Si particles, and (b) the cracking of a π-phase iron intermetallic particle.
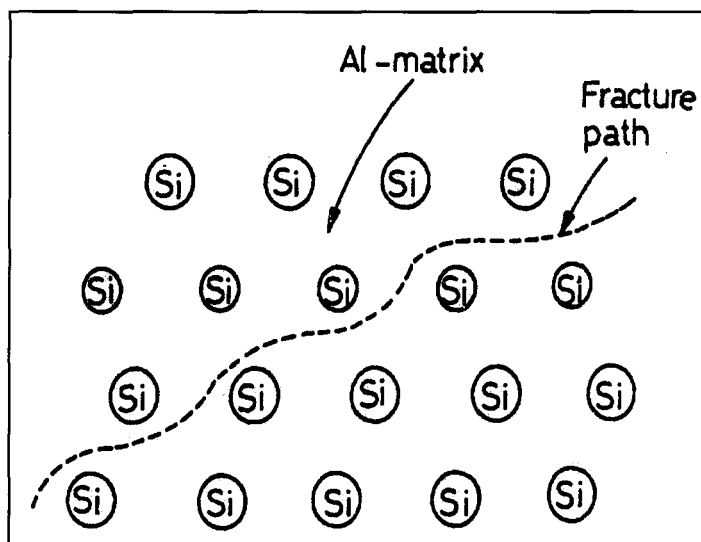
Figure 5.16 Model for the fracture mechanism of modified Al-Si alloys.

This fracture behavior was explained by Surappa *et al.*[124] in their study on the deformation and fracture of A356 alloys. They posited that the microcracks which formed in the small iron intermetallics and the Si particles in A356 alloys which solidified at a high cooling rate are short and that they are difficult to link with each other due to the presence of large ductile α-Al region, consequently that the microcrack linkage occurred by ductile fracture of the α-Al between the cracks. Figure 5.15(b) reveals that the crack propagates through the splitting of the π-phase iron intermetallic as well as through the formation of microcracks inside the bulk of the π-phase.

The preceding discussion may explain the reason that the Sr-modified as-cast 6C alloy, when solidified at the high cooling rate, leads to the highest toughness level among the as-cast alloys studied. Figure 5.17(a) and (b) show the fracture paths of 6CS alloy sample solidified at the low cooling rate and then subjected to a T6 standard heat treatment
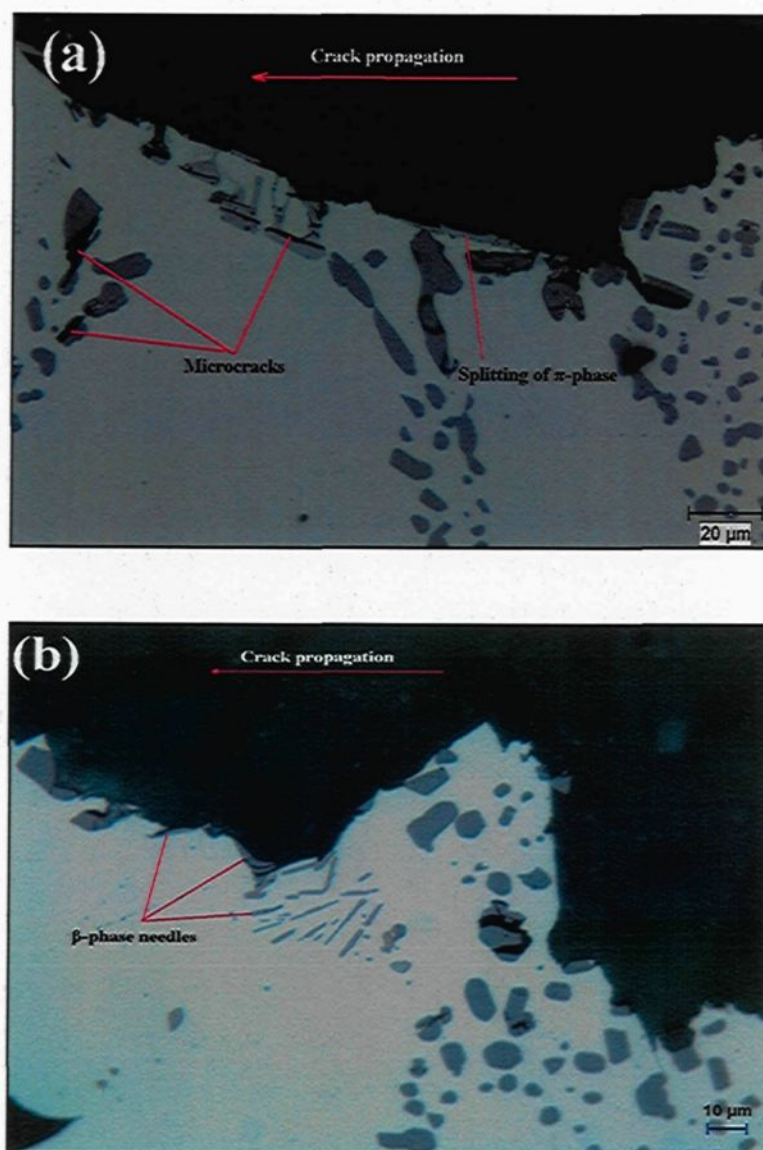
Figure 5.17 Optical micrographs obtained from longitudinal sections below the fracture surface of T6-6CS alloy sample solution heat treated for: (a) 8hr/540oC, and (b) 80hr/540oC; samples were obtained at low cooling rate SDAS~110 μm.

using 8-hr and 80-hr solution treatment time durations, respectively. Figure 5.17 (a) reveals that the main fracture path went through the eutectic region together with the undecomposed π-phase iron intermetallic particles and also shows the influence maximum Si particle spheroidization in increasing the interparticle spacing, thereby reducing the number of the microcracks formed beneath the fracture surface. Figure 5.17(b) shows that the primary crack passes through the eutectic Si particles and newly-formed β-phase needles which came into being as a result of π-phase decomposition. Based on the fracture profile analysis, it appears that the presence of these needles may be responsible for lowering the value of the total impact energy in these samples after 80 hours of solution treatment, as was observed in Figure 5.6.

5.5   Tensile Test Results

The tensile strength of defect-free 357 alloys is controlled by the SDAS, the eutectic particle size and aspect ratio, as well as by the iron intermetallic phases, all of which are strongly dependent on the cooling rate, Mg content, Fe content, Sr modification, and heat treatment. It has been reported that the yield strength is more sensitive to the Mg content of the matrix and to the aging condition than to the eutectic Si particle characteristics, SDAS and iron intermetallic phases. [125, 126, 127, 128] Consequently, the tensile properties were selected in order to examine the response of the same 6C and 6CS alloys obtained from ASTM B-108 permanent mold castings to an increase in Mg content of the matrix during solution heat treatment. This increase resulted from the dissolution of Mg_2Si as well as the decomposition of the π-phase during the solution heat treatment process. The tensile

properties, UTS, YS, and %El, were measured using a Servohydraulic Mechanical Testing Machine. The details of sample preparation and testing procedures are provided in Chapter 3, subsection 3.5.

Figures 5.18 (a), (b), and (c) show the YS, UTS, and %El, respectively, for the as-cast and heat-treated 6C and 6CS alloys solidified at a cooling rate corresponding to SDAS 23μm. For the as-cast alloys, Sr modification had no significant effect on the YS value compared to the non-modified value, as shown in Figure 5.18(a) which was in reasonable agreement with the values reported by Shivkumar.[87] This response may be explained by Saigal and Berry[129] who reported that the stress required for localized yielding varies marginally with Si particle size or aspect ratio. The UTS and %El values for Sr-modified as-cast samples show improvements when compared to non-modified samples. This improvement is mainly related to the changes occurring in the Si particle characteristics as a result of Sr modification.[130] The low ductility and UTS of the non-modified as-cast alloys is usually ascribed to the presence of large Si particles and iron intermetallics. Large elongated particles tend to crack early during plastic deformation, lowering the strength and ductility of the material.[131,132]

Solution heat treatment leads to two types of competing changes in the microstructure. First, an increase in the Mg and Si content of the matrix to attain the maximum level, thereby resulting in the formation of the hardening Mg_2Si precipitates after aging. These Mg_2Si precipitates hinder the movement of dislocations leading to an overall
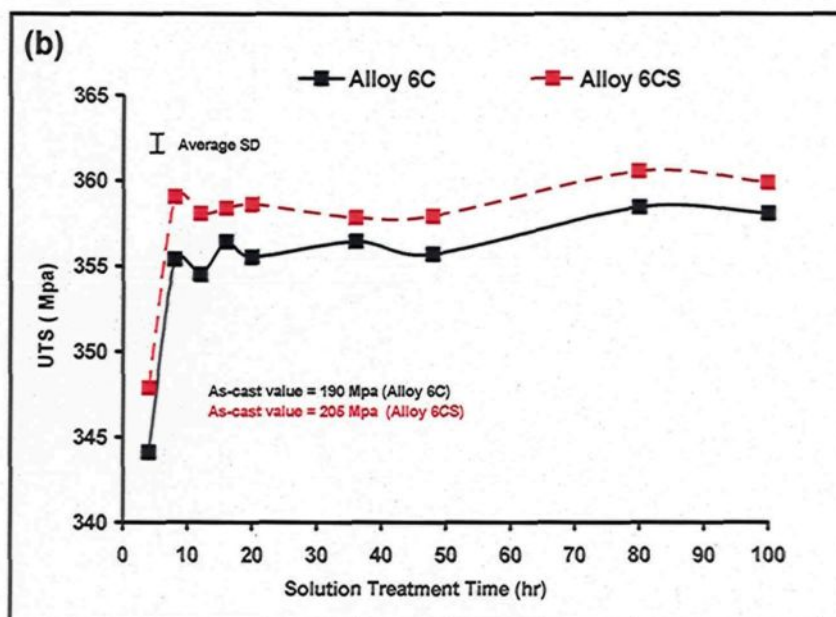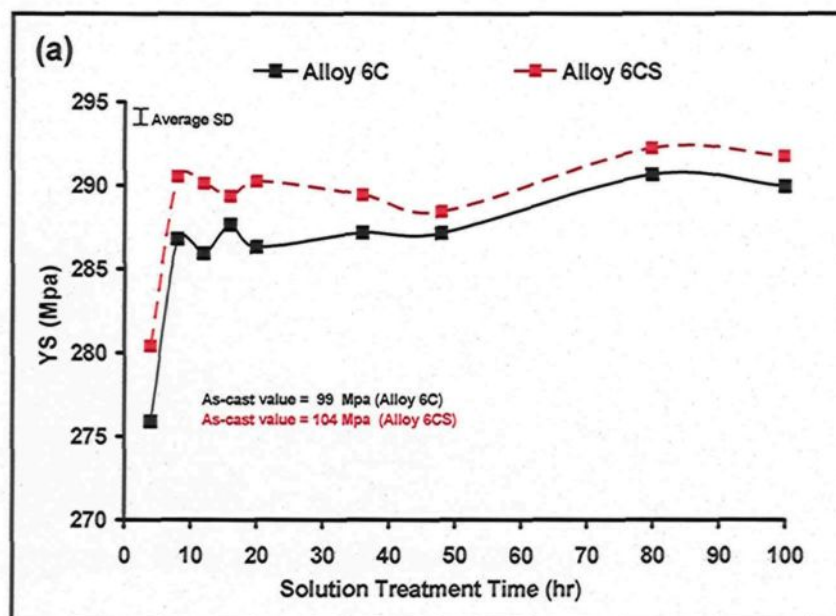
Figure 5.18(a) and (b)
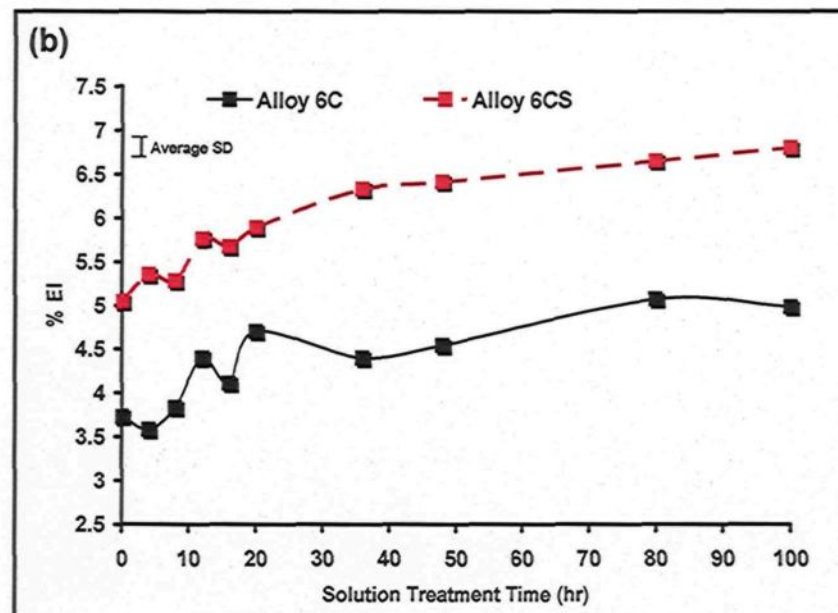
Figure 5.18 Average (a) UTS, (b) YS, and (c) %El values exhibited by non-modified and Sr-modified T6-357alloys, as a function of solution treatment time at 540°C.

reduction in ductility and an increase in strength.[4, 133] Secondly, as pointed out in subsection 5.3, solution heat treatment reduces the aspect ratio and increases the roundness of the Si particles, thereby leading to improvements in the ductility and UTS of the alloy compared to the as-cast state. In a previous study carried out on A357 alloys,[134] the results indicated that the UTS value increased from 300 to 350 mpa with a decrease in the Si particle aspect ratio from 2.15 to 1.55.

Based on the above discussion, the results shown in Figures 5.18(a), (b), and (c) reveal an improvement in YS, UTS, and %El, respectively, in all heat-treated non-modified and Sr-modified samples compared to the as-cast ones. The improvement of the tensile properties observed after 16 and 8 hours solution heat treatment for non-modified and Sr-

modified alloys, respectively, as shown in Figures 5.18(a) and (b), can be attributed to two factors:

(i)   in view of the fact that the Mg_2Si phase in A375 alloys dissolved completely during solution treatment in less than 2hour,[108] the Mg required to form Mg_2Si precipitates after 5 hour aging at 155°C is derived from said dissolution of Mg_2Si phase as well as from the partial dissolution of the π-phase;

(ii)   the fact that there is a partial spheroidization and a reduction in the aspect ratio of the Si particles as a result of solution treatment.

It should be noted that the degree of spheroidization is higher in Sr-modified alloys than in the non-modified ones as discussed previously in subsection 5.2, thus the amount of the crack initiation sites is reduced, and consequently the UTS and %El values for Sr-modified alloys will be greater than these for the non-modified alloys.

With a further increase in the solution treatment time of up to 48 hours, the increased amount of Mg content in the Al matrix resulting from further decomposition of the π-phase is not expected to be large enough to have any significant effect on increasing the amount of Mg_2Si precipitates after aging in both the non-modified and Sr-modified alloys. Consequently, there is no significant change to be observed in the strength values in this period of time. The effects of further improvement in the roundness and aspect ratio, as well as the relative coarsening of Si particles with increasing solution heat treatment from

20 to 48 hours lead to fluctuations in the strength values of 2 to 3 MPa around the values obtained at 8 hours and 16 hours for non-modified and Sr-modified alloys, respectively.

Prolonged solution treatment time of up to 100 hours results in a coarsening of the Si particles and an increase in the amount of ductile α-Al present; also, more Mg_2Si precipitates may be expected to form as a result of further Mg diffusion into the matrix after the decomposition of large amounts of the π-phase particles. These two effects result in improving the ductility values and in marginally increasing the strength values. Warren *et al.*[135] attributed the increase in the percentage of elongation with increasing solution treatment time to the refinement occurring in the silicon-rich structure together with the uniformity of the precipitate distribution. As mentioned previously in subsection 5.2, Sr addition and heat treatment affect the modification and spheroidization of the eutectic Si particles. The combination of Sr and solution treatment thus increase the ductility of 6CS alloys significantly when compared to 6C alloys, as may be observed in Figure 5.18(c). Figures 5.18(a) and (b) also indicate that the heat-treated modified samples showed appreciably higher strength values than the non-modified specimens; this may be explained in terms of the fact that the number of Mg_2Si particles in the Sr-modified alloys is greater and finer than those observed in non-modified alloys. [137,136]

Figure 5.19 shows the main precipitates observed in the 6CS alloy after applying an aging treatment for 5 hours at 155°C using an 8-hour solution treatment time. These precipitates are responsible for increasing the strength of the alloys beyond 8 hours solution of treatment. Figure 5.19(a) illustrates an SEM image taken from the matrix at a
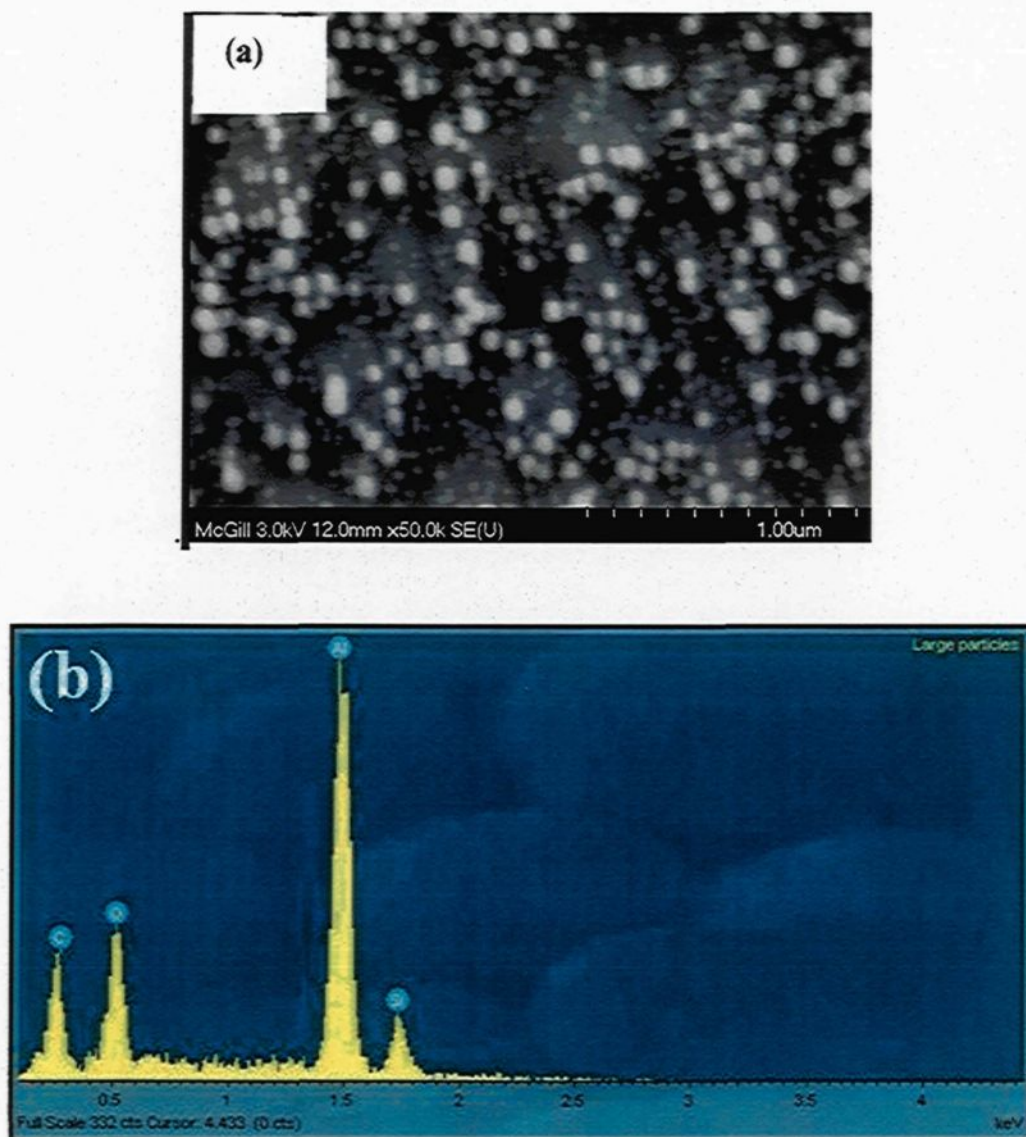
Figure 5.19 FESEM analysis of the precipitates observed in 6CS alloys: (a) SEM image taken from the matrix of 6CS alloy solution-treated for at 540°C for 8hrs and aged at 155°C for 5hrs; (b) EDX spectrum corresponding to the bright particles in (a).

magnification of 10,000x, displaying a mixture of gray and bright spherical types of precipitate. The bright particles, of the gray spherical should correspond to Mg_2Si precipitates, based on similar observation of the same gray spherical Mg_2Si precipitates detected in D357 heat-treated alloys by Chaudhury *et al.*[137] using SEM and analysis. The EDX in the work of The EDX spectrum shown in Figure 5.19(b) corresponds to the bright particles shown in Figure 5.19(a); from this spectrum and the documentation listed in the relevant literature,[138, 139] it may be concluded that the bright particles are silicon precipitates.

Figure 5.20 shows optical micrographs taken from longitudinal section obtained from as-cast and 80hr/540oC solution heat treated 6CS tested alloy samples the microstructure beneath the fracture surface in order to determine the cause of the crack initiation. The microstructure beneath the fracture surface of the as-cast 6CS alloy shown in Figure 5.20(a) reveals that the cracks initiated at sites on the surface where both silicon and π-phase iron intermetallic particles were found, as indicated by the arrows. As described earlier in subsection 5.4 for Sr-modified alloys, the cracks usually initiate at partially modified Si particles and iron intermetallic phases because of the hard brittle nature of these phases when compared to the Al matrix. It is apparent from the figure that the Si particles and π-phase iron intermetallics do in fact affect crack propagation; it should be noted, however, that the crack shows a preferential tendency to pass through the Si
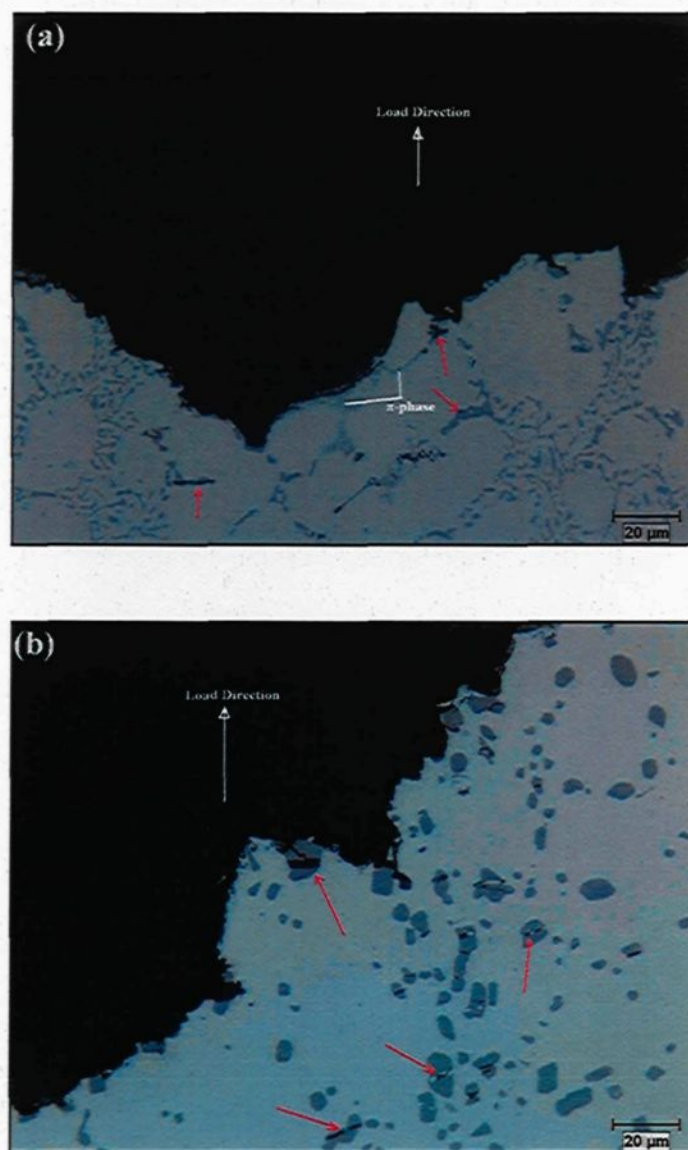
Figure 5.20 Optical micrographs obtained from longitudinal sections below the fracture surface of (a) as-cast, and (b) 540°C/80hr solution heat treatment 6CS alloy samples solidified at a high cooling rate, (SDAS ~23μm).

particles. This observation implies that the Si particles affect the crack propagation more than the iron intermetallic phases.

The large Si particles remaining after 80 hours solution heat treatment act as crack initiation sites as indicated by the arrows in Figure 5.20(b). It will also be seen from this figure that there were no newly-formed β-phase needles to be observed in the microstructure of the fractured samples affecting the fracture behaviour as observed earlier in Figure 5.17(b); this may be ascribed to the much higher cooling rate which had been applied to these samples (SDAS:23μm). Based on the fractography analysis, ductility is observed to be controlled by features of the Si eutectic when the solution time is prolonged. The present results show that the Sr modification has no significant effect on the formation of porosity due to the very high cooling rate applied to these samples.

Figure 5.21 illustrates the variation of quality index (Q) in the as-cast and heat-treated 6C and 6CS alloys as a function of solution treatment time. The concept of quality index as described in Chapter 2, subsection 2.4.2, correlates both the tensile strength and the percentage of elongation to the different microstructural constituents. Accordingly, the Q values for the various samples were calculated based on the following equation:

$$Q = UTS + K \log (\%El)$$

Where the Q value expressed in MPa units and the constant K, for the current condition is equivalent to 150. The results shown in Figure 5.21 reveal a significant increase of about
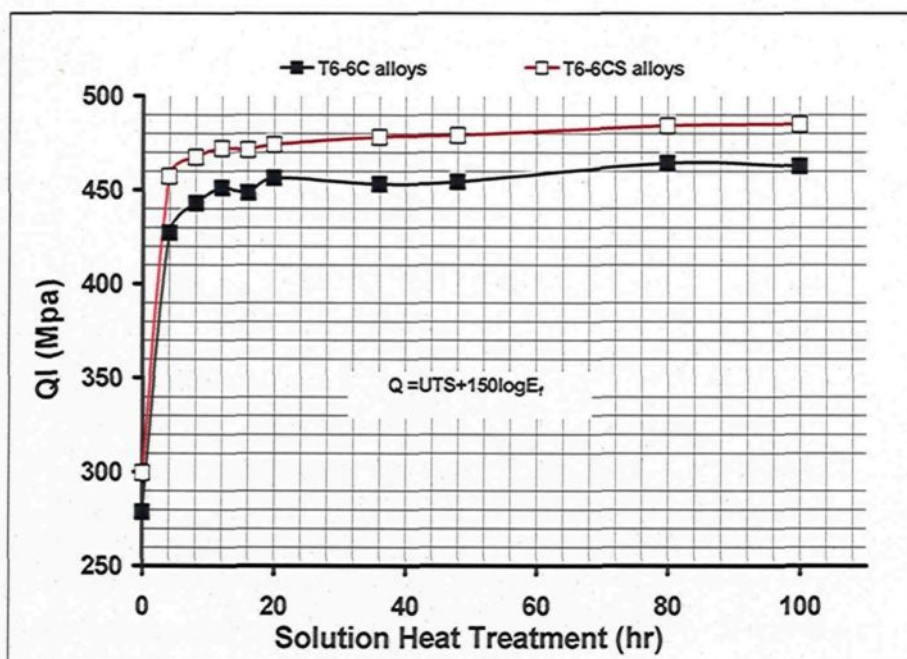
Figure 5.21 Effects of solution heat treatment on the Quality Index of heat-treated samples obtained from 6C and 6CS alloy castings.

52% - 53% in the Q value of the non-modified and Sr-modified alloys after 4 hours of solution treatment, when compared to the corresponding as-cast values. With further solution treatment, the Q values increase gradually until they reach a maximum value at the 80-hr mark after which the Q value remains constant up to 100 hours of solution treatment.

As will be observed, the Sr-modified casting displays a higher quality index than the non-modified casting. It will also be observed upon comparing Figure 5.21 with Figure 5.18, that the Q values are more sensitive to variations in ductility than to variations in tensile strength. Increasing the solution treatment time from 20 hours to 100 hours for Sr-modified alloys causes an increase of about 4.5 % in the Quality Index, which is not so high as to be considered a significant increase. Thus, from a practical point of view, the 12 to 20

hours range may be considered the optimum solution treatment time duration for the Sr-modified alloys to achieve high strength values with reasonable ductility.

Based on the results shown and the above discussion, the changes occurring in the morphology of the π-phase and the Si particles during solution treatment, however, have a greater effect on the ductility values than on the strength values. These changes in Si particle characteristics and π-phase iron intermetallics, however, are more clearly reflected in the previously presented results from impact testing than in those from tensile testing. Consequently, no further experiments were considered necessary at this juncture in regard to tensile properties.

5.6   Conclusions

From the analysis and discussion of the results presented in this chapter, the following conclusions may be drawn.

1. Results obtained from Si particle characterization show that the Sr modification, rather than a high cooling rate, is the most influential factor in bringing about observable improvements in the Si particle characteristics.

2. Increasing the solution treatment time increased the average impact values for the alloys studied. This was accomplished by:

      (i)   Changing the shape of the eutectic Si particles;

      (ii)   Decreasing the number of silicon particles;

(iii)   Increasing the interparticle spacing between Si particles;

(iv)   Decreasing the amount of the π-phase iron intermetallic particles.

3. The improvement in the impact properties resulting from changes in the Si particle parameters in the first 20 hours of solution treatment compensates largely for the loss in the impact energy arising from the presence of the π-phase, the newly-formed β-phase needles, and the strengthening of the Al-matrix.

4. A combination of Sr-modification and solution treatment significantly improves the initiation and propagation energies and tensile values of the alloys studied, particularly at a high cooling rate.

5. Newly-formed β-phase needles contribute significantly to reducing the total impact energy of the alloys studied for a prolonged solution treatment time of 60 to 80 hours.

6. The decrease in the cooling rate does not have as direct an effect on the impact properties as Sr modification does. Increasing the cooling rates, however, provides the fine microstructure with a uniform distribution of the eutectic mixture.

7. The fracture mode shows a dependence on the microstructural features of the eutectic Si phase. Fine silicon particles displaying a high degree of sphericity reveal a ductile mode. By contrast, coarse long Si particles lead to a brittle fracture mode.

8. The π-phase iron intermetallic undergoes cracking in the non-modified and Sr-modified 357 alloys, providing another source for microcrack initiation and further paths for crack propagation.

9. A dimpled pattern was observed on the fracture surface of the modified samples.

10. Fine Si particles with a low aspect ratio and a high degree of spheroidization provide an increase in the crack initiation and crack propagation energies.

11. Sr-modification has no significant effects on the strength values of the as-cast alloys. Its effects are appreciable, however, in improving the strength and ductility values of all the heat-treated alloys studied.

12. The changes which occur in the Si particle characteristics and the π-phase iron intermetallics as a result of prolonged solution heat treatment affect the alloy ductility more significantly than the strength.

13. The optimum quality index (Q) values may be obtained in the 12-20hrs range of solution treatment time for Sr-modified alloys. Solution treatment time beyond this range produce only a marginal increase of ~ 4.5% in the Q value.

14. An analysis of the microstructure beneath the fracture surface reveals that the Si particles and the π-phase iron intermetallics play a significant role in reducing the ductility of the as-cast alloys.

15. The changes occurring in the Si-particle characteristics, as well as in the π-phase iron intermetallics, as a result of cooling rate, Sr-modification, and solution treatment time are all clearly reflected in the impact test results. Tensile properties, however, are not as sensitive to these changes.

16. The tensile properties, in particular the ductility of 357 alloys obtained at high cooling rates (SDAS of ~23μm) is strongly dependent on the Si particles characteristics which are regulated by solution treatment time and Sr modification.

RECOMMENDATIONS FOR FUTURE WORK

1. Since the addition of Be is considered to be a health hazard, another study is suggested in order to investigate the effects of adding a controlled amount of iron-neutralizing elements such as Cr, Co, or Ni on the amount as well as the decomposition of the π-phase after the application of heat treatment.

2. The current results show that the addition of Sr has an effect on increasing the amount of the π-phase iron intermetallic; consequently, other possible study on investigating the effects of using a different modifier may be proposed.

3. It is also suggested that a detailed study of selected compositions be set up at high temperatures to follow on the decomposition of π-phase and its role in preservation the alloys tensile properties at temperatures as high as 350oC for operating times of up to 100h.

REFERENCES

1   S. Murali, K. S. Raman and K.S.S. Murthy, "Effect of Magnesium ,Iron (impurity) and Solidification Rates on the Fracture Toughness of Al-7Si-0.3Mg Casting Alloy," *Material Science and Engineering*, A151,1992, pp.1-10.

2   A. T. Joenoes and J. E. Gruzleski, "Magnesium Effects on the Microstructure of Unmodified and Modified Al-Si Alloys," *Cast Metals*, Vol. 4, No. 2, 1991.pp.62-71

3   A. Thirugnanam, K. Sukumaran, U.T.S. Pillai, and K. Raghukandan, "Effect of Mg on the Fracture Characteristics of Cast Al-7Si-Mg Alloys," *Materials Science and Engineering A*, Vol. 445-446, 2007, pp. 405-414.

4   S. Shivkumar, C. Keller, M. Trazzera and D. Apelian, "Precipitation Hardening in 356 Alloys," *Proceedings International Symposium on Production, Refining, Fabrication and Recycling of Light Metals*, Hamilton, Ontario, August 26-30, 1990, pp. 264-278

5   C. H. Cáceres, C. J. Davidson, J.R. Griffiths and Q. G. Wang, "The Effect of Mg on the Microstructure and Mechanical Behavior of Al-Si-Mg Casting Alloys," *Metallurgical and Materials Transactions A*, Vol. 30A, March 1999, pp. 1999-2611.

6   Q. G. Wang, and C. J. Davidson, "Solidification and Precipitation Behaviour of Al-Si-Mg Casting Alloys," *Journal of Materials Science*, Vol. 36, 2001, pp.739-750.

7   H. Mäller, G. Govender, W. E. Stumpf and P.C. Pistorius, "Comparison of Heat Treatment Response of Semisolid Metal Processes Alloys A356 and 357," *International Journal of Cast Metals Research*,Vol.23, No.1, 2010, pp.37-43.

8   Barresi, M. J. Kerr, H. Wang and M. J. Couper, "Effect of Magnesium, Iron and Cooling Rate on Mechanical Properties of Al-7Si-Mg Alloys," *AFS Transactions*, Vol. 108, 2000, pp. 563-570.

9   Zalensas DL (2001) Aluminum Casting Technology. AFS, 2nd Ed., 19-104. Des Plaines, Illinois.

10   J. A. Taylor, D. H. StJohn, Barresi, and M. J. Couper, "Influence of Mg Content on The Microstructure and Solid Solution Chemistry of Al-7Si-Mg Casting alloys During Solution Treatment," *Materials Science Forum*, Vol. 331-337, 2000, pp. 277-282.

11   William F. Smith, "Introduction to Aluminum," ASM International, Materials Engineering Institute Materials Park, Ohio, 1993.

12   Warmuzek Malgorzata, Aluminum-Silicon Casting Alloys, "An Atlas of Microfractographs," Materials Park, Ohio; ASM International, Vol. 124, 2004.

13   J. Gilbert and Elwin Leroy, "Aluminum Alloy Castings: Properties, Processes and Applications," *AFS, ASM, and International Materials Park*, Dec. 2004.

14   Ned. Tenekedjiev, H. Mulazimoglu, B. Closset and J. Gruzleski, "Microstructures and Thermal Analysis of Strontium Treated Aluminum Silicon Alloys," *AFS*, 1995.

15   S. L. Bäckerud, G. Chai, J. Tamminen, Solidification Characteristics of Aluminum alloys, AFS/Skanaluminium, Oslo, Norway, Vol.2, 1990.

16   Gösta Phragmén, "On The Phases Occurring in Alloys of Aluminum with Copper, Magnesium, Manganese, Iron, and Silicon," *Journal of the Institute of Metals*, Vol. 77, 1950, pp. 498-553.

17   S. K. Tang and T. Sritharan, "Morphology of β-AlFeSi Intermetallic in Al-7Si Alloy Castings," *Materials Science and Technology*, Vol.14, No.8, Aug., 1998, pp.738-742.

18   S. Foss, A. Olsen, C. J. Simensen and J Tafto, "Determination of the Crystal Structure of The π-AlFeMgSi Phase Using Symmetry and Site-Sensitive Electron Microscope Techniques," *Acta Crystallographica*, Section B, B59, 2003, 36-42.

19   L. F. Mondolfo, "Aluminum Alloys: Structure and Properties," Butterworths, London, 1976.

20   G. Gustafsson, T. Thorvaldsson, and G. L. Dunlop "The Influence of Fe and Cr on The Microstructure of Cast Al-Si-Mg Alloys," *Metallurgical and Materials Transactions A* Vol. 17A, Jan.1986, pp. 45.

21   B. Closset and J. E. Gruzleski, "Structure and Properties of Hypoeutectic Al-Si-Mg Alloys Modified with Pure Strontium," *Metallurgical and Materials Transactions A,* Vol. 13(A), 1982, pp. 945-951.

22   John A. Taylor, "The Effect of Iron in the Al-Si Casting Alloys," Casting Concepts, *35th Australian Foundry Institute National Conference Adelaide*, South Australia, 31 Oct. 2004.

23   J. D Evensen and T. B. Pedsesen, "Microstructural Aspects of the Fracture Behavior of Al-Si-Mg Casting Alloys," *Proc. of the 7th International Light Metals Congress*, Loeben / Vienna, June 22-26, Aluminum-Verlag Gmbh, 1981, pp. 77-79.

24   S. Yaneva, N. Stoichev, Z. Kamenova, and S. Budurov, "Quaternary Iron-Containing Phases in Al-Si Cast Alloys," *Zeitschrift fur Metallkunde*, Vol. 75, 1984, pp. 395-398.

25   L. Lu, A. K. Dahle, and M. J. Couper, "Formation of Iron Intermetallic Phases During Solidification of the Aluminum Casting Alloys," *Solidification of Aluminum Alloys*, TMS (The Minerals, Metals and Materials Society), 2004.

26   T. O. Mbuya, B. O. Odera and S. P. Nganga," Influence of Iron on Castability and Properties of Aluminum Silicon alloys: Literature review," *International Journal of Cast Metals Research*, Vol.16 (5), 2003.pp.451-465

27   J. A. Taylor, G. B. Schaffer, and D. H. StJohn, "The Role of Iron In The Formation of Porosity in Al-Si-Cu Based Casting Alloys: Part III A Microstructural Model," *Metallurgical and Materials Transactions A*, Vol. 30A, June 1999, pp. 1657-1662.

28   O. Vorren, J. E. Evensen, and T. B. Pedersen, "Microstructure and Mechanical Properties of Al-Si-Mg Casting Alloys," *AFS Transactions,* Vol. 92, 1984, pp.459-466.

29   S. Musmar, "In-Situ Thermal Analysis Probe," PhD Thesis, Faculty of Graduate Studies and Research, McGill University, Montreal, Canada, 2006.

30   Taylor, J. A. StJohn, D. H. Zheng, L H. Edwards, and G. A. Barresi, "Solution Treatment Effect of Al-Si-Mg Casting Alloy: part 1: Intermetallic Phase," *Aluminum Transactions*, Vol. 4, No 5, 2001, pp. 95-110.

31   C. H. Cáceres, C. J. Davidson, J. R. Griffiths, and Q. G. Wang, "The effect of Mg on the Microstructure and Mechanical Behavior of Al-Si-Mg Casting Alloys," *Metallurgical and Materials Transactions A*, Vol.30A, March 1999, pp. 1999-2611.

32   Makhlouf M. Makhlouf and Sumanth Shankar, "The Mechanism of Eutectic Nucleation in Hypoeutectic Al-Si Alloys Applied to the Design of New Casting Alloys," *Proceedings of the Second International Light Metals Technology Conference*, H. Kaufmann ed., St. Wolfgang, Austria, June 2005, pp. 21-26.

33   F .H. Samuel, P. Ouellette, A. M. Samuel and H. W. Doty, "Effect of Mg and Sr Additions on the Formation of Intermetallics in Al-6 %Si - 3.5 % Cu-(0.45) to (0.8) % Fe 319-Type Alloys," *Metallurgical and Materials Transactions A*, Vol. 29A, 1998, pp. 2871-2884.

34   Q. G. Wang, "Microstructural Effects on the Tensile and Fracture Behavior of Aluminum Casting Alloys A356/357," *Metallurgical and Materials Transactions A*, Vol. 34A, Dec. 2003, p. 2887.

35   B. Zhang, M. Garro, and C. Tagliano, "Dendrite Arm Spacing in Aluminum Alloy Cylinder Heads Produced by Gravity Semi-Permanent Mold," *Metallurgical Science and Technology*, Vol. 21, No. 1, June 2003.pp.3-9

36   C. Triveno Rios, C. Bolfarini, W. J. Botta F. and C. S. Kiminami," Rapidly Solidified Al-Si-Mg alloy," *Journal of Metastable and Nanocrystalline Materials* Vol. 20-21, 2004, pp. 594-598.

37   R. Maniara, L.A. Dobrzanski, J. H. Sokolowski, W. Kasprzak, and W.T.Kierkus, "Influence of Cooling Rate on The Size of the Precipitates and Thermal Characteristic of Al-Si Cast alloys," *Advanced Materials Research*, Vol.15-17, 2007, pp. 59-64.

38   J. Barresi, M. J. Kerr, H. Wang and M. J. Couper, "Effect of Magnesium, Iron and Cooling Rate on Mechanical Properties of Al-7Si-Mg Alloys," *AFS Transactions*, Vol. 108, 2000, pp. 563-570.

39   S. G. Shabestari and J.E. Gruzleski, "The Effect of Solidification Conditions and Chemistry on the Formation and Morphology of Complex intermetallic Compounds in Aluminum-Silicon Alloys", *Cast Metals*, Vol. 6, No. 4, 1994, pp. 217-224.

40 J. Z. Yi, Y. X. Gao, P. D. Lee and T. C. Lindley, "Effect of Fe Content on Fatigue Crack Initiation and Propagation in a Cast Aluminum–Silicon Alloy (A356–T6)," Materials Science and Engineering A, Vol. 386,pp.396-407, 2004.

41 K. Abedi and M. Emamy, "The Effect of Fe, Mn and Sr on the Microstructure and Tensile Properties of A356–10% SiC Composite," *Material Science and Engineering A*, Vol. 527, No. 16-17, 2010, pp.3733-3740.

42 Q. G. Wang, "Plastic Deformation Behavior of Aluminum Casting Alloys A356/357," *Metallurgical and Materials Transactions A*, Vol. 35A, Sept. 2004, pp. 2707-2718.

43 Cameron M. Dinnis, John A. Taylor and Arne K. Dahle, "As-cast Morphology of Iron–Intermetallics in Al-Si Foundry Alloys," *Scripta Meterialia*, Vol. 53, 2005 pp.955-958,.

44 S. Murali, K. S. Raman and K. S. S. Murthy, "Effect of the Trace Additions (Be, Cr, Mn and Co) on The Mechanical Properties and Fracture Toughness of Fe-Containing Al-7Si-0.3Mg Alloy," *Cast Metals*, Vol. 6, No.4, 1994,pp.189-198.

45 Z. Ma, A. M. Samuel, F. H. Samuel, H. W. Doty and S. Valtierra, "Effect of Fe Content and Cooling Rate on the Impact Toughness of Cast 319 and 356 Aluminum Alloys," *AFS Transactions*, paper 03-101, 2002, pp. 1-11

46 P. N. Crepeau, "Effect of iron in Al-Si Casting Alloys: A Critical Review," AFS Transactions, Vol. 103, 1995, pp. 361-366.

47 A. Couture, "Iron in Aluminum Casting Alloys - A Literature Survey," *AFS International Cast Metals Journal*, Vol. 89, 1981, pp. 9-17.

48 N. D. Alexopoulos, and Sp. G. Pantelakis, "Quality Evaluation of A357 Cast Aluminum Alloy Specimens Subjected to Different Artificial Aging Treatment," *Materials and Design*, Vol. 25, 2004, pp. 419-430.

49 Murat Tirykoglu, John Campbell, and Nikolaos D. Alexopoulos, "On the Ductility of Cast Al-7Si-Mg Alloys," *Metallurgical and Materials Transactions A*, Vol. 40A, April 2009, pp. 1000-1007.

50 C. H. Cáceres, "Microstructure Design and Heat Treatment Selection for Casting Alloys Using the Quality Index," *Journal of Materials Engineering and Performance*, Vol. 9, No. 2, April 2000, pp. 215-221.

51   M. Drouzy, S. Jacob and M. Richard, "Interpretation of Tensile Results by Means of Quality Index and Probable Yield Strength," *AFS International Cast Metals Journal*, Vol. 5, 1980, pp. 43-50.

52   A. Granger and R. R. Sawtell, "Effect of Beryllium on the properties of A357 Castings," *AFS*, Vol. 115, 1984, pp. 579.

53   M. Tsukuda, M. Harada, T. Suzuki and S. Koike, "The effect of Si, Mg, Fe on the mechanical properties of Al-Si-Mg alloys for casting," *Journal of Japan Institute of Light Metals*, Vol. 28(3), 1978, pp. 109-115.

54   M. Tsukuda, M. Harada, T. Suzuki and S. Koike, "Interaction of Mg and Fe Content and Aging Temperature on mechanical Properties of Al-7%Si-Mg Alloys," *Journal of Japan Institute of Light Metals*, Vol. 29, No.4, 1979, pp.131-138.

55   Y. Kaneko, H. Murakami, K. Kurada and S. Nakasaki, *Die Casting Engineer*, May-June 1979, p. 26.

56   G. E. Nagel and J. P. Mouret, "A357 Type Alloy with Improved Properties," *AFS Transactions*, Vol, 91, 1983, pp. 157-160.

57   D. Apelian, S. Shivkumar and G. Sigworth, "Fundamental Aspects of Heat Treatment of Cast Al-Si-Mg Alloys," AFS Transactions, Vol. 97, 1989, pp. 727-742.

58   G. K. Sigworth, S. Shivkumar and D. Apelian, "The Influence of Molten Metal Processing on Mechanical Properties of Cast Al-Si-Mg alloys," *AFS.*, Vol. 97, 1989, pp.811-823

59   C. H. Cáceres, I. L. Svensson and J. A. Taylor, "Strength- Ductility Behavior of Al-Si-Cu-Mg Casting Alloys In T6 Temper," *Int. J. Cast Metals Res.*, Vol. 15, 2003, pp. 531-543.

60   K. T. Kashyap, S. Murali, K. S. Raman, and K. S.S. Murthy, "Overview-Casting and Heat Treatment Variables of Al-7Si-Mg Alloy," *Material Science and Technology*, Vol. 9, 1993, pp. 189-202.

61   N. Komatsu, M. Nakamura and Y. Yamamoto, "Relationship Between Si Crystallized Form and Impact Strength of Al-Si Alloys-Observation of Impact

Strength of Al-Si Alloys (1st.Report)," *Journal of Japan Institute of Light Metals*, Vol. 19, No. 9, 1969, pp. 398-408.

62   T. Takaai, Y. Nakayama, N. Ohnishi, and A. Dionisio, "High Temperature Solutionizing and Mechanical Properties of the A356 Aluminum Casting Alloy," *Light Metals 1996*, Montreal, Quebec, Canada, 25-29 Aug, 1996, pp. 307-314

63   C. H. Câceres, C. J. Davidson and J. R. Griffiths, "The Deformation and Fracture Behavior of an Al-Si-Mg Casting Alloy," *Materials Science and Engineering A*, Vol. 197, 1995, pp. 171-179.

64   A. Bayram and A. Uguz, "The Effect of Spheroidising and Na-Modification On the Mechanical Properties of Al-Si Cast Alloys," *Metall. (Germany)*, Vol. 53, No.3, 1999, pp. 131-134.

65   I. Akira, M. Tsujikawa, K.Okabyashi and M. Kawamoto, "Relationship Between Fracture Properties and Microstructure of Hyper-Eutectic Al-Si Alloy Castings," *Transaction of The Japan Foundrymen's*,1987, 6 P18-22ISSN 0287-041X TS, pp.18-22.

66   G. K. Sigworth, "The Modification of Al-Si Casting Alloys: Important Practical and Theoretical Aspects," *International Journal of Metal Casting*, Vol.2, Issue 2, Spring 2008, p.1940.

67   SHU-ZU Lu and A. Hellawell, "The Mechanism of Silicon Modification in Aluminum-Silicon Alloys: Impurity Induced Twinning," *Metallurgical Transactions A*, Vol. 18A, October 1987, pp. 1721-1733.

68   J. G. Conley, J. Huang, Jo Asada and Kenji Akiba, "Modeling The Effects of Cooling Rate, Hydrogen Content, Grain Refiner and Modifier On Microporosity Formation in Al A356 Alloys," *Materials Science and Engineering A*. 285 (1-2), 2000, pp. 49 - 55.

69   S. M. Miresmaeili, W. D. Griffiths, J. Campbell, S.G. Shabestari and S. M. A. Boutorabi, "'Precipitation of Sr-Rich Intermetallic Particles and Their Effect on Pore Formation in A356 Alloy," *Journal of Metallurgical and Materials Transactions A*, Vol. 36A, Sept. 2005, pp. 2341-2349.

70   F. H. Samuel , P. Ouellet , A. M. Samuel , H. W. Doty, "Effect of Mg and Sr Additions on the Formation of Intermetallics in Al-6 Wt Pet Si-3.5 Wt Pet Cu-(0.45) to (0.8) Wt Pet Fe 319-Type Alloys," *Metallurgical and Materials Transactions A*, 1998, Vol. 29A, pp 2871-2884.

71   Peyman Ashtari, Hiroyasu Tezuka and Tatsuo Sato, "Influence of Sr and Mn Addition on Intermetallic Compound Morphologies in Al-Si-Cu-Fe Cast Alloys," *Materials Transactions*, Vol. 44, No. 12, 2003, pp. 2611-2616.

72   A. M. Samuel, F. H. Samuel, and H. W. Doty, "Observations on the Formation of β-AlFeSi Phase in 319 Type Al-Si Alloys," *Journal of Materials Science,* Vol. 31, 1996, pp. 5529-5539.

73   A. pennors, A. M. Samuel, F. H. Samuel and H. W. Doty, "Precipitation of β-Al$_5$FeSi Iron Intermetallic in Al-6Si-3.5Cu (319) Type Alloys: Role of Sr and P," *AFS Transactions*, Vol. 106, 1998, pp. 251-264.

74   F. Paray and J. E. Gruzleski, "Factors to Consider in Modification," *AFS Transactions*, Vol.92, 1994, pp. 833-842.

75   G. K. Sigworth, 'The Modification of Ai-Si Casting Alloys: Important Practical and Theoretical Aspects," *International Journal of Metal Casting*, Vol. 2, 2008, pp.19-40.

76   Florence Paray, "Heat Treatment and Mechanical Properties of Aluminum Silicon Modified Alloys," PhD Thesis, McGill University, Montreal, Quebec, Canada, 1992, p. 375

77   M. Hafiz, and T. Kobayashi, "Metallurgical Factors Affecting Impact Toughness of Eutectic Al-Si Casting Alloy," *Zeitschrift Fur Metallkunde*, Vol. 89, No. 6, 1998, pp. 445-449.

78   S. Kamado, M. Tsukuda, I. Tokutomi and Hirose, "Effect of Solidification Condidtion on Mechanical Properties of Directionally Solidified 356 Aluminum alloy," *Journal of Japan Institute of Light Metals*, Vol. 37. No. 4, 1987, pp. 268-276.

79   E. Kato and T. Kobayashi, "Effect of Solidified Structure on the Fracture Toughness of Unidirectionally Solidified Al-Si System Alloys," Journal of Japan Institute of Light Metals, Vol. 30(3), 1980, pp. 140-146.

80   S. G. Shabestari and F. Shahri, "Influence of modification, solidification conditions and heat treatment on the microstructure and mechanical treatment of A356 aluminum alloy," Journal of Materials Science, Vol. 39, 2004, pp. 2023-2032.

81   Donna L. Zalensas, "Aluminum Casting Technology," AFS, 2nd Edition, Des Plaines, Illinois, 2001, pp. 19-104.

82   G. A. Edwards, K. Stiller, G.L. Dunlop and M.J. Couper, "The Precipitation Sequence in Al-Mg- Si Alloys," *Acta Materialia*, Vol. 46 (11), 1998, pp. 3893-3904.

83   J. L. Jorstad, "Heat Treatment and Strengthening of Aluminum Castings," Aluminum Casting Technology, 2nd edition, *AFS*, 1993, p.287.

84   ASM Handbook, "Heat Treating," ASM International, Metals Park, Ohio, U.S.A., Vol. 4, 1991.pp. 844-858.

85   L. A. Narayanan, F. H. Samuel and J. E. Grazleski, "Dissolution of Iron Intermetallics in Al-Si Alloys through Nonequilibrium Heat Treatment," *Metallurgical and Materials Transactions A,* Vol. 26A, 1995, pp. 2161-2174.

86   Villeneuve and F. H. Samuel, "Fragmentation and Dissolution of β-Al5FeSi Phase During Solution Heat Treatment of Al-13%Si-Fe Alloys," *International Journal of Cast Metals Research,* Vol. 12, 1999, pp. 145-160.

87   S. Shivkumar, S. Ricci Jr., B. Steenhoff, D. Apelian and G. Sigworth, "An Experimental Study to Optimize the Heat Treatment of A356 Alloy," *AFS Transactions*, Vol. 97, 1989, pp. 791-810.

88   F. Paray, B. Kulunk and J. E. Gruzleski, "Impact properties of Al-Si foundry alloys," International Journal of Cast Metals Research, 2000, Vol. 13, pp. 17-37.

89   M. Tsukuda, S. Koike and M. Harada, "The Heat Treatment of Al-7%Si-0.3Mg Alloy," *Journal of Japan Institute of Light Metals*, Vol. 28 No.1, 1978, pp. 8-14

90   Carolyn W. Meyers and Jed S. Lyons, "Fracture Toughness-Second Particle Interactions in A357 Alloys," Technology for Premium Quallity Casting, Denver, Colorada, USA, 1988, pp.151-178.

91   L. Lu and A. K. Dahle, "Iron-Rich Intermetallic Phases and Their Role in Casting Defect Formation in Hypoeutectic Al-Si Alloys," *Metallurgical and Materials Transactions A,* Vol. 36(3), March 2005, pp. 819-835.

92   Aluminum Beryllium Master Alloys, www.freedomalloyssusa.com.

93   Keith G. Wikle, "Improve Aluminum Castings with Beryllium," *AFS*, 1978, Vol.119, pp. 513.

94   Yen Hung Tan, Sheng Long Lee, and Yu Lin., "Effect of Be and Fe Additions on the Microstructure and Mechanical properties of A357 Alloys," *Metallurgical and Materials Transactions A*, Vol. 26A, May 1995, p. 1195.

95   Y. Wang, and Y. Xiong, "Effects of Beryllium in Al-Si-Mg-Ti alloy," *Materials Science and Engineering A*, Vol. 280 (1), March 2000, pp. 124-127.

96   S. S. Sreeja Kumari, R. M. Pillai, T. P. D. Rajan and B. C. Pai., "Effect of Individual and Combined Additions of Be, Mn, Ca and Sr on The Solidification Behavior, Structure and Mechanical Properties of Al-7Si-0.3Mg-0.8Fe Alloy," *Materials Science and Engineering A*, Vol. 460-461, 2007, pp. 561-573.

97   S. Murali, K. S. Raman, K. S. S. Murthy, "The Formation of β-phase and Be-Fe phases in Al-7Si-0.3Mg Alloy Containing Be," *Materials Science and Engineering A*, Vol. 190, 1995, p. 165.

98   S. Murali, A. Trivedi, K. S. Shamanna and K. S. S. Murthy, "Effect of Iron and Combined Iron and Beryllium Addition on the Fracture Toughness and Microstructures of Squeeze-Cast Al-7Si-0.3Mg Alloy," *Journal of Materials Engineering and Performance*, Vol. 5(4), 1996, pp. 462-468.

99   L. Lu and A. K. Dahle, "Iron-Rich Intermetallic Phases and Their Role in Casting Defect Formation in Hypoeutectic Al-Si Alloys," *Metallurgical and Materials Transactions A*, Vol. 36, No.3, March 2005, pp. 819-835.

100   M. A. Moustafa, F. H. Samuel, H. W. Doty and S. Valtierra, "Effect of Mg and Cu Additions on the Microstructural Characteristics and Tensile Properties of Sr-Modified Al-Si Eutectic Alloys," *Int. J. Cast Metals Res.*, 2003, Vol.15, pp. 609-626.

101   Y. H. Tan, S. L. Lee, and Y. Lin, "Effect of Be and Fe Additions on the Microstructure and Mechanical properties of A357 Alloys," *Metallurgical and Materials Transactions A*, Vol. 26A, May 1995, pp. 1195-1205.

102   C. Y. Yang, S. L. Lee, C. K. Lee and J. C. Lin, "Effect of Be and Fe on the Mechanical and Corrosion Behaviour of A357 Alloys," *Materials Chemistry and Physics*, Vol. 93, 2005, pp. 412-419.

103   D. Apelian and S. K. Chaudhury, "Heat Treatment of Aluminum Cast Components: Recent Developments and Future Challenges," WFO Technical Forum-St. Louis, Missouri, USA, April 19, 2005.

104   J. Espinoza-Cuadra, P. Gallegos-Acevedo, H. Mancha-Molinar and A. Picado, "Effect of Sr and Solidification Conditions on Characteristics of Intermetallic in Al-Si 319 Industrial Alloys," *Materials and Design*, Vol. 31, 2010, pp.343-356.

105   D. A. Porter, K. E. Easterling (1992), *Phase Transformation in Metals and Alloys*, Second Edition, Chapman & Hall, London, UK.

106   W. B. Alexander, and L. M. Slifkin, "Diffusion of Solutes in Aluminum and Dilute Aluminum Alloys," Physical Review B1, 1970, pp.3274:3282.

107   Lawrence V. Olivante, Material Science Research Trends, Nova Science Publishers, New York, US, 2008, pp. 251-271.

108   P. A. Rometsch, L. Arnberg and D. L. Zhang, "Modelling Dissolution of Mg_2Si and Homogenisation in Al-Si-Mg Casting Alloys," *International Journal of Cast Metals Research*, Vol.12, 1999, pp. 1-8.

109   J. A. Taylor, D. H. StJohn and M. J. Couper, "Solution Treatment Effects in Al-Si-Mg Casting Alloys: Part II Solid Solution Chemistry," *Aluminum Transactions*, Vol. 4-5, 2001, pp. 111-124.

110   Q. G. Wang and C. H. Cáceres, "Mg Effect on the Eutectic Structure and Tensile Properties of Al-Si-Mg Alloys," *Materials Science Forum* Vol. 242, 1997, pp.159-164.

111   F. Paray and J. E. Gruzleski, "Microstructure-Mechanical Properties Relationships in 356 Alloy. Part I: Microstructure," *Cast Metals*, Vol.7, No.1, 1994, pp 29-40.

112   M. M. Haque and M. A. Maleque, "Effect of Process Variable on Structure and Properties of Aluminum-Silicon Piston alloy," *Journal of Material Processing Technology*, Vol. 77, 1998, pp.122-128.

113   P. Y. Zhu, Q. Y. Liu and T. X. Hou, "Spheroidization of Eutectic Silicon in Al-Si Alloys," *AFS Transactions*, Vol. 93, 1985, pp.609-614.

114   A. Thirugnanam, K. Sukumaran, K. Raghukandan, U.T.S. Pillai and B.C. Pai, "Microstructural Aspects and Fracture Behavior of A356/357 Alloys-an-Overview," *Transactions of The Indian Institute of Metals*, Vol. 58, No. 5, October 2005, pp. 777-787.

115   M. Hafiz and T. Kobayashi, "Mechanical Properties of Modified and Non-modified Eutectic Al-Si Alloys," *Journal of Japan Institute of Light Metals*, Vol. 44, No.1, Jan.1994, pp. 28-34.

116   M. Hafiz and T. Kobayashi, "Metallurgical Factors Affecting Impact Toughness of Eutectic Al-Si Casting Alloy," Zeitschrift Fur Metallkunde, Vol. 89, No. 6, 1998, pp. 445-449.

117   R. C. Voigt and D. R. Bye, "Microstructural Aspects of Fracture in A356," *AFS Transactions*, Vol. 99, 1991, pp. 33-50.

118   S. Shivkumar, L. Wang, and C. Keller, "Impact Properties of A356-T6 Alloys," *Journal of Materials Engineering and Performance*, Vol. 3, Feb. 1994, pp. 83-90.

119   S. Hotta, K. Saruki, and M. Nakamura, "Effects of T6 Heat Treatment on the Impact Strength of AC4C and AC2B Aluminum Alloy Castings Solidified for a Long Time," *Journal of Japan Institute of Light Metals*, Vol. 37, No. 7, July 1987, pp. 478-482.

120   S. Shivkumar, 'The Interactive Effect of Sr Modification and Heat Treatment on The Mechanical Properties of Cast Aluminum Alloys,' *17th ASM Heat Treating Society Conference Proceedings*, Vol. 15-18, 1998, pp. 265-269.

121   Fractography: Observing, Measuring and Interpreting Fracture Surface Topography. Derek Hull. Cambridge University Press, 40 W. 20th St., New York, NY 1001 24211. 1999.

122   N. Fat-Halla, "Structural Modification of Al-Si Eutectic Alloy by Sr and its Effect on Tensile and Fracture Characteristics," *Journal of Materials Science*, Vol. 24, 1989, pp. 2488-2492.

123   Q. G. Wang and C. H. Câceres, "The Fracture Mode in Al-Si-Mg Casting Alloys," *Materials Science and Engineering A*, Vol. A 241, 1998, pp. 72-82.

124   M. K. Surappa, E. W. Blank, and J. C. Jaquet, "Microstructural Approach to Deformation and Fracture of Cast Al-7Si-0.3Mg," *3rd International Conference on Solidification Processing*, Sheffield, UK, 1987, pp. 424-427.

125   H. Beumler, A. Hammerstad, B. Wieting and R. Dasgupta, "Analysis of Modified 319 Aluminum Alloy", *AFS Transactions*, Vol. 96,1988, pp.1-12.

126   Cáceres, C. H., Griffiths, J.R., Wang Q. G., and Davidson, C. J., "The Effect of Mg on the Microstructure and Mechanical Behaviour of two Al-Si-Mg Casting Alloys". Metallurgical and Materials Transactions, 30A, 1999, pp. 2611-261.

127   Q. G. Wang and C. H. Câceres, "Mg Effects on the Eutectic Structure and Tensile Properties of Al-Si-Mg Alloys," Materials Science Forum, Vol. 242, 1997, pp. 159-164.

128   James M. Boileau, Jacob W. Zindel, and John E. Allison "The Effect of Solidification Time on the Mechanical Properties in a Cast A356-T6 Aluminum Alloy," *SAE Transactions*, Vol.106, 1997, pp. 63-74.

129   A. Saigal and J. T. Berry, "Finite Element Method Analysis of the Effect of Chilling and Modification on Localized Yielding and Crack Initiation in Al-Si Alloys," *AFS Transactions*, 1984, pp. 703-708.

130   E. N. Pan, J. F. Hu and C. C. Fan, "Solution-Treatment Conditions for Optimal Tensile Properties in A357 Alloy," *AFS Transactions*, Vol. 104, 1996, pp. 1119-1132.

131   Q. G. Wang, C. H. Caceres and J. R. Griffiths, "Damage by Eutectic Particle Crackingin Aluminum Casting Alloys A356/357", *Metallurgical and Materials TransactionsA*, Vol. 34A, 2003, pp. 2901-2912.

132   G. Guiglionda and W.J. Poole, "The Role of Damage on the Deformation and Fracture of Al–Si Eutectic Alloys," *Materials Science and Engineering A*, Vol. 336, 2002, pp. 159-169.

133   Hetke A., and Gundlach R. B., "Aluminum Casting Quality in Alloy 356 Engine Components," *AFS Transactions*, Vol. 102, 1994, pp. 367-380.

134   L. Ceschini Alessandro Morri, Andrea Morri, A. Gamberini and S.Messieri, "Correlation Between Ultimate Tensile Strength and Solidification Microstructure For the Sand Cast A357 Aluminum Alloy," *Materials and Design*, Vol. 30, 2009, pp. 4525-4531.

135   A. Warren and J. Campbell, "The Al-7Si-0.5Mg Aerospace Casting Alloys," *The Metallurgy of Light Alloys*, 1983, pp. 196-208.

136   Mulazimoglu, M. H., Zaluska, A., Paray, F. and Gruzleski, J. E. "The Effect of Strontium on the Mg_2Si Precipitation Process in 6201 Aluminum Alloy," *Metallurgical and Materials Transactions A*. Vol. 28A, pp. 1289-1295.

137   S. K. Chaudhury, D. Apelian, "Effects of Rapid Heating on Solutionizing Characteristics of Al-Si-Mg Alloy Using a Fluidized Bed", *Metallurgical and Materials Transactions A*, Vol. 37A, March 2006, pp. 763-778.

138   L. Zhen, W.D. Fei, S.B. Kang and H.W. Kim, "Precipitation Behaviour of Al-Mg-Si Alloys with High Silicon Content," *Journal of Materials Science*, Vol. 32, 1997, pp. 1895-1902.

139   A. K. Gupta, D. J. Lloyd and S. A. Court, "Precipitation Hardening in Al-Mg-Si Alloys with and without Excess Si," *Materials Science and Engineering A*, Vol. 316, 2001, pp. 11-17.